

Oxygen and Hydrogen Isotopes in the Porphyry Copper Deposit at El Salvador, Chile

SIMON M. F. SHEPPARD AND LEWIS B. GUSTAFSON

Abstract

$\delta^{18}\text{O}$ and/or δD values were measured for quartz (11 samples), plagioclase (3), K-feldspar (3), biotite (4), hornblende (1), sericite (3), chlorite (1), kaolinite (2), and pyrophyllite (1) from the porphyry copper deposit at El Salvador, Chile. The samples analyzed were chosen to represent the hypogene evolution from early K-silicate alteration and quartz veining to late pyritic veining and sericitic alteration to very late advanced argillic alteration, as well as supergene kaolinization.

The isotopic compositions of the biotites are identical to those from most other porphyry copper deposits, and the sericite compositions are similar to those from Santa Rita. The requirements for equilibrium isotopic geothermometry are met only for unmineralized "L" Porphyry and K-silicate alteration assemblages, yielding minimum temperatures of about 650° and 525°C, respectively. Temperatures estimated from various other geologic evidence are used to calculate the equilibrium isotopic compositions of hydrothermal solutions. These solutions show a distinct trend of ^{18}O depletion and deuterium enrichment from early to late stages and from high to low temperatures. The $\delta^{18}\text{O}$ and δD values of fluids responsible for Early K-silicate alteration assemblages are similar in isotopic composition to magmatic waters but are enriched in deuterium relative to the later unmineralized "L" Porphyry even though it is petrologically similar to the earlier mineralized porphyries. Later fluids are dominantly meteoric waters enriched in ^{18}O by reaction with the host rock. Late and presumably shallow advanced argillic assemblages developed from acid geothermal waters of meteoric origin that were enriched in deuterium and ^{18}O by near-surface evaporation processes. There was possibly some mixing between these fluids and the deeper meteoric-hydrothermal fluids. The similar isotopic compositions of both meteoric and magmatic waters and the variety of possible processes modifying their isotopic compositions prevent a quantitative analysis of the relative proportions of each at the different stages in the evolution of the hydrothermal fluids.

Introduction

GUSTAFSON and Hunt (1975) have documented in detail the development of the porphyry copper deposit at El Salvador, Chile, which was formed near the end of a long series of Tertiary volcanic and intrusive events. A thick sequence of Cretaceous andesitic flows and related sedimentary rocks is overlain by Lower Tertiary andesitic and rhyolitic extrusives, including ignimbrites. These rocks were intruded by a series of rhyolitic and quartz porphyry intrusions which in turn were intruded by the main granodioritic porphyry complex. The main stages of mineralization and alteration accompanied and followed the intrusion of this final porphyry complex.

Most of the copper was emplaced during the period (termed Early) of alteration-mineralization associated with the two major intrusions ("X" and "K" porphyries). The younger "L" Porphyry was intruded during the waning stages of Early mineralization after much, but not all, of the alteration. K-silicate alteration assemblages and veins of quartz-perthitic feldspar - anhydrite - chalcopyrite - bornite,

called "A" veins, characterize this Early hydrothermal mineralization. These were repeatedly formed, being closely associated in both space and time with the consolidation of several surges of porphyry magma.

"B" quartz-molybdenite veins, without alteration halos, cut "A" veins and K-silicate alteration assemblages. They formed only after the emplacement of the last major intrusion ("L" Porphyry) and mark a transition in the pressure-temperature regime and chemical character of the mineralizing fluids. Subsequent Late mineralization-alteration associated with K-feldspar- and biotite-destructive alteration, produced pyrite-sericite assemblages and pyrite-rich "D" veins with sericitic alteration halos. These Late pyrite- and sericite-forming environments collapsed inward and downward as the inferred ground-water system invaded the cooling mineralized intrusive center. A very late stage hot spring system produced advanced argillic alteration near the surface and over the mineralized center of the deposit. This study presents part of a stable

TABLE 1. Description and Location of Samples

ES-2689	"L" Porphyry, practically unaltered and unmineralized; fresh hornblende and sphene, a few anhydrite veinlets; 2,400 m elevation, 20,059 N-8,530 W.
ES-2691	"L" Porphyry near andesite contact, practically unmineralized; incipient alteration assemblage limited to biotization of hornblende, local sericite "dusting," interstitial anhydrite and K-feldspar-sericite-chlorite veinlets; 2,400 m elevation, 20,034 N-8,530 W.
ES-2699	"X" Porphyry, moderate K-silicate alteration and bornite-chalcopyrite mineralization, cut by "B" quartz-anhydrite-chalcopyrite-vein; 2,400 m elevation, 19,875 N-8,200 W.
ES-1910	"Andesite," strong biotization and bornite-chalcopyrite mineralization, cut by "A" quartz-K-feldspar-anhydrite-bornite-chalcopyrite veins; 2,400 m elevation, 19,894 N-8,160 W.
ES-4304	"A" quartz vein in well-mineralized "K" Porphyry; quartz-perthite-chalcopyrite-bornite, with anhydrite leached out; 2,600 m elevation, 19,840 N-7,766 W.
ES-7536	"B" quartz-anhydrite-chalcopyrite-molybdenite-pyrite vein cutting biotized andesite with chalcopyrite-bornite; 2,400 m elevation, 19,950 N-7,613 W.
ES-1116	"X" Porphyry with strong sericite-chlorite-anhydrite alteration but residual alkali feldspar; pyrite-chalcopyrite mineralization; 2,400 m elevation, 19,720 N-8,420 W.
ES-7576	"D" pyrite-anhydrite vein cutting very weakly mineralized "L" Porphyry, sericite-pyrite halo with minor chalcopyrite and anhydrite; anhydrite largely hydrated to gypsum; 2,400 m elevation, 19,950 N-7,921 W.
ES-1417	"D" pyrite vein cutting very weakly mineralized "L" Porphyry, inner sericite-pyrite halo and outer kaolinite-calcite halo; 2,400 m elevation, 20,054 N-8,530 W.
ES-7486	"D" quartz-pyrite vein cutting sericitic pyroclastics with pyritic fringe mineralization; supergene alunite in vugs; 2,872 m elevation, 19,340 N-8,740 W.
ES-6573	Intense pyrophyllite-alunite alteration of a pebble dike cutting advanced argillic altered quartz porphyry; leached capping; 2,980 m elevation (surface), 20,118 N-8,875 W.
ES-1855	Andesite with sericite-kaolinite alteration and "chalcocite"-enriched pyritic mineralization; supergene kaolinite; 2,710 m elevation, 19,580 N-8,519 W.
ES-6	"L" Porphyry, with kaolinitic alteration, leached capping; location unknown, from Sheppard et al. (1969).
ES-8	"K" Porphyry, enriched "chalcocite" ore with kaolinitic alteration; location unknown, from Sheppard et al. (1969).

isotope investigation which attempts to supplement and quantify these interpretations (see also Field and Gustafson, 1976).

Many studies of the D/H and $^{18}\text{O}/^{16}\text{O}$ ratios of minerals and natural waters over the past several years, recently reviewed by Taylor (1974), have gone far toward defining the isotopic characteristics of different geologic environments and the origins of hydrothermal fluids. Data on hydrogen and oxygen isotope ratios from several porphyry copper and molybdenum deposits have been presented by Sheppard et al. (1969, 1971), Hall et al. (1974), and Sheppard and Taylor (1974).

Specimens representative of assemblages typical of different zones and stages of mineralization at El Salvador were collected by Gustafson. Mineral separations were made by Judy Montoya in the Anaconda Geology Laboratory and were analyzed by Sheppard at the California Institute of Technology. Several of these same samples were also subjected to chemical analyses (Gustafson and Hunt, 1975, table 1) and provided sulfide and sulfate separates for sulfur isotope analyses (Field and Gustafson, 1976). The reader is referred to the article by Gustafson and Hunt (1975) for a description of the geology of the deposit and an explanation of the terminology used.

Sample Selection

A list of samples with their locations and descriptions are given in Table 1 and summarized in Table 2, which gives the hydrogen and oxygen isotope analyses for minerals analyzed from each sample.

The two "L" Porphyry samples from the deep central part of the deposit are representative of a relatively late and barren intrusion which shows minimum effects of mineralization and alteration. Both samples are practically unmineralized, but ES-2691 contains appreciable biotite replacing hornblende, anhydrite in veinlets, and anhydrite replacing plagioclase.

ES: 2699R and 1910R are representative of Early K-silicate alteration with chalcopyrite-bornite, and ES: 1910V and 4304 are typical of the "A" quartz veins accompanying this Early mineralization. Transitional "B" quartz veins are represented by ES: 2699V and 7536, while Late "D" veins and halos are represented by ES: 7576 and 1417. The halo on ES-1417 is a zoned halo, with kaolinite-calcite found peripheral to the inner sericite halo. The sericite-chlorite alteration assemblage from the inner part of the deep pyritic fringe is represented by ES-1116. All of these samples are from the deep "sulfate zone," which was protected from supergene effects, and all but ES-1116 and the "D" vein samples are free from important visible influences of Late mineralization-alteration effects.

The "D" vein sample ES-7486 and kaolinite-altered samples ES: 1855 and 8 are from the zone of supergene alteration and enrichment. Kaolinite in ES-6 from the leached capping at the surface is supergene. The pyrophyllite formed by Late advanced argillic alteration in a pebble breccia, ES-6573, shows no visible effect of superimposed supergene alteration.

Experimental Methods

The method used for extracting hydrogen and oxygen quantitatively from the silicate minerals and

analyzing the gases mass spectrometrically were similar to those discussed in Sheppard et al. (1969) and Sheppard and Taylor (1974). Thus, all labile absorbed water and interlayer water were removed before commencing the isotopic analysis. The general analytical precision for oxygen is 0.1 to 0.2 per mil and for hydrogen 2 to 3 per mil. Quantitative determination of the H₂ gas yield during the hydrogen extraction processes enabled the H₂O content of the sample to be determined. Water contents are precise to about ±1 percent.

Both the hydrogen and oxygen isotope data are relative to standard mean ocean water (SMOW) in per mil. The fractionation of isotopes between any

two minerals A and B is reported as Δ_{A-B} defined as:

$$\Delta_{A-B} = 1,000 \ln \alpha_{A-B} \approx \delta_A - \delta_B$$

where α is the fractionation factor.

Isotopic Results

δD and $\delta^{18}O$ values in hydrous minerals

All the hydrogen and oxygen isotope data (Table 2) for the hydrous minerals analyzed—biotite, hornblende, chlorite, sericite, pyrophyllite, and kaolinite—are plotted on Figure 1. The kaolinite samples from within the supergene zone analyzed by Sheppard et al. (1969) are also included. The two reference

TABLE 2. Hydrogen and Oxygen Isotope Analyses of Minerals

Sample no.	Sample/location	Mineral*	$\delta^{18}O$ ‰	δD ‰
ES-2689	"L" Porphyry, deep central	Plagioclase	7.1	
		Biotite(H ₂ O = 3.0%)**	4.5	-83
		Hornblende(H ₂ O = 1.9%)	5.9	-73
ES-2691	"L" Porphyry deep central	Plagioclase	7.6	
		Biotite(H ₂ O = 3.7%)	5.0	-78
ES-2699R	"X" Porphyry K-silicate, deep central	Quartz	9.2	
		K-feldspar	8.3	
		Plagioclase	8.2	
		Biotite(H ₂ O = 3.2%)	4.3	-73 ± 1 (2)
ES-1910R	Biotized andesite	Biotite	4.0	-75
ES-1910V	"A" vein deep central	Quartz	9.3 ± 0.1 (2)	
		K-feldspar	8.5	
		Quartz	9.4	
ES-4304	"A" vein intermediate central	K-feldspar	9.9	
ES-7536	"B" vein, deep central	Quartz	10.3	
ES-2699V	"B" vein, deep central	Quartz	9.3 ± 0.2 (2)	
ES-1116	"X" Porphyry ser-chl, deep fringe	Quartz	9.7	
		Sericite(H ₂ O = 3.4%)	6.9 ± 0.1 (2)	-59
		Chlorite(H ₂ O = 9.8%)	4.5	-65
ES-7576V	"D" vein, deep central	Quartz	12.0 ± 0.1 (2)	
ES-7576H	"D" vein halo, deep central	Quartz	10.7 ± 0.1 (2)	
		Sericite(H ₂ O = 4.1%)	9.3 ± 0.0 (2)	-68
ES-1417	"D" vein halo, deep central	Quartz	9.2	
		Sericite	8.2	-78 ± 1 (2)
		Kaolinite(H ₂ O = 9.0%)	9.4	-79
ES-7486	"D" vein, shallow	Quartz	10.9	
ES-6573	Pebble breccia, surface	Pyrophyllite(H ₂ O = 5.0%)	8.7 ± 0.1 (2)	-51
ES-1855	Andesite, ser-kaol, intermediate central (supergene)	Kaolinite(H ₂ O = 5.4%)	12.4	-96
		Quartz + kaolinite	9.1	
ES-6 (SNT 1969)	Kaolinized "L" Porphyry, leached capping	Kaolinite	15.1	-99
ES-8 (SNT 1969)	Kaolinized "K" Porphyry, chalcocite blanket	Kaolinite	15.0	-87

* Purity of mineral separates was 95 percent or better except ES-1855 kaolinite which contained major sericite impurity. Biotites typically contained about 5 percent chlorite.

** H₂O contents are given in weight percent.

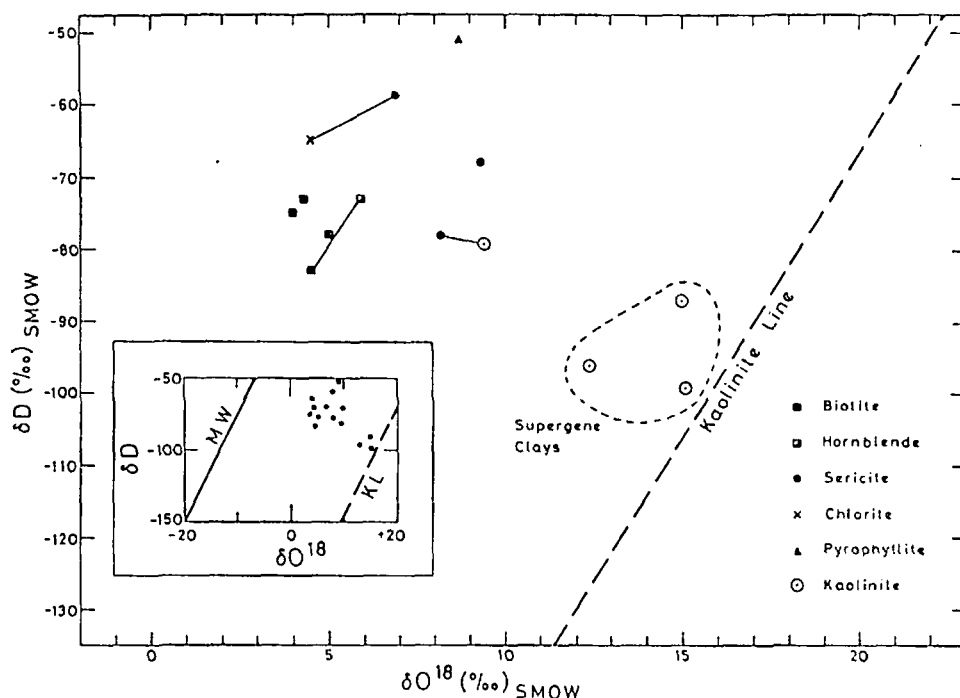


FIG. 1. Plot of δD versus $\delta^{18}O$ for all of the hydrous minerals. Tie lines connect minerals from the same sample. The meteoric water line (Craig, 1961) and the kaolinite line (Savin and Epstein, 1970) are given for reference.

lines shown are the meteoric water line, MW (Craig, 1961), and the kaolinite line, KL (Savin and Epstein, 1970). The meteoric water line defines the isotopic variations of most natural precipitations. The kaolinite line defines the isotopic variations of kaolinites from surface weathering environments.

The three supergene kaolinites, ES: 6, 8, and 1855, plot just to the left of the kaolinite line in agreement with their geologically inferred low temperature supergene origin. In contrast, hypogene kaolinite from the outer halo of the "D" vein, in sample ES-1417, is distinctly different and plots close to the sericite with which it was formed. The isotopic composition of the other sericite (ES-7576H) analyzed from the "D" vein halo, also plots close to the hypogene kaolinite.

The hornblende (ES-2689) and the four biotites from the "L" Porphyry (ES: 2689 and 2691), from the K-silicate alteration assemblages in andesite (ES-1910), and from the "X" Porphyry (ES-2699) all have very similar δD and $\delta^{18}O$ values.

The sericite and chlorite from the "X" Porphyry (ES-1116) from the inner edge of the pyritic fringe are slightly enriched in D and depleted in ^{18}O relative to the "D" vein sericites. The pyrophyllite from the advanced argillic altered pebble breccia from the surface (ES-6573) has a δD value of -51 per mil which is distinctly enriched in deuterium relative to all other minerals analyzed from El

Salvador. Its $\delta^{18}O$ is similar to "D" vein sericites. Based on theoretical arguments (Sheppard and Taylor, 1974), pyrophyllite should be isotopically similar to sericites formed under the same conditions.

The isotopic compositions of biotite from El Salvador fall within the well-defined δD - $\delta^{18}O$ range of biotites from other porphyry copper deposits at Santa Rita, Bingham, and Ely (Sheppard et al., 1971) and the tungsten-base metal deposit at Pasto Bueno, Peru (Landis and Rye, 1974). El Salvador sericites, chlorite, and hypogene kaolinite fall largely within the range of sericite and hypogene clays at Santa Rita.

$\delta^{18}O$ variations in quartz, K-feldspar, biotite, and sericite

The oxygen isotope compositions of some of the minerals from the different assemblages are plotted in Figure 2 and are compared to the range of $\delta^{18}O$ values of quartz from "unaltered" plutonic and hypabyssal granodiorites and quartz monzonites (Taylor and Epstein, 1962; Taylor, 1968) and to the major oxygen-bearing minerals from the K-silicate and quartz-sericite assemblages of eight North American porphyry copper deposits (not including Butte) (Sheppard et al., 1971).

The $\delta^{18}O$ values of the four biotites analyzed fall between 4 and 5 per mil. The oxygen isotopic compositions of the three K-feldspar samples analyzed

fall between 8.3 and 9.9 per mil. The variation in the $\delta^{18}\text{O}$ of the three sericite samples is between 6.9 and 9.3 per mil. Quartz has $\delta^{18}\text{O}$ values between 9.2 and 12.0 per mil.

The two heaviest quartz samples are late "D" vein quartz, leaving all other samples of "rock" quartz, K-silicate alteration quartz, and quartz from sericitic and kaolinitic assemblages (which show no textural evidence of having been recrystallized during this late superimposed alteration) to fall within an even narrower range of 9.2 to 10.7 per mil. These values are all typical of values found in other porphyry copper deposits and contrast with the large 14.0 per mil range observed for quartz from the various alteration assemblages at Butte (Garlick and Epstein, 1966; Sheppard and Taylor, 1974).

The "L" Porphyry magma had a $\delta^{18}\text{O}$ value of about 7 to 8 per mil as deduced from the isotopic composition of the minerals. This is at the ^{18}O depleted end of the "normal" granitic igneous range (Taylor, 1968) and is similar to many other small granitic plutons including those associated with porphyry Cu-Mo deposits in North America (Sheppard et al., 1971).

Oxygen Isotope Geothermometry

The oxygen isotope fractionation data from some coexisting minerals are given in Table 3. The relationships between mineral-mineral equilibrium isotope fractionations and temperatures are derived from calibration data based on the experiments and theories of O'Neil and Taylor (1967, 1969) and Bottinga and Javoy (1973, 1975).

Essentially concordant isotopic temperatures of about 650° and 525°C are given by the minerals analyzed from the unmineralized "L" Porphyry (ES-2689) and the K-silicate altered "X" Porphyry (ES-2699), respectively. The thermometric properties of the plagioclase-hornblende fractionation are known only very qualitatively and are interpreted

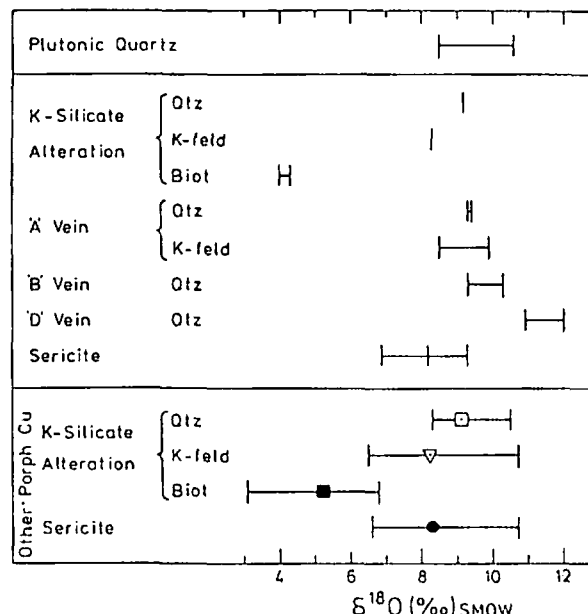


FIG. 2. Comparison of the $\delta^{18}\text{O}$ values of alteration and vein minerals from El Salvador with those from other porphyry copper deposits (Sheppard et al., 1971) and quartz from plutonic intrusions (Taylor and Epstein, 1962; Taylor, 1968). For the other porphyry copper deposit data, the mineral symbol (see Fig. 3) indicates the average isotopic composition.

here to support the close attainment of concordant fractionations in ES-2689. The quartz-feldspar fractionations are slightly disturbed from their equilibrium values at these temperatures and reflect the high sensitivity of these fractionations to differential exchange processes which, on this small scale, do not significantly affect the derivation of a temperature from the quartz-biotite or feldspar-biotite fractionations. Most plagioclase in both the "L" and "X" porphyries analyzed is about An_{30} and this probably crystallized in equilibrium with hornblende and part of the quartz; the rims are more sodic, about An_8 .

TABLE 3. Oxygen Isotope Fractionations (Δ -values) and Isotopic Temperatures for Selected Mineral Pairs

	Sample numbers					
	ES-2689	ES-2691	ES-2699	ES-1116	ES-7576	ES-1417
$\Delta_{\text{Q-Hbl}}$			4.9			
$\Delta_{\text{Q-Ser}}$				2.8 ^d	1.4 ^d	1.0 ^d
$\Delta_{\text{KF-Bi}}$			4.0			
$\Delta_{\text{Pl-Bi}}$	2.6	2.6	3.9			
$\Delta_{\text{Pl-Hbl}}$	1.2					
$T_{\text{Q-Bi}}$			540°			
$T_{\text{KF-Bi}}$			500°			
$T_{\text{Pl-Bi}}$	660°	660°	500°			
$T_{\text{Pl-Hbl}}$	~650°					

^d Size of fractionation is indicative of isotopic disequilibrium and gives an isotopic "temperature" that is geologically unreasonable high.

Abbreviations: Q = quartz, KF = K feldspar, Pl = plagioclase, Bi = biotite, Ser = sericite, Hbl = hornblende.

TABLE 4. Calculated $\delta^{18}\text{O}$ and δD Values of the Hydrothermal Fluids.

Sample no.	Temperature* (°C)	Mineral	$\delta^{18}\text{O}_{\text{H}_2\text{O}}$ **	$\delta\text{D}_{\text{H}_2\text{O}}$ **	
ES-2689	"L" Porphyry	750-625	Plagioclase	$\sim 7.7 \pm 0.4$	
			Biotite	7.3 ± 0.1	-62 ± 4
ES-2691	"L" Porphyry	750-625	Hornblende	7.5 ± 0.4	-55 ± 4
			Plagioclase	8.2 ± 0.4	
ES-2699R	"X" Porphyry	650-520	Biotite	7.8 ± 0.1	-57 ± 4
			Quartz	7.2 ± 0.8	
ES-1910R	Andesite	650-520	Biotite	6.9 ± 0.1	-45 ± 5
			Quartz	6.6 ± 0.1	-47 ± 5
ES-1910V	"A" Vein	650-520	Quartz	7.3 ± 0.8	
			K-feldspar	7.9 ± 0.7	
ES-4304	"A" Vein	650-520	Quartz	7.4 ± 0.8	
			K-feldspar	9.2 ± 0.7	
ES-7536	"B" Vein	450-350	Quartz	4.8 ± 1.4	
ES-2699V	"B" Vein	450-350	Quartz	3.8 ± 1.4	
ES-1116	"X" Porphyry	400-300	Quartz	4.2 ± 1.4	
			Sericite	5.0 ± 0.8	-32 ± 5
ES-7576V	"D" Vein	350-200	Chlorite	5.2 ± 0.8	-25 ± 5
			Quartz	1.2 ± 3.8	
ES-7576H	"D" Vein Halo	350-200	Quartz	-0.1 ± 3.8	
			Sericite	5.6 ± 1.9	-33 ± 5
ES-1417	"D" Vein Halo	350-200	Sericite	4.5 ± 1.9	-43 ± 5
			Kaolinite	6.1 ± 1.5	-44 ± 5
ES-7486	"D" Vein	350-200	Quartz	0.1 ± 3.8	
ES-6573	Pebble breccia	250-150	Propylite	2.9 ± 2.0	-15 ± 5

* From fluid inclusion and isotopic geothermometry (see text).

** The mean δ -value is given; the range is derived from the temperature limits.

and are in equilibrium with K-feldspar biotite and the rest of the quartz.

Temperatures of about 650°C for the two "L" Porphyry samples (ES: 2689 and 2691) apparently represent isotopic equilibrium at subsolidus temperatures, but they are reasonable minimum temperatures. Similarly, the three concordant temperatures in the K-silicate altered "X" Porphyry indicate attainment of isotopic equilibrium and give an independent minimum temperature of about 525°C for the development of this assemblage at El Salvador. This evidence firmly supports other indications of high temperatures for Early events presented by Gustafson and Hunt (1975).

The quartz-sericite fractionations for ES: 1116, 7576, and 1417 give geologically unrealistically high "isotopic temperatures." This is apparently because most of the quartz is inherited from Early assemblages, as indicated by microscopic textures, and evidently did not recrystallize and equilibrate with the sericite (Sheppard et al., 1971, p. 525). Also for sample ES-7576 the quartz in the vein is not in isotopic equilibrium with the sericite in the adjacent halo presumably because of some retrograde exchange in the sericite.

Even though the indicated lack of isotopic equilibrium between quartz-feldspar and quartz-sericite of the "X" Porphyry (ES: 2699 and 1116), "A" vein (ES: 4304 and 1910V), and "D" vein halo samples (ES: 7576 and 1417) precludes isotopic geothermometry, departures from equilibrium are

not necessarily large (less than 1 to 2 per mil). There is no evidence of major retrograde exchange in any of the minerals analyzed. The high deuterium content of the supergene kaolinites argues against major exchange with present-day meteoric waters. At a surface elevation higher than 2,700 m, present-day meteoric water is largely derived from snow and is probably strongly depleted in deuterium compared to the meteoric water at the time of the ore formation.

Calculation of Isotopic Compositions of Hydrothermal Solutions

Experimentally determined mineral-water fractionation factors can be used to calculate, from measured isotopic compositions of the minerals, the composition of the hydrothermal fluids in which they were formed if: (1) the minerals formed in isotopic equilibrium with the fluid; (2) there has not been significant isotopic exchange after mineral formation; (3) known fractionation factors are indeed appropriate to the composition of the analyzed minerals and of the hydrothermal fluids; and (4) the temperature of formation is known.

The minor isotopic exchange which may have occurred in some of the El Salvador samples is much too slight to affect their usefulness for calculations of this sort. Errors of even a per mil or two are not critical.

The mineral-H₂O fractionation factors used in this study are the same as those reviewed by Taylor

(1974). In addition, we assume that isotopic fractionation between pyrophyllite and sericite at the same temperature is negligible. Hydrogen isotope fractionation factors are strongly dependent on the Mg/Fe ratios of biotites (Suzuki and Epstein, 1976). A single analysis of primary "L" Porphyry biotite indicates a Mg/Fe ratio of 0.87/1.0 (atomic fraction) and analyses of K-silicate alteration biotite for ES: 2699 and 1910 indicate ratios of 0.83/1.0 and 0.75/1.0 respectively. Plagioclase-H₂O oxygen isotope fractionations are also compositionally dependent; most plagioclase in both the "L" and "X" Porphyry samples analyzed is about An₃₀. The calculated isotopic compositions of water listed in Table 4 take these compositional data into account. The $\delta^{18}\text{O}$ values of the hydrothermal fluids are not adjusted for the possible second order salinity effects (Truesdell, 1974). Although the calculations may require some adjustment when more complete experimentally determined isotopic fractionation data become available, the uncertainties associated with the calculated values relative to each other will probably not change very much. Thus the conclusions drawn here are unlikely to be affected.

No precise and consistent measurement of the temperatures of the analyzed assemblages is available (Gustafson and Hunt, 1975). The "L" Porphyry, the only major intrusive rock that is found unaltered, crystallized at roughly 750°C, the solidus temperature of a water-saturated melt at 2 to 3 km depth. Its oxygen isotope temperature is approximately 650°C. Early K-silicate alteration and "A" quartz veining were accomplished at temperatures approaching those of the associated porphyry magmas (oxygen isotope temperature, about 525°C). The assemblage andalusite-K-feldspar indicates temperatures greater than 550°C probably at the beginning of the Transitional mineralization. Filling temperatures of a few fluid inclusions in Early "A" and Transitional "B" quartz veins suggest temperatures of 350° to greater than 650°C. Sulfur isotope temperatures for sulfate-sulfide mineral pairs in "A" and "B" veins indicate a 400° to 600°C temperature range (Field and Gustafson, 1976). Late "D" veins and pyritic sericite-chlorite assemblages formed on a cooling trend following Transitional "B" vein time. A few filling temperatures of from 175° to 300°C have been obtained on fluid inclusions in "D" vein quartz. The temperature estimates listed in Table 4 are based on the above evidence and a large measure of geologic intuition. A range of $\delta^{18}\text{O}_{\text{H}_2\text{O}}$ is calculated for the given range of estimated temperatures. The tie lines shown in Figures 3 and 4 connecting isotopic compositions calculated for the estimated range of temperatures illustrate the effect of uncertainties about the temperatures. The composition

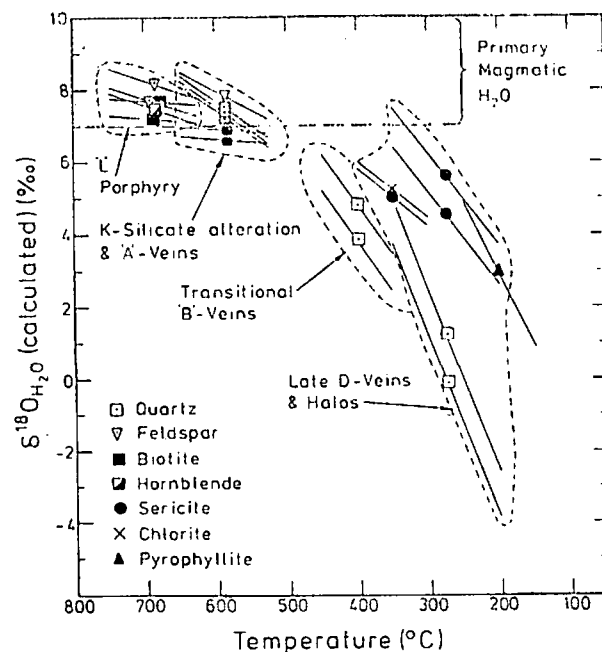


FIG. 3. Plot of calculated $\delta^{18}\text{O}$ of the hydrothermal waters versus the estimated temperature of formation of the minerals. The tie lines connect the isotopic composition of the waters for the estimated range of temperatures with the mineral symbol indicating the median temperature (see text for discussion). The primary magmatic water field is also shown.

calculated for the median temperature is indicated by the position of the symbol for the appropriate mineral. As with the uncertainty in fractionation factors, the inaccuracies in relative isotopic compositions of hydrothermal fluids introduced by the temperature uncertainty are probably significantly smaller than the inaccuracies in actual composition.

Implications of Calculated Isotopic Compositions of Hydrothermal Solutions

An interpretation of the calculated isotopic compositions of the hydrothermal fluids in terms of geologic processes and origins involves knowledge about the isotopic composition of the potential source fluids and the processes which may have modified the isotopic compositions of the fluids during their hydrothermal history. Taylor (1974) has reviewed the variety of processes which are associated with hydrogen and oxygen isotope fractionations.

Supergene solutions

The isotopic compositions of the supergene solutions are considered first because they place certain constraints on the isotopic compositions of the meteoric waters that may have been present during the development of the main hypogene mineralization. K-Ar dating of supergene alunite indicates

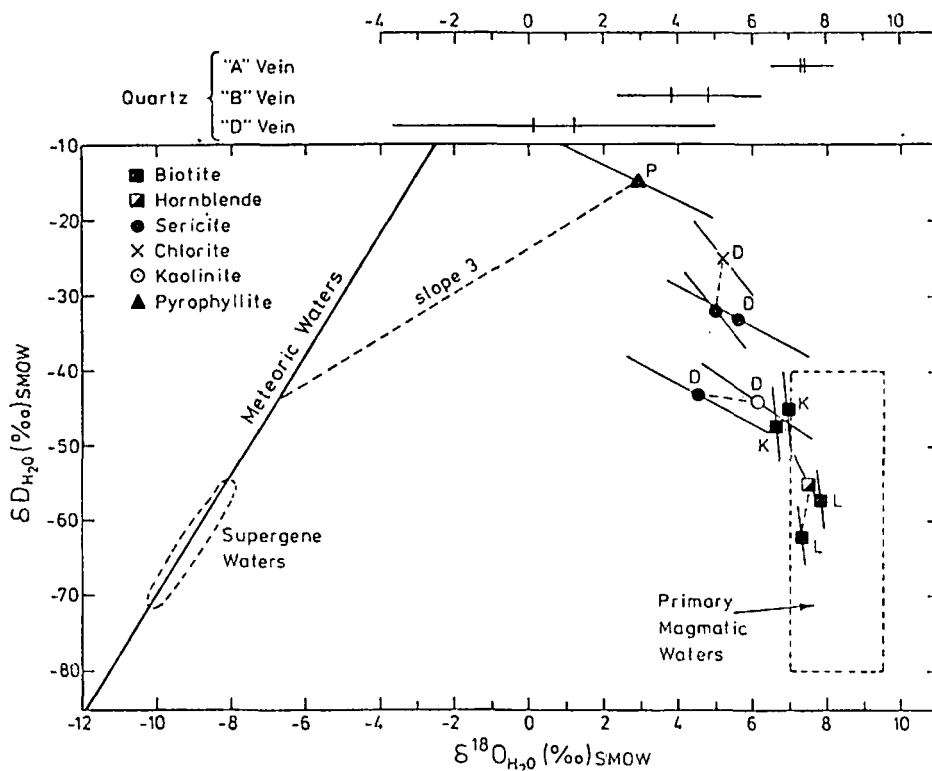


FIG. 4. δD versus $\delta^{18}O$ diagram for the calculated isotopic composition of H_2O that would be in equilibrium with the alteration minerals over the range of temperatures given in Table 4. Also given are the oxygen isotope compositions of H_2O in equilibrium with the vein quartz. Dashed lines connect minerals from the same sample. A line of slope 3, drawn between the pyrophyllite sample point P and the meteoric water line, represents the proposed trend of acid geothermal waters (see text). Fields for primary magmatic water and supergene waters derived from the supergene kaolinite data are also given. Abbreviations are: L = "L" Porphyry; K = K-silicate alteration; D = "D" vein alteration assemblages; P = pyrophyllite from the advanced argillic alteration.

that supergene alteration at El Salvador followed hypogene mineralization by less than a few million years during the early Oligocene.

Of our three supergene kaolinites, ES-6 from the leached capping at the surface plots closest to the kaolinite line of Savin and Epstein (1970) (Fig. 1). This clay was apparently formed at temperatures similar to earth surface ones. The calculated composition of the 25°C meteoric water is on the order of $\delta D = -70$ per mil and $\delta^{18}O = -10$ per mil. The isotopic composition of the other two kaolinites from within the chalcocite enrichment zone could also have resulted from similar meteoric waters but at slightly higher temperatures. This is consistent with the greater depth of their occurrence. The three supergene kaolinites together indicate that meteoric waters probably had δD values on the order of -55 to -70 per mil and $\delta^{18}O \approx$ values on the order of -8 to -10 per mil during supergene alteration. This range gives us an estimate of the isotopic composition of the meteoric waters during the earlier hypogene mineralization providing that there was no significant

change in altitude between these events. These values are appreciably heavier than those for meteoric water normally derived from snow fall at an elevation greater than the present 2,700 m surface elevation of El Salvador. The data support the interpretation that the major uplift of the Andes has occurred since the Pliocene (Salas et al., 1966).

Hypogene fluids

Trends in the calculated isotopic composition of hypogene hydrothermal fluids are evident in Figures 3 and 4. Although no unaltered "X" or "K" Porphyry is exposed for analysis, the petrologically similar "L" Porphyry, closely associated with them in space and time and with a local development within it of Early alteration-mineralization features identical to those developed in the more strongly mineralized porphyries, can probably be taken as representative of the premineralized porphyries. If we make this assumption, we find that the isotopic composition of the hypogene hydrothermal fluids shows a well-defined and consistent decrease in $\delta^{18}O$ and increase in

δD : from unmineralized porphyry to K-silicate alteration biotite to "B" vein quartz to sericite and kaolinite associated with Late "D" veins to pyrophyllite in advanced argillic alteration. The trend is clear despite the effect of the temperature uncertainties. This sequence corresponds to decreasing temperatures and, with the exception of samples from K-silicate alteration and "A" veins which are mostly older than "L" Porphyry, to decreasing age.

In Figure 4 waters in equilibrium with the unmineralized "L" Porphyry plot in the field for primary magmatic water (Sheppard et al., 1969; 1971). Waters associated with the two Early K-silicate alteration samples plot on the boundary of this primary magmatic water field. However, these waters appear to be distinctly enriched in deuterium relative to the "L" Porphyry waters. Because the "L" Porphyry is younger than much of the Early alteration-mineralization assemblage, we cannot say whether the Early hydrothermal fluids underwent a deuterium enrichment process or whether the "L" Porphyry underwent deuterium depletion.

The Early hydrothermal solutions could be primary magmatic waters which were modified to a minor extent relative to "L" Porphyry waters through (1) subsolidus exchange with hot igneous rocks, (2) mixing with a relatively small quantity of nonmagmatic water, (3) leakage of hydrogen relative to H_2O , or (4) some other process involving the gain of deuterium relative to hydrogen. Gustafson and Hunt (1975) have proposed that hydrogen leaked from the mineralizing system and caused the apparent massive oxidation of sulfur, because significant mechanical influx of oxidized meteoric water was precluded by the near-magmatic pressures and temperatures attending intrusion of the porphyry. (Most of the 10^9 tons of sulfur emplaced during early stages was fixed as sulfate rather than sulfide.) The shift in δD from roughly -60 per mil in fluids in equilibrium with biotite that crystallized from the "L" Porphyry melt to about -45 per mil in fluids that produced biotite in K-silicate alteration assemblages might be due to this process. Alternatively, these Early hydrothermal fluids could be recording their essentially unmodified D/H ratios for magmatic water, defined as H_2O -rich solutions that have thoroughly exchanged chemically and isotopically at magmatic temperatures with relatively large magma systems (Sheppard et al., 1969). Many magmas become saturated with H_2O during their crystallization history and lose a substantial part of their original hydrogen content. Under the normal oxygen fugacity conditions associated with most igneous systems, H_2O is overwhelmingly the dominant species carrying hydrogen in the fluid phase (Eugster and Skippen, 1967). Because H_2O concentrates deuterium

relative to biotite and/or hornblende at solidus temperatures (Suzuoki and Epstein, 1976), the fluid crystallized igneous rock may be depleted in deuterium relative both to magmatic water and the original D/H ratio of the magma prior to saturation. Thus our "L" Porphyry sample may be depleted in deuterium relative to earlier crystallized porphyry melts at El Salvador.

We cannot at present determine whether either hydrogen leakage or H_2O loss was the effective process at El Salvador. Either interpretation supports the geologic arguments presented by Gustafson and Hunt (1975) that hydrothermal solutions responsible for Early K-silicate alteration were derived from the porphyry melts and their underlying magma chamber. Because the range in the calculated δD value of meteoric waters at the time of mineralization falls within the accepted range for magmatic water, the possibility of mixing with relatively small quantities of nonmagmatic water cannot be evaluated.

"A" vein quartz is isotopically indistinguishable from the Early K-silicate assemblages with which it is associated (Fig. 4). "B" quartz veins appear to be transitional isotopically as well as temporally and chemically. Though no hydrogen was fixed in the "B" vein minerals, the $\delta^{18}O$ values of fluids in equilibrium with "B" vein quartz appear to be shifted toward the distinctly lighter values relative to Early assemblages. Thus, the trend to lighter $\delta^{18}O$ in later assemblages is observed whether or not hydrous phases are present.

Fluids in equilibrium with "D" vein minerals and their halo are further enriched in deuterium and depleted in ^{18}O . The most important evidence for the extent of this ^{18}O depletion in the fluids is derived from the "D" vein quartz samples (Fig. 3). Quartz is much more resistant to retrograde isotopic exchange than sericite. We have shown above that the sericites are too enriched in ^{18}O to be in equilibrium with vein quartz and therefore the calculated $\delta^{18}O$ values of the fluids, using the sericite data, are too high at these temperatures. At the lower temperatures inferred for this Late mineralization, the isotopic uncertainty related to the temperature uncertainty is greater than that of earlier assemblages. However, the isotopic ratios of chlorite and hypogene-kaolinite also formed during the Late mineralization time are compatible with the compositions of fluids calculated from the sericite data. All the oxygen isotope compositions of these "B" and "D" vein fluids are distinctly depleted in ^{18}O relative to unmodified magmatic waters.

The trend to ^{18}O depleted water in pyrite-sericite-forming environments is typical of other porphyry copper deposits (Sheppard et al., 1971). Sheppard et al. (1971) interpret this trend to show that there

These
teoric
eleva-
eleva-
rpre-
s oc-

on of
gures
Por-
simi-
m in
ithin
ntical
alized
ative
this
on of
ll-de-
se in

was a significant component of meteoric water in the hydrothermal fluids involved during sericitization. This is in complete accord with the interpretation of Gustafson and Hunt (1975), based on several lines of geologic evidence, that the influx of meteoric water was responsible for the evolution of Early to Late mineralization-alteration environments at El Salvador.

The trend to deuterium enrichment in Late hydrothermal solutions is similar to the trend at Santa Rita, but unlike any at Bingham, Ely, and Climax where sericitization was accomplished by solutions relatively depleted in deuterium (Sheppard et al., 1971, fig. 10; Hall et al., 1974). All of these situations can and have been interpreted as indicating meteoric water, with the deuterium enrichment or depletion trend largely reflection differences in the isotopic composition of the meteoric waters from one deposit to another.

The isotopic composition of magmatic water which continues to emanate from an underlying magma chamber and re-equilibrates with a relatively large mass of unaltered igneous rocks at temperatures declining continuously from about 700° to 300°C would evolve along a path similar to that shown in Figure 4. Although such magmatic-hydrothermal waters could be responsible for the evolving alteration-mineralization features seen in the deposit, two lines of reasoning argue against such a cause (Gustafson and Hunt, 1975). (1) The geologic evidence for inward and downward collapsing zonal patterns and for the saturation of the fractured rocks with fluid at hydrostatic pressure in the Late stages of mineralization strongly suggests flooding of the area with ground water. (2) The similarity of the mineralogic and isotopic patterns with those from other deposits where such deuterium enrichment is not seen suggests that deuterium enrichment is not an essential feature of a common process in all deposits; an influx of meteoric water fits the evidence but cooling magmatic water does not. In addition one possible interpretation of the sulfur isotope data suggests a source of sulfur for Late fluids which was different from that associated with the Early magmatic-hydrothermal fluids (Field and Gustafson, 1976), but this is a much more tentative argument.

The pebble dike with pyrophyllite was interpreted by Gustafson and Hunt (1975) as forming in an overlying acid hot spring system. The deuterium enrichment of such fluids, relative to those associated with the deeper main stages of hydrothermal activity (Fig. 4) supports this conclusion. Acid-type hot spring waters which undergo evaporation at temperatures on the order of 70° to 90°C experience a kinetic isotope effect (Craig, 1963). Such waters become systematically enriched in deuterium relative

to the local unheated meteoric water and plot along a line with a slope of about 3. Using this slope to project back from the composition of water in equilibrium with pyrophyllite gives for the composition of unheated meteoric waters at El Salvador: δD values equal to -30 to -60 per mil and $\delta^{18}O$ values equal to -5 to -9 per mil.

This range of δD values for advanced argillic assemblages is similar to that calculated for the fluids responsible for the earlier sericitization events but higher than the values calculated for the later supergene waters. If meteoric waters involved in "D" vein formation were enriched in deuterium relative to later supergene waters, certain processes must have operated which at least partially modified some of the δD values. A mixing of meteoric waters, with unmodified D/H ratios, with those associated with the transitional advanced argillic alteration which had been modified by evaporation processes is possible. Modification through hydrogen leakage, although possible, is unlikely to have been an effective mechanism at this late stage because (1) the oxygen isotope data for the vein quartz indicate that the fluids were dominantly of meteoric origin and (2) the amount of H_2 present in such a fluid was probably negligible under the prevailing oxygen fugacity conditions. In light of the evidence of some limited oxygen isotope retrogradation in the sericites, we should also suspect that their δD values have been modified, too. Assuming that the D/H ratio of the system was largely controlled by the meteoric-hydrothermal fluids (very reasonable from the $^{18}O/^{16}O$ values of the fluid), then the actual δD values of the hydrothermal fluids were probably slightly more deuterium rich than our calculated values, although sericite-water hydrogen isotope fractionation factors are not very temperature sensitive under our temperature conditions. Even though we cannot isolate the dominant modifying process from our data, our main conclusion that meteoric waters were dominant in these late-stage fluids is not affected.

The meteoric waters involved in the Late hydrothermal systems could have been slightly more deuterium rich than those involved with supergene alteration that followed within a few million years. However, the difference in their δD value implies that uplift of the Andes at this latitude had begun by late Eocene.

Acknowledgments

We gratefully acknowledge stimulating discussions with H. P. Taylor, Jr., N. F. Davis, J. J. Hemley, C. Meyer, and J. P. Hunt. We thank N. F. Davis, W. E. Hall, and H. P. Taylor, Jr. for providing helpful reviews of the manuscript; the Anaconda Company for financing the study and permitting its

publication; and S. Epstein and H. P. Taylor, Jr., at the California Institute of Technology for the use of their stable isotope facilities.

S. M. F. S.

SCOTTISH UNIVERSITIES RESEARCH AND REACTOR
CENTRE

EAST KILBRIDE, GLASGOW, SCOTLAND

L. B. G.

AUSTRALIAN NATIONAL UNIVERSITY

CANBERRA, A. C. T., AUSTRALIA

July 24, 1975; May 27, 1976

REFERENCES

- Bottinga, Y., 1969, Calculated fractionation factors for carbon and hydrogen isotope exchange in the system calcite-carbon dioxide-graphite-methane-hydrogen-water: *Geochim. et Cosmochim. Acta*, v. 33, p. 49-64.
- and Javoy, M., 1975, Comments on oxygen isotope geothermometry: *Earth Planet. Sci. Letters*, v. 20, p. 250-265.
- 1975, Oxygen isotope partitioning among the minerals in igneous and metamorphic rocks: *Rev. Geophys. Space Phys.*, v. 13, p. 401-418.
- Craig, H., 1961, Isotopic variations in meteoric waters: *Science*, v. 133, p. 1702-1703.
- 1963, The isotopic geochemistry of water and carbon in geothermal areas: *Conf. on Nuclear Geology in Geothermal Areas*, Spoleto, Italy, p. 17-53.
- Eugster, H. P. and Skippen, G. B., 1967, Igneous and metamorphic reactions involving gas equilibria, in Abelson, P. H., ed., *Researches in geochemistry*, v. 2: New York, John Wiley and Sons, p. 492-520.
- Field, C. W., and Gustafson, L. B., 1976, Sulfur isotopes in the porphyry copper deposit at El Salvador, Chile: *ECON. GEOL.*, v. 71, p. 1533-1548.
- Garlick, G. D., and Epstein, S., 1966, The isotopic composition of oxygen and carbon in hydrothermal minerals at Butte, Montana: *ECON. GEOL.*, v. 61, p. 1325-1335.
- Gustafson, L. B., and Hunt, J. P., 1975, The porphyry copper deposit at El Salvador, Chile: *ECON. GEOL.*, v. 70, p. 857-912.
- Hall, W. E., Friedman, I., and Nash, J. T., 1974, Fluid inclusion and light stable isotope study of the Climax molybdenum deposits, Colorado: *ECON. GEOL.*, v. 69, p. 884-901.
- Landis, G. P., and Rye, R. O., 1974, Geologic, fluid inclusion, and stable isotope studies of the Pasto Bueno tungsten-base metal ore deposit, Northern Peru: *ECON. GEOL.*, v. 69, p. 1025-1059.
- O'Neil, J. R., and Taylor, H. P., Jr., 1967, The oxygen isotope and cation exchange chemistry of feldspars: *Am. Mineralogist*, v. 52, p. 1414-1437.
- 1969, Oxygen isotope fractionation between muscovite and water: *Jour. Geophys. Research*, v. 74, p. 6012-6022.
- Salas, R., Kast, R., Montecinos, F., and Salas, I., 1966, Geología y recursos minerales del Departamento de Arica—Provincia de Tarapaca: Instituto de Investigaciones Geológicas (Chile), Bol. 21.
- Savin, S. M., and Epstein, S., 1970, The oxygen and hydrogen isotope geochemistry of clay minerals: *Geochim. et Cosmochim. Acta*, v. 34, p. 25-42.
- Sheppard, S. M. F., and Taylor, H. P., Jr., 1974, Hydrogen and oxygen isotope evidence for the origins of water in the Boulder batholith and the Butte ore deposits, Montana: *ECON. GEOL.*, v. 69, p. 926-946.
- Sheppard, S. M. F., Nielsen, R. L., and Taylor, H. P., Jr., 1969, Oxygen and hydrogen isotope ratios of clay minerals from porphyry copper deposits: *ECON. GEOL.*, v. 64, p. 755-777.
- 1971, Hydrogen and oxygen isotope ratios in minerals from porphyry copper deposits: *ECON. GEOL.*, v. 66, p. 515-542.
- Suzuoki, T., and Epstein, S., 1976, Hydrogen isotope fractionation between OH-bearing silicate minerals and water: *Geochim. et Cosmochim. Acta*, v. 40, p. 1229-1240.
- Taylor, H. P., Jr., 1968, The oxygen isotope geochemistry of igneous rocks: *Contr. Mineralogy Petrology*, v. 19, p. 1-71.
- 1974, The application of oxygen and hydrogen isotope studies to problems of hydrothermal alteration and ore deposition: *ECON. GEOL.*, v. 69, p. 843-883.
- and Epstein, S., 1962, Relationship between O^{18}/O^{16} ratios in coexisting minerals of igneous and metamorphic rocks; Part 1: Principles and experimental results: *Geol. Soc. Amer. Bull.*, v. 73, p. 461-480.
- Truesdell, A. M., 1974, Oxygen isotope activities and concentrations in aqueous salt solutions at elevated temperatures: Consequences for isotope geochemistry: *Earth Planet. Sci. Letters*, v. 23, p. 387-396.

ECONOMIC GEOLOGY

AND THE

BULLETIN OF THE SOCIETY OF ECONOMIC GEOLOGISTS

VOL. 70

AUGUST, 1975

No. 5

The Porphyry Copper Deposit at El Salvador, Chile

LEWIS B. GUSTAFSON AND JOHN P. HUNT

Abstract

The formation of the porphyry copper deposit at El Salvador culminated volcanic activity in the Indio Muerto district. Host rocks for the ore are Cretaceous andesitic flows and sedimentary rocks overlain unconformably by lower Tertiary volcanics. Early rhyolite domes, formed about 50 m.y. ago and roughly contemporaneous with voluminous rhyolitic and andesitic volcanics, were followed by irregularly shaped subvolcanic intrusions of quartz rhyolite and quartz porphyry about 46 m.y. ago. Minor copper-molybdenum mineralization accompanied this event. A steep-walled granodioritic porphyry complex and the closely associated main center of mineralization and alteration were emplaced 41 m.y. ago.

The oldest of these porphyries, "X" Porphyry, is fine grained, equigranular to weakly porphyritic. Porphyritic textures are seen in deep exposures, whereas strong K-silicate alteration at higher elevations has developed the equigranular texture. Next, a complex series of feldspar porphyries was intruded. These include an early group, "K" Porphyry, and a late group, "L" Porphyry, defined by mapped age relations at intrusive contacts. Strong alteration and mineralization of most "K" Porphyry bodies have partially obliterated the porphyry texture. The larger "L" Porphyry complex is relatively unaltered and unmineralized. A wide range of textural variation in "L" Porphyry is spatially related to its contacts and evidences reaction with intruded andesite. Relatively minor porphyry dikes and igneous breccia cut the composite porphyry stock and are followed by postmineral latite dikes and clastic pebble dikes. Below the present surface, pebble dikes exhibit a striking decrease in abundance and a change from a radial-concentric to a nearly orthogonal pattern.

Petrologic trends are obscured because most intrusive rock types are not exposed away from the area affected by alteration and mineralization and because chemical and mineralogical variation within a single fresh major intrusive unit, "L" Porphyry, is apparently greater than it is across the entire porphyry series. However, rhyolitic volcanism in the district was clearly more felsic than younger granodioritic porphyries and produced higher K_2O/Na_2O ratios. Compared to average granodiorite, the El Salvador porphyries are low in total iron and have a smaller K_2O/Na_2O ratio. Compositional trends in "L" Porphyry correlate with textural variations. The initial $^{87}Sr/^{86}Sr$ ratio of early siliceous extrusive rocks and domes, as well as of the main porphyry series and all alteration products, is a consistent 0.704.

Early alteration-mineralization was mostly accomplished before the intrusion of the last major feldspar porphyry ("L" Porphyry) and contributed probably three-quarters of the 5 million tons of copper in the orebody. Early mineralization is characterized by distinctive quartz veins and largely disseminated K-silicate assemblages of alkali feldspar-biotite-anhydrite-chalcocyanite-bornite or chalcocyanite-pyrite. Early quartz veins are typically granular quartz-K-feldspar-anhydrite-sulfide, generally lack internal symmetry, and are irregular and discontinuous. K-silicate alteration of some porphyries appears to have occurred during final consolidation of the melts as well as later. Biotization of andesitic volcanics and an apparently contemporaneous outer fringe of propylitic alteration were produced during this Early period. Except at deepest exposed elevations in the younger porphyries, incipient K-silicate alteration converted hornblende phenocrysts to biotite-anhydrite-rutile, ilmenite to hematite-rutile, and sphene to rutile-

UNIVERSITY OF UTAH
RESEARCH INSTITUTE
EARTH SCIENCE LAB.

anhydrite. Anhydrite deposition occurred through the entire history of primary mineralization, and probably more sulfur was fixed as sulfate in anhydrite than in sulfides.

Outward within a central zone of K-silicate alteration with chalcopyrite-bornite, the proportion of bornite decreases until pyrite appears and increases as chalcopyrite diminishes. Pyrite abundance increases, then decreases in an outer propylitic zone with epidote-chlorite-calcite. In the outermost propylitic zone, minor chalcopyrite-magnetite veins give way outward to specular hematite. Pyrite is very closely associated with sericite or sericite-chlorite, and pyrite-sericite-chlorite veining is clearly younger than both K-silicate and propylitic assemblages. The major fringe zone of pyrite-sericite appears to be a relatively late feature superimposed across the transitional boundary of the Early-formed zones. Patterns of alteration-mineralization are strongly influenced by the intrusion of "L" Porphyry, which removed part of the previously formed Early pattern and largely controlled subsequent Late events.

A Transitional type of quartz vein was formed after consolidation of all major intrusions and prior to the development of Late pyritic and K-feldspar-destructive alteration assemblages. Transitional quartz veins occupy continuous planar fractures, which tend to be flat. They are characterized by a lack of K-feldspar and associated alteration halos and by the presence of molybdenite. The assemblage K-feldspar-andalusite on deep levels is probably a Transitional alteration assemblage. Tourmaline in veinlets and breccias is closely associated in time with Transitional quartz veins. The abundance of tourmaline increases upward toward the present surface.

Late mineralization, characterized by abundant pyrite and K-feldspar-destructive alteration, tends to be more fracture controlled than Early and more disseminated mineralization. Late sulfide veins and veinlets cut all rock types, except latite, and all Early and Transitional age veins. They contain pyrite and lesser but upward-increasing amounts of bornite, chalcopyrite, enargite, tennantite, sphalerite, or galena. Quartz and anhydrite are the most common gangue minerals. Alteration halos surrounding these pyrite veinlets are principally sericite or sericite-chlorite. These veins occupy a radial-concentric fracture set at all levels of exposure.

Vertical zoning of Late alteration and sulfide assemblages is well developed. Peripheral sericite-chlorite gives way upward to sericite, which encroaches inward on central zones. Upper level assemblages are dominated by sericite and andalusite and are superimposed on Early K-silicate assemblages. Sericite-andalusite assemblages are gradational with underlying andalusite-K-feldspar zones. Deep-level Early sulfide zones, with antithetic pyrite and bornite, are abruptly truncated by later disseminated sulfide zones containing contact assemblages of pyrite and bornite and variable amounts of chalcopyrite and "chalcocite." Evidence for sulfide zoning higher within the leached capping is based on study of relict sulfide grains. Pyrite-bornite sulfide zones are generally found with sericite or advanced argillic alteration assemblages, but the "roots" of these zones extend downward into K-feldspar-bearing lower level alteration zones. Advanced argillic alteration assemblages containing abundant pyrophyllite, diaspore, alunite, amorphous material, and local corundum are strongly developed at high elevations. These assemblages, present in postore pebble dikes, were formed very late in the evolution of mineralization. Where preserved, the associated sulfide is pyrite.

Two types of fluid inclusions are found in Early and Transitional quartz veins but never in Late pyritic veins. They contain high-salinity fluid coexisting with low-density fluid. Both exhibit homogenization temperatures in the range of 360° to >600°C. A third type of inclusion is found in veins of all ages, contains low-salinity fluid, and homogenizes at less than 350°C.

Supergene enrichment formed the commercial orebody, roughly 300 million tons of 1.6% Cu. Secondary Cu-S minerals extensively replaced chalcopyrite and bornite but coated pyrite with little or no replacement. Kaolinite and alunite are the principal supergene alteration products. Kaolinite replaces feldspar, biotite, and chlorite but not sericite. The zones of supergene kaolinite are developed beneath the upper level zones of strong sericitic alteration and within the upper preserved portions of the underlying K-silicate and sericite-chlorite zones. Magnetite is oxidized to hematite by supergene alteration. Anhydrite is hydrated to gypsum and then dissolved by supergene water to depths as great as 900 m beneath the present surface.

Sulfides originally present in the leached capping have been oxidized to limonite, composed mostly of jarosite, goethite, and hematite. A dominantly jarositic capping overlies most of the orebody and the inner pyritic fringe. This is surrounded by a

As su
a critic
orebod
Indio
as a p
to abo
Potrer
superi
March
favora
Area"
Salva
diggir
quoise

goethitic capping. A thin hematite-goethite capping between the jarosite and the enrichment blanket was apparently formed during a second stage of oxidation and leaching. Copper was mostly removed from the sericitic capping, but iron, molybdenum, and gold were relatively immobile during supergene leaching.

Interpretation of the space-time patterns and relations of the mineralization, alteration, volcanism, and intrusion allows reconstruction of the depositional environments of the El Salvador porphyry copper deposit. The bulk of the primary mineralization and alteration accompanying emplacement of the porphyries was accomplished in less than one million years, at the end of an extended period of volcanism. The granodioritic stocks intruded their cogenetic volcanic pile, which extended probably less than 2,000 meters above the present surface. Early mineralization-alteration formed simultaneous with, adjacent to, and within recurrent intrusions of porphyry. The pressure-temperature environment was close to that of the final crystallization of the melt. The saline aqueous fluids responsible for the bulk transport of metals and sulfur at this time were boiling, limited in quantity, and of largely magmatic origin. They were generally depleted at present levels of exposure prior to the emplacement of the last porphyry mass. The relatively oxidized state of sulfur during this Early period probably reflects leakage of hydrogen from the mineralizing system.

As cooling of the intrusive complex progressed, the structural and chemical character of the mineralizing environment shifted, largely in response to the inflow of meteoric water. This water was part of a deep convective system driven by heat from the cooling intrusive center. With continued cooling, upper and peripheral zones of Late alteration and mineralization progressively collapsed inward and downward over zones of Early mineralization, penetrating deepest along continuous vein structures. There was extensive reworking of previously deposited sulfides and wall-rock alteration, especially at high elevations. In the last stages, an acid hot-spring system was established in the upper portions of the deposit. Final and relatively minor intrusion of latite dikes into this hot-spring system caused pebble brecciation along Late vein structures. Erosion and supergene leaching and enrichment followed within 5 m.y. and may have overlapped the final stages of hot-spring activity.

A genetic model is proposed for the emplacement and deposition of porphyry copper deposits in general. Essential elements of this genetic model are (1) shallow emplacement of a usually complex series of porphyritic dikes or stocks in and above the cupola zone of a calc-alkaline batholith; (2) separation of magmatic fluids and simultaneous metasomatic introduction of copper, other metals, sulfur, and alkalis into both the porphyries and wall rocks; and (3) the establishment and inward collapse of a convective ground-water system, which reacts with the cooling mineralized rocks.

The well-known similarities of porphyry copper deposits from many parts of the world are variations on a common theme. The differences and unique features exhibited by individual deposits reflect the imprint of local variables upon the basic model. The local variables include depth of emplacement, availability of ground water, volume and timing of successive magma advances, and the concentration of metals, sulfur, and other volatiles in the magmas, as well as depth of exposure.

Introduction

As summarized by Perry (1960) geology played a critical role in the discovery of the El Salvador orebody beneath the iron-stained slopes of Cerro Indio Muerto. Interest in Indio Muerto Mountain as a possible important copper prospect went back to about 1922 and the early years of the nearby Potrerillos mine and metallurgical plant. Then mine superintendent Greninger, and mine geologists March, Reed, Watson, and Wendell all commented favorably on certain aspects of the so-called "Camp Area", about two miles north of the present El Salvador orebody. Even the ancient turquoise diggings of the Incas, in what is now known as Turquoise Gulch, excited interest and speculation. In

1944, Reno Sales and Vincent Perry, accompanied by March and Wendell, visited the Camp Area. During this visit Perry was impressed by porphyry float containing glassy quartz veinlets in the gravel-filled arroyo leading from Turquoise Gulch, and which reminded him of quartz veining he had previously mapped over the fabulous La Colorada orebody at Cananea, Mexico. The following year he assigned Roland Mulchay and E. C. Stephens to map and appraise the surface of Indio Muerto. They reported favorably on the Camp Area as a copper prospect but stressed its limited tonnage possibilities. In 1950 Perry again visited the district, this time accompanied by William Swayne as well as then Potrerillos geologists Swensen and Brinley, and

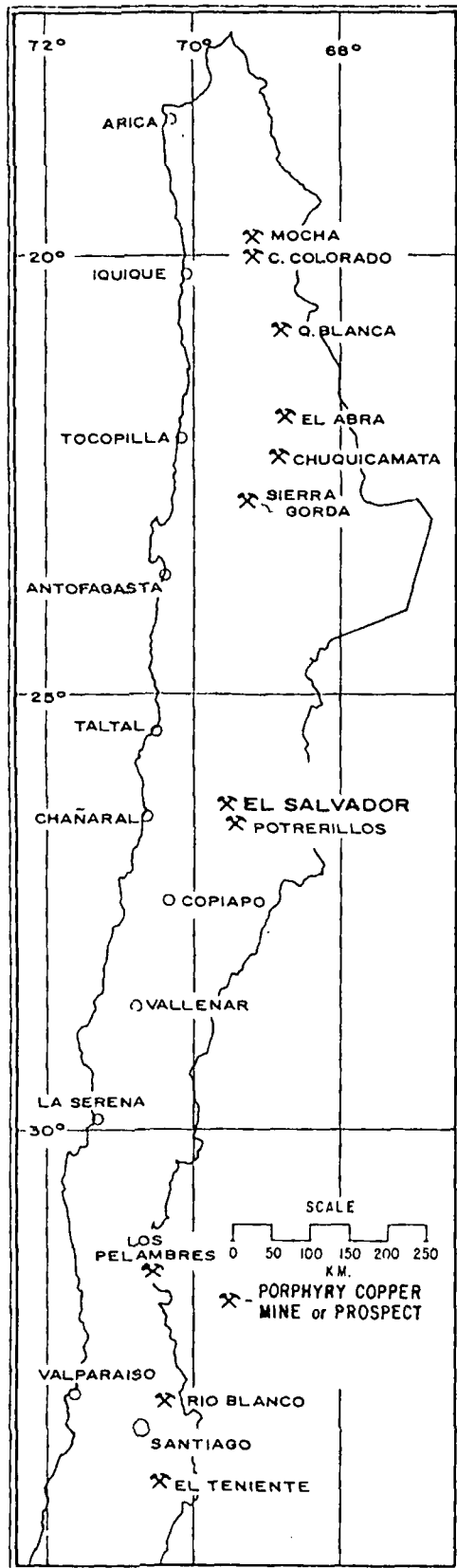


FIG. 2. Location map of northern Chile.

using the Mulchay and Stephens map as a guide examined the leached outcrops within Turquoise Gulch. During this visit particular emphasis was placed on the distribution of quartz mineralization and other features of limonite and alteration, indicating a favorable exploration target. Subsequently, Anaconda's management approved Perry's vigorous recommendation for a major exploration effort to test the possibility of a secondary, enriched target beneath Turquoise Gulch. Swayne, assisted by John Bain and Hans Langerfeldt, was then assigned to map in detail the rugged slopes of Indio Muerto and the surrounding district and to plan a drilling campaign. The mapping project was a major undertaking as no adequate base maps, roads, or water existed within the district. These difficulties were overcome and an accurate map was prepared upon which Perry and Swayne together laid out four initial test holes. Swayne's mapping and interpretations were supplemented by mineralogical studies of rock specimens by Charles Meyer in Anaconda's Butte laboratories. Meyer was then in charge of Anaconda's geological research and also inspected the prospect accompanied by Sales and Perry during the subsequent drilling campaign.

In 1951, approval for drilling was given by Anaconda management. A single drill rig was allocated for the initial exploration program. The prime target in Turquoise Gulch was inaccessible at the start and the first two holes were drilled in more easily reachable locations. They intersected interesting but low-grade secondary copper sulfides in what subsequently proved to be the outer pyritic fringe of the orebody. The third hole was drilled to explore the readily accessible Camp Area target and intercepted 1,000 feet of plus one percent primary copper mineralization. Such an encouraging showing threatened to divert management's interest from the secondarily enriched target in Turquoise Gulch, and a fourth hole was drilled near Hole 3. In spite of the tempting distraction of the Camp prospect, Swayne moved the rig back to the relatively inaccessible prime target area in Turquoise Gulch, where, in the meantime, a drill road and site had been completed, and started Hole 5. Completion of this hole was delayed due to management's interest in the intercept of primary mineralization in the Camp Area, where two additional holes were finished. Finally, in 1954, Swayne, supported by Perry, managed to complete Hole 5, intercepting high-grade secondarily enriched ore beneath the barren outcrops of Turquoise Gulch, and it was evident that a major discovery had been achieved.

The development of the El Salvador Mine following the discovery of the Turquoise Gulch orebody through 1959, the first year of production, has

also been Trask (19 of the m mapping a Salvador. were repo 1964, 190 Hunt, 197

During El Salvador years of e invested i the privile this effort of manpo the broad concepts a of a majo was select plete geol good rock overlying drill hole 900 mete

The m: dor was anatomy body. B Turquoise centers in itself in tory of th completed and chem alteration never cor

The p: consider conda's g description tions of concurre in the m:

The I Muerto Chile, sc 2). Du the mine averagin enrichment up to 20 area. S ization c in a nor

also been described by Perry (1960). Swayne and Trask (1960) described many of the general features of the mine and district as well as the geologic mapping and office procedures routinely used at El Salvador. Several important aspects of the geology were reported during the course of the work (Hunt, 1964, 1969; Hemley, 1969; and Gustafson and Hunt, 1971).

During the period of Anaconda management of El Salvador prior to July 1971, more than 80 man-years of detailed geologic mapping and study were invested in the property. The present authors have the privilege of summarizing some of the results of this effort. A significant part of this commitment of manpower and money was deliberately aimed at the broad objective of developing new exploration concepts and tools through a "case-history" analysis of a major porphyry copper deposit. El Salvador was selected for study because of excellent and complete geologic records and because of the unusually good rock exposure, consisting of surface outcrops overlying more than 200 km of tunnels and diamond drill holes which extend over a vertical range of 900 meters.

The main thrust of geologic research at El Salvador was directed at understanding the detailed anatomy and evolution of the Turquoise Gulch orebody. Broader studies, such as the relation of the Turquoise Gulch orebody to other smaller mineralized centers in the district and the geology of the district itself in relation to the Mesozoic and Cenozoic history of the Andean Cordillera, were begun but never completed. We also regret that critical petrological and chemical studies of both the regional rocks and alteration-mineralization suites within the mine were never completed.

The present paper attempts to focus on what we consider to be the main scientific result of Anaconda's geologic effort at El Salvador, namely, description and interpretation of the space-time relations of volcanism and porphyry intrusion with the concurrently evolving mineralization and alteration in the main orebody beneath Turquoise Gulch.

Geologic Setting

The El Salvador mine is located in the Indio Muerto district in the Atacama Desert of northern Chile, some 800 km north of Santiago (Figs. 1 and 2). During 12 years of operation under Anaconda, the mine produced 80 million short tons of sulfide ore averaging 1.5% Cu. The orebody is a "chalcocite" enrichment blanket roughly 1.5 km in diameter and up to 200 m thick, underlying the Turquoise Gulch area. Surface indications of alteration and mineralization can be observed in the Indio Muerto district in a north-northeast elongate zone of some 5 by 10

km. Actual ore reserves prior to production (January 1, 1957) were about 300 million short tons averaging 1.6 percent total copper, approximately 5 million tons of copper metal. This represents roughly one-third to one-half of the total amount of copper deposited in the district.

The Indio Muerto district and the Potrerillos porphyry copper deposit, 25 km southeast of El Salvador, both lie along the northern edge of a dissected and eroded lower Tertiary volcanic field, roughly 50 × 200 km in extent, which contains rhyolite and andesite extrusives and numerous granodiorite and quartz monzonite stocks. These lower Tertiary volcanics were laid down unconformably over folded and eroded Upper Cretaceous andesitic volcanic and related sedimentary rocks. The Quaternary volcanic belt, lying some 60 km east of El Salvador in the High Andes, appears to be a recent analogue of the lower Tertiary field. Erosion and dissection of the lower Tertiary rocks were aided by major northerly trending faults, most showing down-to-the-west relative displacements and unknown strike-slip components. Both El Salvador and Potrerillos have been exposed by erosion, which progressed to the point of largely stripping the lower Tertiary volcanics but not deeply eroding the underlying Mesozoic rocks.

Upper Cretaceous (?) rocks, approximately 3 to 5 km thick, are exposed in the northern half of the Indio Muerto district and at lower elevations within Cerro Indio Muerto itself (Fig. 3). The lower part of this Cretaceous section is dominantly sedimentary and composed of andesitic conglomerates and sandstone, tuffaceous in part, with subordinate andesite flows. The upper part of the Cretaceous section contains numerous andesite flows, subordinate andesitic conglomerates and sandstones, and at least one silicic pyroclastic unit. These rocks are very similar to and probably correlate with the lower and upper members of the Cerrillos formation in the Copiapo area (summarized by Segerstrom, 1967). In the Indio Muerto district, the Upper Cretaceous rocks are folded into a faulted antiformal structure trending northerly and having a steep western limb. In the vicinity of the orebodies, distinction between igneous and clastic units within this formation is impossible because of strong alteration and they have been mapped simply as "andesite."

A series of lower Tertiary andesitic and rhyolitic extrusives, including abundant ignimbrites, overlies the Cretaceous rocks and comprises intertongued volcanic piles whose thickness has not been determined. In the vicinity of Turquoise Gulch, at least 400 m of siliceous ignimbrites overlie the unconformity and dip gently to the south. The fact that the steep porphyry contacts and sulfide veins in the

mine dip northerly, perpendicular to these volcanics, suggests minor southerly tilting or warping of the district after mineralization. These volcanics probably correlate with the Hornitos formation in the Copiapo area (Seegerstrom, 1967), and therefore the unconformity has been named the "Hornitos unconformity".

On the southeast flank of Cerro Indio Muerto, a second unconformity with sharp local relief is seen cutting through the Hornitos volcanics into an underlying window of Cerrillos rocks. This unconformity and the thick series of overlying andesitic and rhyolitic volcanics and sediments have been called the Indio Muerto unconformity and series, respectively. Mapping to define the extension of this unconformity and the detail within the volcanics on the south slope of the mountain was never completed, so these features on Figure 3 are somewhat speculative. The Indio Muerto series rocks probably correlate with the Cerro La Peineta volcanics in the Copiapo region (Clark et al., 1967).

Intrusive activity centered in the Indio Muerto district began during mid-Eocene with the emplacement of a group of rhyolite domes, which apparently formed one of the volcanic centers for the Indio Muerto series extrusives. A second group of quartz rhyolite and quartz porphyry intrusions was followed by the granodioritic porphyry complex around Turquoise Gulch at the end of the Eocene. It is not clear how much of an edifice was built by either of these volcanic episodes or how much erosion preceded the intrusion of the main porphyry sequence. Only minor copper and molybdenum mineralization was related to the quartz rhyolite and quartz porphyry volcanic events, but the bulk of mineralization and alteration accompanied the emplacement of the final porphyry complex. Subsequent supergene oxidation and sulfide enrichment of the primary mineralization formed the commercial orebodies at El Salvador. Supergene enrichment was accomplished long before the present erosion surface was formed, as noted elsewhere in the Atacama desert (Sillitoe et al., 1968). Oxidized portions of the original enrichment blanket are exposed on the lower slopes of Indio Muerto and are overlain by Miocene gravels.

The present paper will concentrate on those events that took place in the Turquoise Gulch area at the culmination of volcanic activity and produced the main orebody of the El Salvador mine.

Principal Intrusive Rock Types

The Turquoise Gulch center of mineralization contains a complex of siliceous to intermediate intrusive rock types.

Indio Muerto Rhyolite domes

The main peak of Cerro Indio Muerto and the high ridge to the southwest (Figs. 1 and 4) are formed by two rhyolite domes. Underground penetrations have partially defined the geometry of each as flaring outward above the elevation of the Hornitos unconformity (Fig. 5). A third rhyolite body, located on the east flank of Indio Muerto, is petrologically very similar to these domes and is probably a more deeply eroded and steep-walled volcanic neck. The smaller irregular masses on the northeast flank of the mountain are dikes and sills of similar rock intruding Cerrillos "andesites." The rhyolite domes clearly intrude the rhyolitic pyroclastics above the Hornitos unconformity near Turquoise Gulch. A flow breccia of identical rock on the southeast slope of the mountain grades downhill into water-worked debris derived from the domes. These rocks directly overlie the Indio Muerto unconformity, which therefore marks the surface at the time of emplacement of these early rhyolites. These rhyolites are clearly older than quartz porphyry and granodiorite porphyry, being cut by dikes of these rocks.

These rhyolites are readily identifiable as a single rock type, called Indio Muerto Rhyolite (Fig. 6A). They contain practically no quartz phenocrysts, but all contain more or less abundant, 1 to 3 mm phenocrysts of alkali feldspar, recognizable even in strongly altered areas. A variety of matrix textures are seen, all suggesting devitrification of glass. Flow banding is common and widespread.

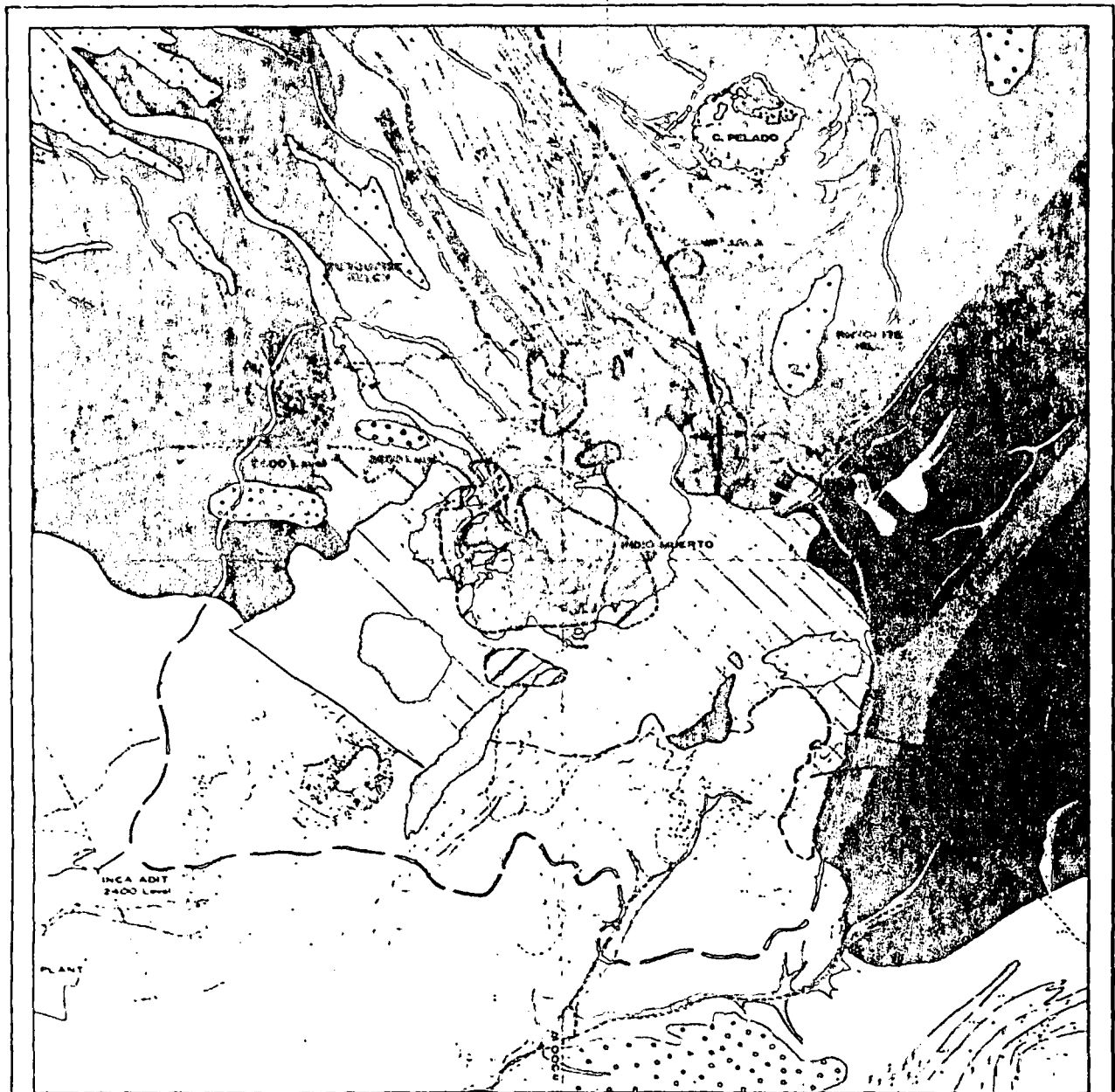
A single complete chemical analysis (Table 1) and a few partial analyses indicate a silica content ranging from about 74% to 77% SiO₂, with K₂O ranging from 4.0% to 6.5% and Na₂O from 1.6% to 3.6%.

Quartz rhyolite

Close to the northeast flank of the mountain lie two hills of quartz rhyolite, known as Cerro Pelado and Rhyolite Hill (Fig. 3). This rock type is characterized by abundant and usually small quartz phenocrysts and relatively abundant feldspar phenocrysts (Fig. 6B). Small biotite books and K-feldspar phenocrysts are commonly present but sparse, and opaques are practically absent. Age relations with the Indio Muerto Rhyolite domes and with quartz porphyry, described below, are inconclusive.

Cerro Pelado is a steep-walled, complex intrusive center. Quartz rhyolite forms an arcuate massive plug with arcuate and tangential dikes. The margins of the plug are strongly brecciated. Enclosed within the circular outline is what is probably a collapsed breccia, containing fragments of andesitic sediment partially engulfed by quartz rhyolite. Cerro Pelado has many of the characteristics of a shallow





SIMPLIFIED GEOLOGIC MAP of the INDIO MUERTO DISTRICT

KILOMETERS

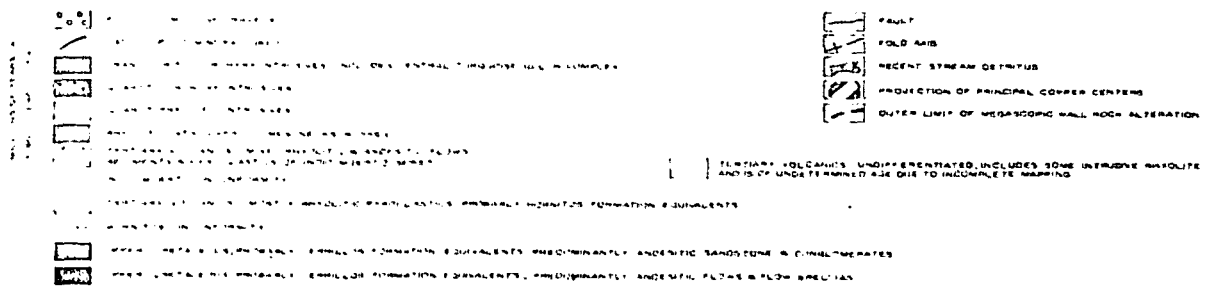
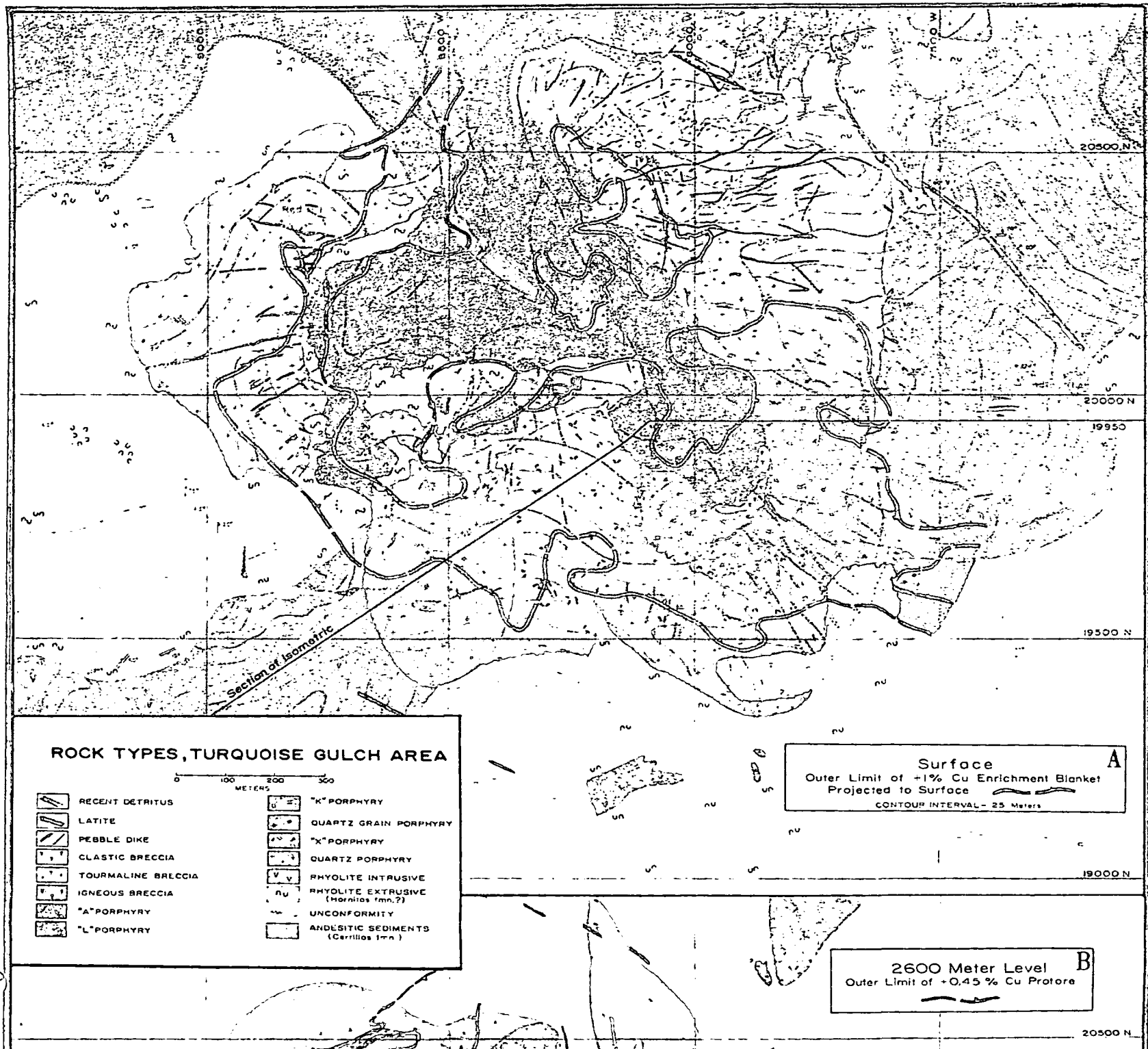


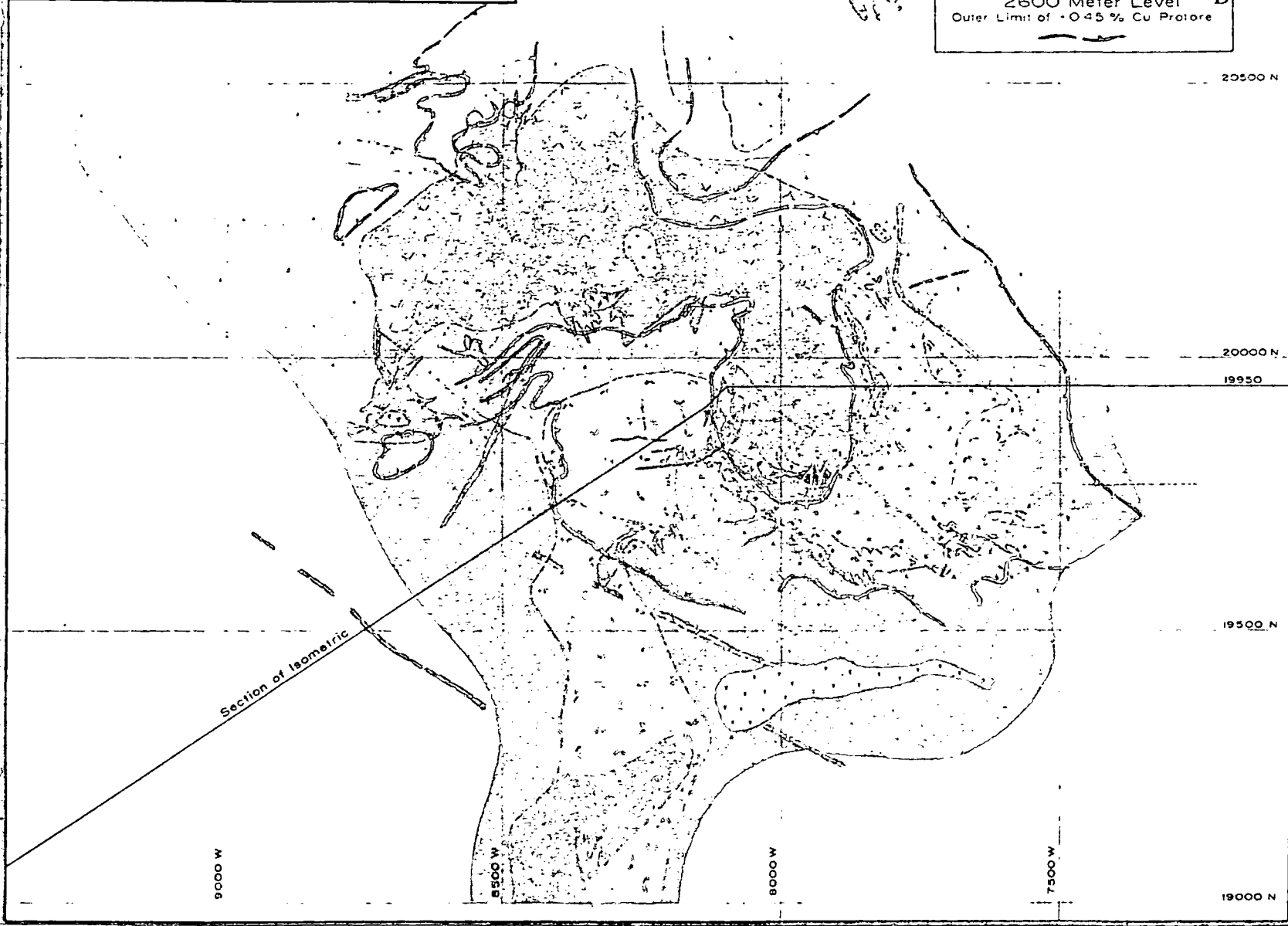
FIG. 3. Simplified geologic map of the Indio Muerto district.

Fig. 4. Rock types, Turquoise Gulch area: A, surface and B, 2,600-meter level.



	100% Cu		50% Cu
	25% Cu		10% Cu
	5% Cu		1% Cu
	0.5% Cu		0.25% Cu
	0.1% Cu		0.05% Cu

2600 Meter Level **B**
 Outer Limit of 0.45 % Cu Profile



9000 W

8500 W

8000 W

7500 W

19000 N

19500 N

19950

20000 N

20500 N

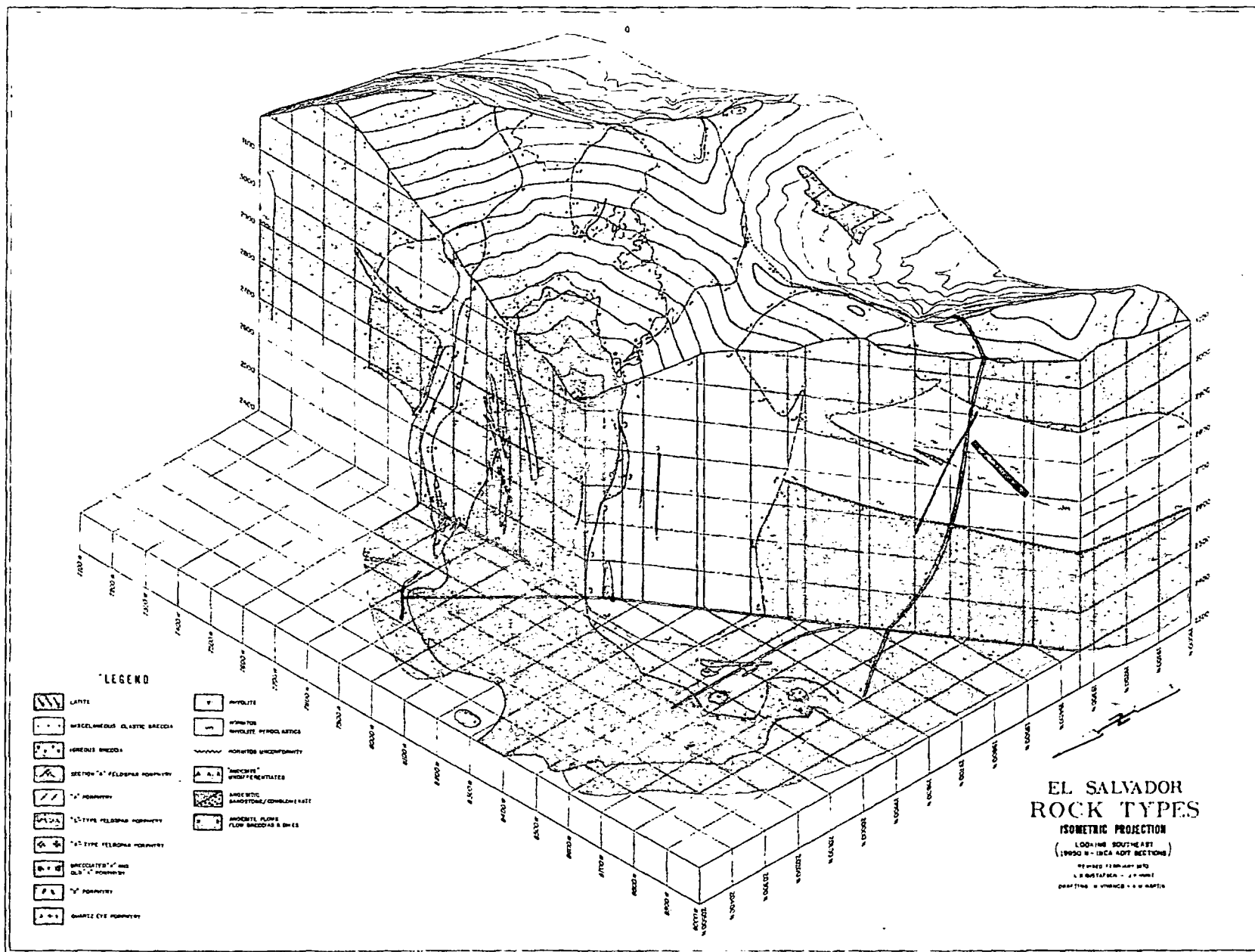


FIG. 5. Rock types in the El Salvador mine, isometric projection.

volcanic neck. It is not certain whether the nearly flat base of the quartz rhyolite in Rhyolite Hill was the surface on which it was extruded or represents merely the base of an intrusive sill.

Quartz porphyry

Quartz porphyry is a major intrusive rock type in the Turquoise Gulch and Old Camp centers of mineralization. It is characterized by usually abundant and large quartz and plagioclase phenocrysts in a siliceous fine-grained groundmass. The texture is similar to the coarsest quartz rhyolite (above), except that plagioclase phenocrysts are larger (some >1 cm) and more abundant and biotite books more prominent (Fig. 6C).

Clearly more than one intrusive unit has been included as quartz porphyry, but only in the Old Camp area have contacts between two quartz porphyries been mapped. The irregular north-trending dike between Turquoise Gulch and the Old Camp area (Fig. 3) contains abundant broken phenocrysts, suggesting that it was a feeder for pyroclastic extrusives. Quartz porphyry at the Old Camp area forms an arcuate dike, presumably a ring dike, which occupies nearly 170 degrees of a circle around Cerro

Pelado quartz rhyolite. The large areas of quartz porphyry in and surrounding Turquoise Gulch are exposures of rather extensive and thick sills of quartz porphyry which were intruded at the base of and within the Hornitos volcanic pile. In mine exposures and drilling beneath these outcrops, only a few small dikes are seen below the Hornitos unconformity (Figs. 4 and 5).

There is a striking difference in shape between the quartz porphyry intrusions and both the earlier Indio Muerto Rhyolite domes and later steep-walled granodioritic porphyries. This suggests that quartz porphyry was intruded at a different depth or at a different rate than these other intrusions. Quartz rhyolite has closer affinities to quartz porphyry than to Indio Muerto Rhyolite in texture and shape. Quartz rhyolite and quartz porphyry are interpreted as being closely related intrusions.

All of the quartz porphyry in the main Turquoise Gulch area is moderately to strongly altered. The single chemical analysis of quartz porphyry (Table 1) is of a sericite-chlorite altered dike rather than of fresh rock. The alteration may account for the relatively high Fe_2O_3/FeO and K_2O/Na_2O ratios reported in the analysis.

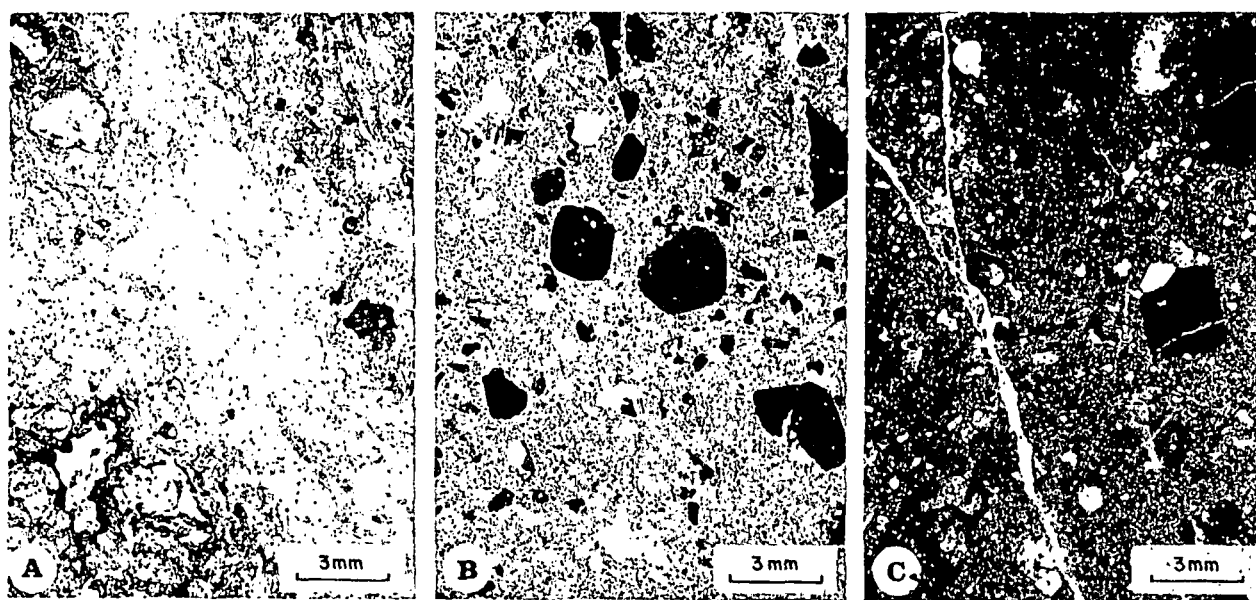


FIG. 6. Textures of intrusive rocks related to early rhyolitic volcanic events.

A. Indio Muerto Rhyolite. Flow banding, devitrification textures (quartz and alkali feldspar), and sparse small phenocrysts of alkali feldspar characterize the cluster of rhyolite domes on and around Cerro Indio Muerto. Quartz or biotite phenocrysts are not seen. (Nonpolarized light)

B. Quartz rhyolite. Abundant phenocrysts of quartz and alkali feldspar are commonly fragmental, and biotite "books" are small and sparse. Groundmass is a very fine granular intergrowth of quartz, alkali feldspar, and sericite, which shows neither flow banding nor the usual devitrification textures. Coarse varieties with some plagioclase phenocrysts approach quartz porphyry in texture. (Cross-polarized light)

C. Quartz porphyry. Large phenocrysts of plagioclase and quartz are set in a fine-grained groundmass of quartz and sericite. Biotite "books" are prominent, but in this specimen are altered to sericite, as is the plagioclase. (Cross-polarized light)

Note that like the photographs in Figures 7, 8, and 9 these are negative prints made by using thin sections directly as negatives in the enlarger, with or without polarizing sheets.

TABLE 1. Chemical Analyses of Intrusive Rocks. The samples are from the freshest and most weakly mineralized exposures of each type in the mine area, but most have been affected by significant mineralization and alteration. Analyses were made by the Japan Analytical Research Institute, except for (1), which was made by The Anaconda Co. In samples with significant amounts of sulfides, the ratio of Fe_2O_3 to FeO is erroneously high.

	(1)	(2)	(3)	(4)	(5)	(6)	(7)	(8)	(9)	(10)	(11)
SiO_2	75.86	60.11	57.75	62.93	56.58	64.31	64.53	65.09	62.46	53.85	59.23
Al_2O_3	12.87	15.01	16.44	14.66	17.41	16.29	16.10	15.03	17.39	16.66	15.59
Fe_2O_3	0.44	1.40	0.59	1.00	3.44	2.63	1.23	2.05	2.42	2.03	3.10
FeO	0.75	0.47	2.22	1.00	2.72	1.77	1.37	1.27	1.64	1.05	1.71
MnO	0.00	trace	0.06	0.01	0.03	0.03	0.01	0.02	trace	0.02	0.05
MgO	0.05	1.36	2.58	1.33	2.15	1.60	1.34	1.31	1.48	2.43	2.13
CaO	0.23	5.44	6.39	4.66	6.14	4.34	4.55	3.87	4.40	6.64	5.41
Na_2O	3.44	1.99	4.04	6.73	4.65	4.79	3.99	3.56	4.29	5.59	4.31
K_2O	5.13	3.77	2.28	1.45	1.57	1.79	2.30	2.68	3.58	1.89	2.73
$H_2O(+)$	0.39	2.55	1.04	0.62	1.18	0.98	1.24	2.47	0.93	1.25	1.32
$H_2O(-)$	—	1.09	0.28	0.95	0.53	0.41	0.53	0.77	0.29	0.51	2.30
P_2O_5	0.00	0.28	0.85	0.55	0.48	0.32	0.26	0.22	0.20	0.22	0.29
TiO_2	0.24	0.14	0.99	0.62	0.73	0.71	0.43	0.48	0.45	0.66	0.96
SO_3	0.00	6.30	3.79	3.43	2.24	0.55	2.27	1.83	0.45	6.23	trace
S	0.02	0.63	0.20	0.38	0.22	0.08	0.28	0.57	0.25	0.07	trace
CO_2	0.17	0.27	0.08	0.26	0.33	0.24	0.40	0.35	0.04	0.53	1.55
F	0.013	0.02	0.04	0.03	0.06	trace	0.04	0.04	0.04	0.04	0.03
Cu	0.00	0.26	0.53	0.50	0.06	0.03	0.15	0.13	0.03	0.27	0.01
Subtotal	99.60	101.09	100.15	101.11	100.52	100.87	101.02	101.74	100.34	99.94	100.72
Less O equivalent for S	-0.01	-0.32	-0.10	-0.19	-0.11	-0.11	-0.14	-0.29	-0.12	-0.04	—
Total	99.59	100.77	100.05	100.92	100.41	100.83	100.88	101.45	100.22	99.90	100.72
Sp. gr.	2.52	2.68	2.69	2.66	2.73	2.67	2.66	2.66	2.66	2.70	2.56

- (1) Indio Muerto Rhyolite, ES 1693; practically unmineralized and unaltered; surface.
- (2) Quartz porphyry, ES 2702; sericite-chlorite-anhydrite-chalcocopyrite-bornite; 2400 level.
- (3) "X" Porphyry, ES 2699; K-feldspar-biotite-anhydrite-chalcocopyrite-bornite; 2400 level.
- (4) "K" Porphyry, DDH 547-180 m; K-feldspar-biotite-anhydrite-chalcocopyrite-bornite; 2,460-m elevation.
- (5) "L" Porphyry, ES 2691; no aplitic groundmass, biotized hornblende and anhydrite veinlets; 2400 level.
- (6) "L" Porphyry, ES 2689; (-) aplitic groundmass, practically fresh and unmineralized; 2400 level.
- (7) "L" Porphyry, ES 2688; (\pm) aplitic groundmass, weak chloritization, sparse chalcocopyrite in "alkali seams"; 2400 level.
- (8) "L" Porphyry, ES 2687; (\pm) aplitic groundmass, weak sericite-Na-plagioclase-chlorite with sparse chalcocopyrite-pyrite; 2400 level.
- (9) "L" Porphyry, ES 2703; (\pm) coarse aplitic groundmass, practically fresh and unmineralized; 2400 level.
- (10) "A" Porphyry, ES 2701; "mineralized" texture, biotitic-alkali feldspar-anhydrite-chalcocopyrite-bornite; 2400 level.
- (11) Latite, ES 2695; moderate montmorillonite-calcite alteration; 2400 level.

"X" Porphyry

The oldest of the main series of granodioritic porphyries in Turquoise Gulch is known as "X" Porphyry. (The main intrusive rock types in the El Salvador mine were arbitrarily given letter designations, X, K, L, etc., referring to crosscuts in original exploration workings where these rock types were well exposed.) This porphyry was referred to by Swayne and Trask (1960) as "fine-grained granodiorite." As shown in Figure 4, there are three main bodies of "X" Porphyry lying along the north-northeast axial trend of the porphyry complex. The central body forms a discontinuous fringe about a younger feldspar porphyry intrusion.

"X" Porphyry characteristically sends many irregular dikes into andesite. Recrystallization of andesite into a relatively coarse, equigranular biotized rock in the immediate vicinity of the contact locally makes recognition of the intrusive contact difficult,

especially where further complicated by superimposed hydrothermal alteration. Definitive age relations at contacts between "X" Porphyry and quartz porphyry have not been found, but gross geometry strongly implies that the steep "X" Porphyry stocks cut the quartz porphyry sills. Younger feldspar porphyries ("K" and "L") clearly intrude "X" Porphyry. "X" Porphyry contacts locally truncate early quartz veins with sulfides in andesite, but most quartz veins cut across these contacts.

The weakly porphyritic texture of "X" Porphyry is best observed in deep underground exposures, where the rock is least altered (Fig. 7A). In exposures at higher elevations, the rock is strongly altered and appears equigranular, with only sparse evidence of a porphyritic texture (Fig. 8C). Plagioclase phenocrysts are commonly obliterated by alkali feldspars and hornblende phenocrysts by biotite and alkali feldspar. Over broad areas, there is no evidence of an originally more porphyritic texture. Small

dikes of
extremite
phyries.
granular
was deve
of the ro
during fir

"K" Porphyry

Follow
plex ser
"Feldspa
porphyry
phenocry
but lacki
crysts.
Turquois
Porphyry
"K" I

the main
Gulch.
phyry to
fringing
not only
veins an
ture, de
location
types, it
tacts th
type.

"K"
complex
tacts be
have be
of text
with "L"
much o
and hov
stage r
(Figs. 1
in the
tassium

"L" Porphyry

The
quoise
steep-w
nearly
porphy
also ye
tion. ar
the or
the ma
seen le
of a m

dikes of "X" Porphyry grade into aplites at their extremities, as do some small dikes of other porphyries. It is not fully clear whether the equigranular texture of "X" Porphyry at upper levels was developed through post-consolidation alteration of the rock or whether it was developed primarily during final stages of consolidation of the melt.

"K" Porphyry

Following emplacement of "X" Porphyry, a complex series of feldspar porphyries was intruded. "Feldspar porphyry" is a textural term meaning porphyry characterized primarily by plagioclase phenocrysts, with an abundance of mafic phenocrysts but lacking prominent quartz and K-feldspar phenocrysts. The main mass of feldspar porphyry in the Turquoise Gulch area is separated into an early "K" Porphyry and a later "L" Porphyry.

"K" Porphyry occupies the southeastern lobe of the main mass of feldspar porphyry in Turquoise Gulch. It is older than the main mass of "L" Porphyry to the northwest but intrudes andesite and the fringing mass of "X" Porphyry. This is established not only by dike shapes but by truncation of quartz veins and alteration assemblages. While rock texture, degree of alteration and mineralization, and location are useful for field recognition of these rock types, it is the age relationships at the intrusive contacts that were used to define each porphyry rock type.

"K" Porphyry is best described as an intrusive complex, as within its main body many local contacts between intrusive surges of "K" Porphyry have been mapped. There is a fairly wide range of textural variation within "K" Porphyry. As with "X" Porphyry, it is not entirely clear how much of this is due to post-consolidation alteration and how much to reaction between crystals and late-stage melt and fluids during final crystallization (Figs. 7B, 8A, 8B). Most "K" Porphyry exposed in the mine is at least moderately altered to potassium silicate assemblages.

"L" Porphyry

The largest mass of feldspar porphyry in Turquoise Gulch is "L" Porphyry. It is a complex steep-walled stock with a crudely arcuate outline, nearly 1 km across. "L" Porphyry cuts quartz porphyry, "K" Porphyry, and "X" Porphyry. It is also younger than much, but not all, of the alteration and mineralization in the deep central part of the ore zone. Although intrusive contacts within the mass are difficult to recognize, enough have been seen locally to indicate that this stock is also made of a number of separate intrusive units. The south-

eastern lobe shows the clearest evidence of multiple intrusion of feldspar porphyry magma. Here dikes of both mafic feldspar porphyry ("A" Porphyry) and igneous breccia which clearly cut "L" Porphyry are in turn cut by dikes of porphyry which are indistinguishable from the host "L" Porphyry. So close is the similarity of early and late surges of "L" Porphyry that contacts between them can be traced for only short distances.

"L" Porphyry is the only one of the major intrusive rocks with exposure fresh enough to determine the original composition and petrography. The texture and composition vary markedly. However, all textural variants are characterized by abundant phenocrysts of plagioclase, biotite, hornblende, and locally quartz. These are enclosed in a matrix of quartz, alkali feldspar, and biotite and (or) hornblende, with accessory zircon, apatite, sphene, magnetite, and ilmenite (Figs. 9 and 10).

The major texture variation is in the abundance and grain size of the groundmass. Where microscopic texture of the groundmass is a "sugary" equigranular mixture of relatively fine grained quartz and alkali feldspar, with mafics and other accessory minerals, it has been called "aplitic" groundmass. This is characteristic of most "L" Porphyry as well as the least altered exposures of "K" Porphyry. Along with variation in the abundance of aplitic groundmass are seen rather systematic variations in the abundance of quartz phenocrysts, color index, and ratio of identifiable biotite and amphibole phenocrysts to total biotite plus amphibole. The sizes of plagioclase phenocrysts and the ratio of hornblende to biotite phenocrysts show no systematic variations.

Systematic textural patterns have been mapped within "L" Porphyry (Fig. 11). Areas of abundant aplitic groundmass, quartz phenocrysts, low mafic content, and a high proportion of mafics as phenocrysts grade into relatively nonporphyritic, more mafic rock with no quartz phenocrysts near contacts with biotitized andesite. This transition is accomplished by both truly gradational and abrupt changes in one or a combination of the textural features. Such mafic contact effects are absent or only weakly developed where "L" Porphyry intrudes early porphyries or previously mineralized and biotitized andesite. A miniature (5 cm), nonporphyritic, mafic porphyry rim has been found surrounding a small (10 cm) inclusion of biotitized andesite within one of the high groundmass porphyry centers. On both scales, Na_2O rises and K_2O drops approaching the "andesite" from high-groundmass porphyry. Evidently, reaction with the intruded "andesite" is the chief cause of the textural variations.

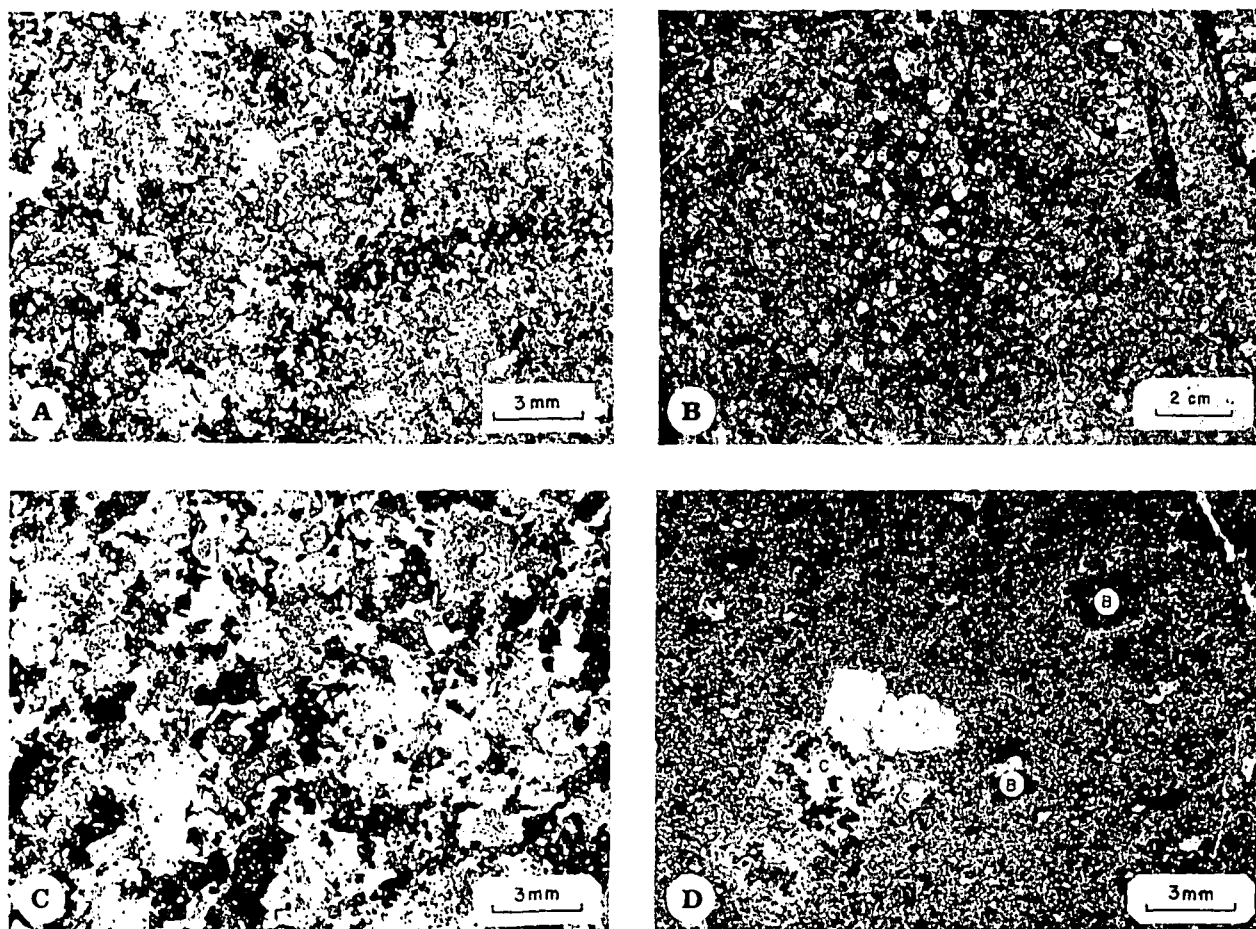


FIG. 8. Textures of strong K-silicate alteration in "X", "K", and "A" Porphyry.

A, "K" Porphyry with porphyritic texture (Fig. 7B) strongly obliterated by replacement of phenocrysts and recrystallization of groundmass. Plagioclase is rimmed and veined by perthite, with oligoclase typically separating any unreplaced andesine from the perthite. The relatively coarse, ragged "perthitic" groundmass (Fig. 10B) assemblage replaces biotite phenocrysts as edges of plagioclase. Diagonal "A" quartz vein. (Cross-polarized light)

B, "K" Porphyry with poorly defined area of fairly clean, residual porphyry texture within an area of texture obliterated by intense K-silicate alteration. Within "K" Porphyry there is a general correlation between intensity of texture obliteration and abundance of "A" quartz veining. (Macrophotograph)

C, "X" Porphyry with much of the plagioclase replaced by alkali feldspar and relatively coarse quartz and perthite in the matrix (Fig. 7A). Irregular clots of "shreddy" biotite do not suggest hornblende pseudomorphs. This texture is widespread in "X" Porphyry with no evidence of any structural control. (Cross-polarized light)

D, "A" Porphyry "mineralized" texture (cf. Fig. 7C). Some plagioclase phenocrysts are replaced by alkali feldspar-biotite-anhydrite (B), and a miarolitic cavity(?) filled with anhydrite-biotite-quartz-bornite is marked C. The trachytic groundmass contains very fine grained plagioclase laths and biotite. This texture characterizes dikes (or extensions of dikes with normal texture, as in Fig. 7C) which intrude previously well mineralized rock in the central portions of the deposit. (Nonpolarized light)

Igneous breccias

Intrusive rocks containing more or less abundant heterogeneous rock fragments in an igneous (i.e., originally magmatic, not elastic) matrix are here called "igneous breccias." Four of the largest breccia masses are shown in Figure 4B, as they are exposed on the 2600 level.

The Main Breccia, which is an arcuate feature near the contact between "L" Porphyry and "K" Porphyry, is the best exposed. Near the 2,600-m elevation, where the Main Breccia cuts several rock types (Fig. 5), it contains abundant heterogeneous rock

fragments in a groundmass of alkali feldspar, quartz, and biotite with chalcopyrite, bornite, and rutile. Sixty meters below, the breccia is smaller, contains practically no fragments, and is confined within "L" Porphyry. The rock, which has a sharp intrusive contact with the "L" Porphyry, looks like little more than a foliated or "stretched out" surge of "L" Porphyry magma. At higher elevations, the Main Breccia crosses into the "K" Porphyry with little change other than an increase in "K" Porphyry fragments. Above the 2,710-m elevation, an arcuate mass of intensely brecciated "K" Porphyry containing abund-

ant quartz fragments overlies the upward projection of the Main Breccia. The deep exposures appear to represent the roots of the breccia. It is not clear

whether the arcuate brecciated zone at higher elevations represents brecciation related to the intrusion of igneous breccia or to a prior structural event which

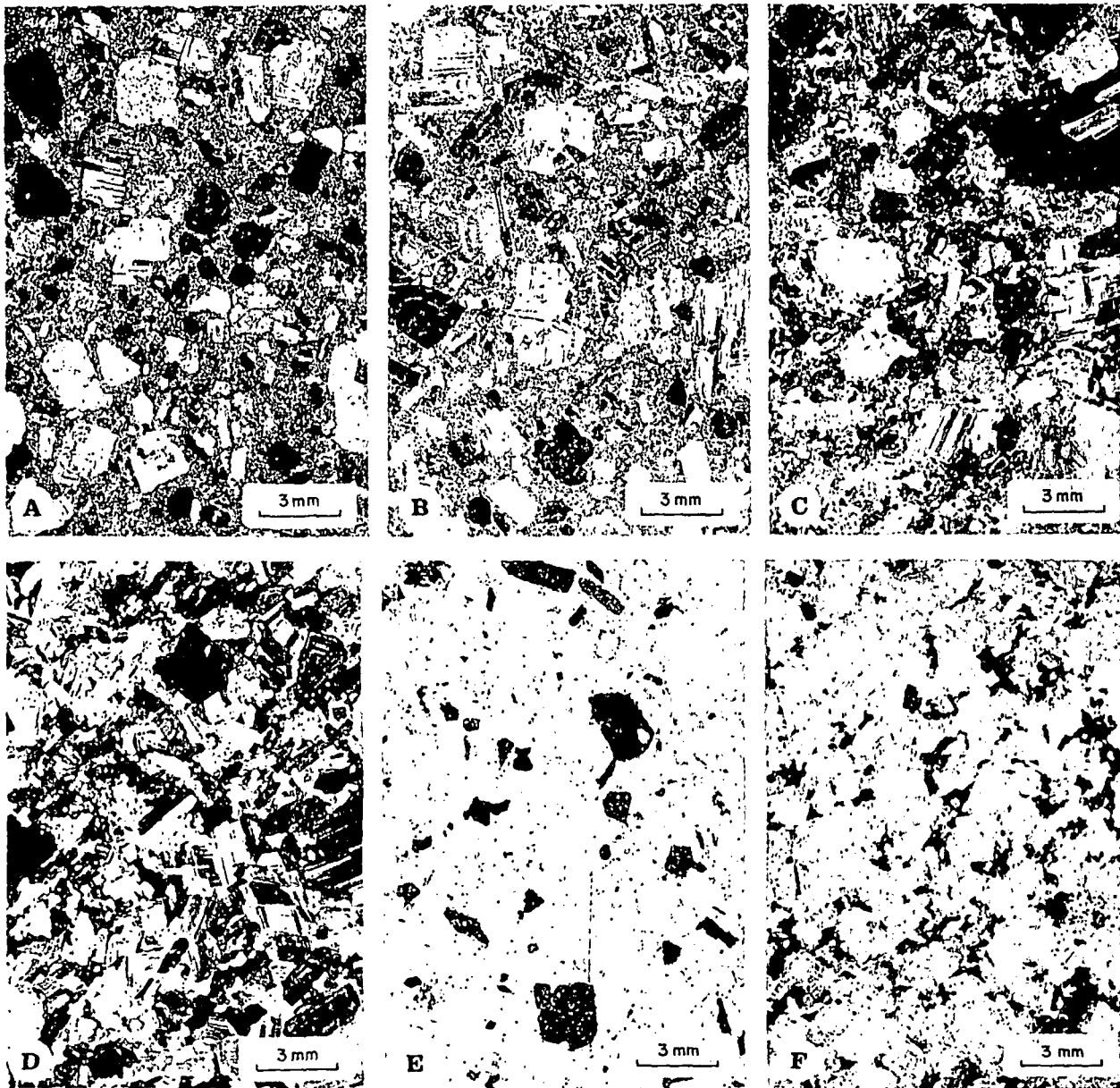


FIG. 9. Textural variations within El Salvador "L" Porphyry.

A, Maximum-groundmass texture. Most plagioclase phenocrysts are isolated in (+) "aplitic" groundmass (see Fig. 10A). Plagioclase are oscillatory zoned \pm An_{50} , usually have normally zoned rims \pm An_5 , have moderately well ordered structures, and range from 1 to 5 mm in size. Phenocrysts also of quartz, biotite, and hornblende (biotized); accessories are zircon, apatite, sphene, magnetite, and ilmenite. (Cross-polarized light)

B, Intermediate-groundmass texture. Most plagioclase phenocrysts in point contact (\pm) "aplitic" groundmass. Plagioclase are slightly altered, but there is no systematic variation in size of plagioclase. (Cross-polarized light)

C, Low-groundmass texture. Most plagioclase phenocrysts in edge contact. (-) "aplitic" groundmass is relatively coarse and ragged and has a relatively low alkali feldspar-quartz ratio. (Cross-polarized light)

D, No-groundmass texture. Quartz and biotite but almost no K-feldspar are interstitial to plagioclase. This texture is developed near contacts with biotized andesite (Fig. 11) and as a reaction rim about an inclusion of andesite within porphyry with (+) "aplitic" groundmass. (Cross-polarized light)

E, Porphyritic habit of mafics, biotite, biotized hornblende within porphyry with maximum "aplitic" groundmass (A). Fine disseminated opaques are magnetite and hematite-rutile after ilmenite. (Nonpolarized light)

F, Irregular "shreddy" habit of biotite within no-groundmass porphyry (D). Degree of anhedral habit of mafics ranges between E and F, correlates well with abundance of "aplitic" groundmass, and is easier to map. (Nonpolarized light)

was merely
breccia. I
"L"-type p

Latite

A series
posed acro
(Figs. 3 &
intrusive
cally all n
mine. Th
latite are

Pebble Di

Pebble
vador, es
Like latit
spatial an
postdate
our unde
is derive
Pebble
filled wi
abundant
these dil
rare bul

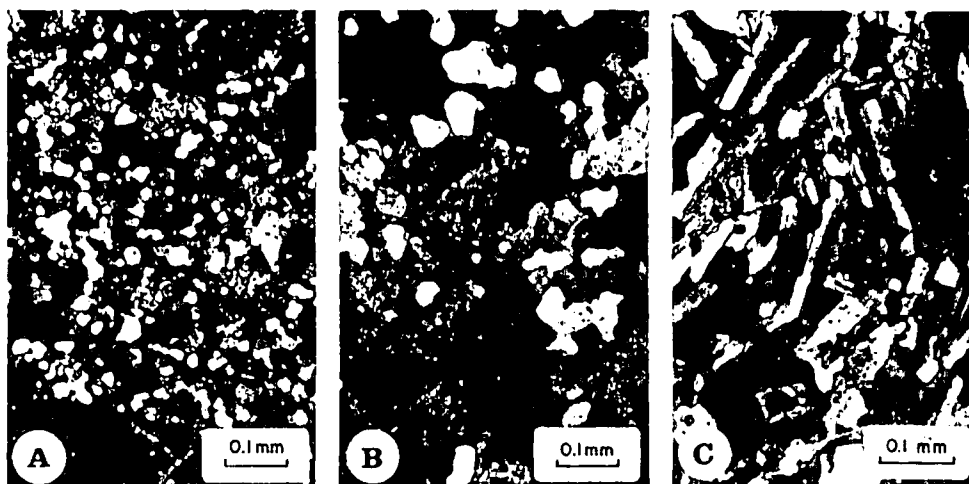


FIG. 10. Microscopic textures of groundmass in porphyritic rocks.

A, "Aplitic" groundmass, typical of unaltered feldspar porphyries. Sugary granular mixture of subround quartz and alkali feldspar with more or less fine grained biotite and accessory Fe-Ti oxides. The alkali feldspar is not perthitic, but its composition and structure are not known. Minor amounts of sodic plagioclase may be present. In hand specimen, especially of rock with no sericitic or argillic alteration where the groundmass is relatively fine grained, this kind of groundmass commonly appears aphanitic. (Cross-polarized light)

B, Perthitic groundmass, typical of strong K-silicate altered feldspar porphyries. Relatively coarse, ragged mixture of quartz and perthitic alkali feldspar with more or less fine grained biotite. This texture is developed both by alteration of "aplitic" groundmass and by original crystallization. Because of its coarseness, this groundmass rarely appears to be aphanitic, even in hand specimens lacking sericite or argillic alteration. (Cross-polarized light)

C, "Feldspathic" groundmass, typical of "A" Porphyry. It is composed largely of plagioclase laths, usually growth zoned with more calcic cores, and abundant mafics with minor quartz and rare K-feldspar. Mafics are most commonly hornblende, usually biotized, and commonly with a fine acicular habit. Groundmass intermediate between this and "aplitic" groundmass occurs in some "L" Porphyry. (Cross-polarized light)

was merely followed by the intrusion of the igneous breccia. Dikes of "A" Porphyry and of still later "L"-type porphyry cut this breccia on the 2600 level.

Latite

A series of northwest-trending latite dikes is exposed across the district, as well as in the mine area (Figs. 3 and 5). These are the only truly postore intrusive rocks at El Salvador. The dikes cut practically all mineralization and alteration features in the mine. The typical texture and petrography of the latite are illustrated in Figure 7D.

Pebble Dikes

Pebble dikes are a conspicuous feature at El Salvador, especially at the surface and on upper levels. Like latite dikes, with which they show very close spatial and temporal relationships, the pebble dikes postdate nearly all primary mineralization. Much of our understanding of the pebble dikes at El Salvador is derived from the work of Langerfeldt (1964a).

Pebbles dikes at El Salvador are dike-like features filled with clastic material, generally containing abundant rounded pebbles (Fig. 12). The width of these dikes ranges from less than 1 cm to 2 m, with rare bulges to 6 m. Their continuity along strike

ranges from a few meters to more than 1 km. Few pebble dikes have a vertical continuity of more than 600 m below the present surface. There is one circular outcrop of pebble breccia on the surface which is presumably a "pebble pipe." The abundance of pebbles relative to matrix varies widely. The matrix consists of pulverized rock and vein material, ranging in size from silt to coarse sand size.

The degree of rounding of a pebble correlates in a rough way with the distance of travel of the pebble. Angular pebbles almost invariably are of the same rock types as the immediate enclosing wall rock. Well-rounded pebbles may have originally come from lower or higher elevations than where exposed, although this is usually indeterminate. The Cretaceous andesites are readily converted to sand matrix and angular slabs, while porphyry rock types tend to round readily and can be found relatively far from their source. There is a general lack of evidence of long-distance transport of pebbles in these pebble dikes. However, in the two largest and deepest known pebble dikes, pebbles of barren, coarse, subporphyritic rock, presumably from significantly deeper levels, are found. These pebbles could be samples of a subjacent cupola of a granodioritic batholith lying below the porphyry complex.

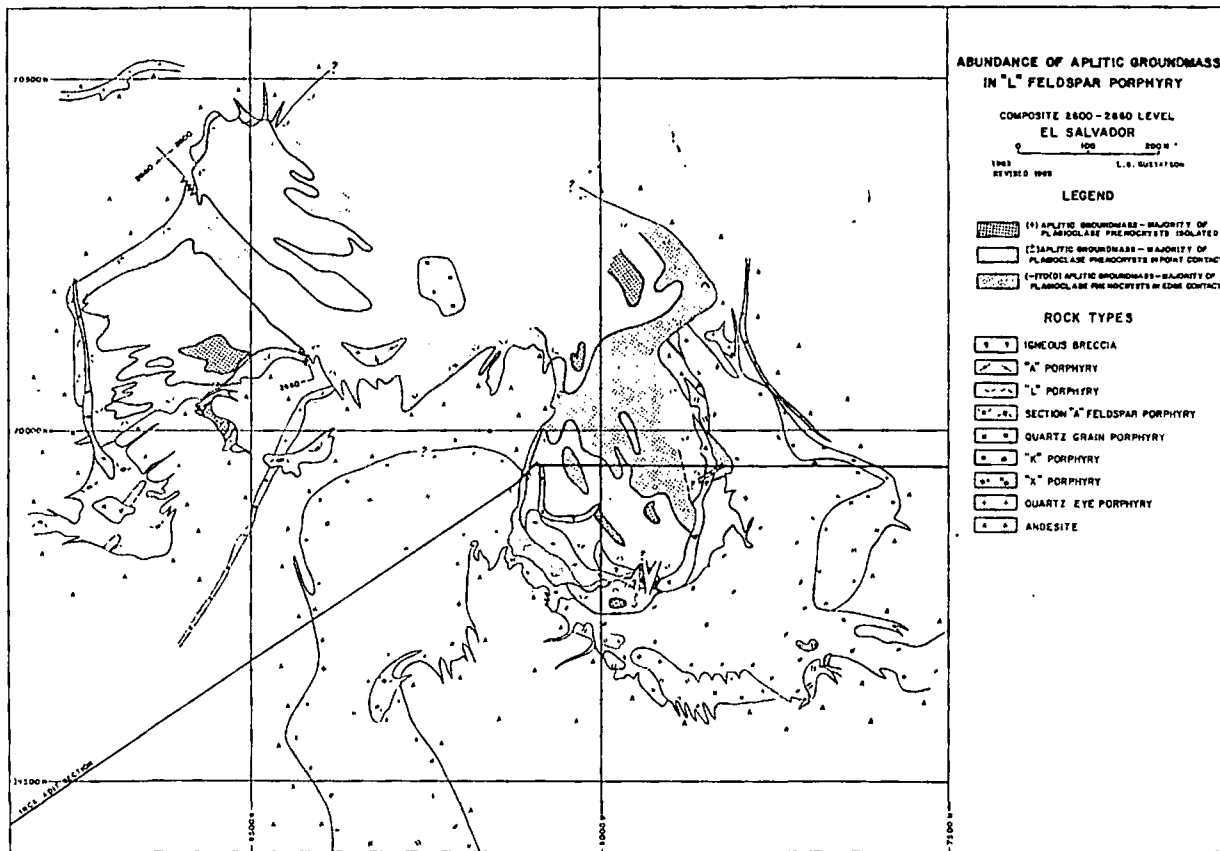


FIG. 11. Abundance of aplitic groundmass in "L" feldspar porphyry.

Flow banding of the matrix of pebble dikes is commonly observed. Many pebble dikes, particularly the small ones, are irregular in both thickness and attitude. These commonly follow sharp changes in direction between intersecting structures.

Pebble dikes occupy preexisting throughgoing structures, especially late hydrothermal vein structures. Late hydrothermal vein material and ground-up alteration halo material are very abundant in pebble dikes. The surface pattern of pebble dikes (Fig. 4A), as mapped by Hans Langerfeldt, shows a distinct radial pattern with a few circumferential structures. There is a strong correspondence of this structural pattern with the pattern of "D" veins described below (see Fig. 22). In striking contrast to this pattern is the nearly orthogonal conjugate pattern of pebble dikes at the lower levels in the mine (Fig. 4B), even at levels where radial vein fractures do exist. On these lower levels, pebble dikes have the northwest and northeast trends of late regional faults in the district and do not occupy the radial vein set except in areas where this trend is parallel to the northwest or northeast directions. Evidently the radial set of fractures was open near

the surface at the time of pebble-dike formation but was not open at depth.

There is a striking decrease in the abundance of pebble dikes from the surface downward, especially below the Hornitos unconformity at roughly 2,800-m elevation. Many pebble dikes seem simply to terminate downward. In other areas, especially where parallel swarms of pebble dikes on the surface overlie single major pebble dikes at depth, a splitting of the major dikes upward is implied.

Very close relationships between latite dikes and pebble breccias have been noted in a number of exposures (Fig. 12). The margins of latite are usually faulted and occupied by pebble dikes. Round, polished pebbles plucked from the pebble dikes are occasionally included in latite, and in at least one instance a pebble dike is clearly truncated by latite. On the other hand, pebble dikes locally contain completely isolated but unrounded fragments of latite. Latite dikes also favor northwest-trending faults, which are the principal loci of the deep pebble dikes.

On deep levels, pebble dikes are relatively fresh, with weak calcite and chlorite alteration of their matrix material. Near the surface, many pebble

dikes ob-
vanced a
nonsilice
alteration
dikes.]
pebble d
different
roughly
episodes

Geochem

Some
able expo
presented
samples
trusive t
represent

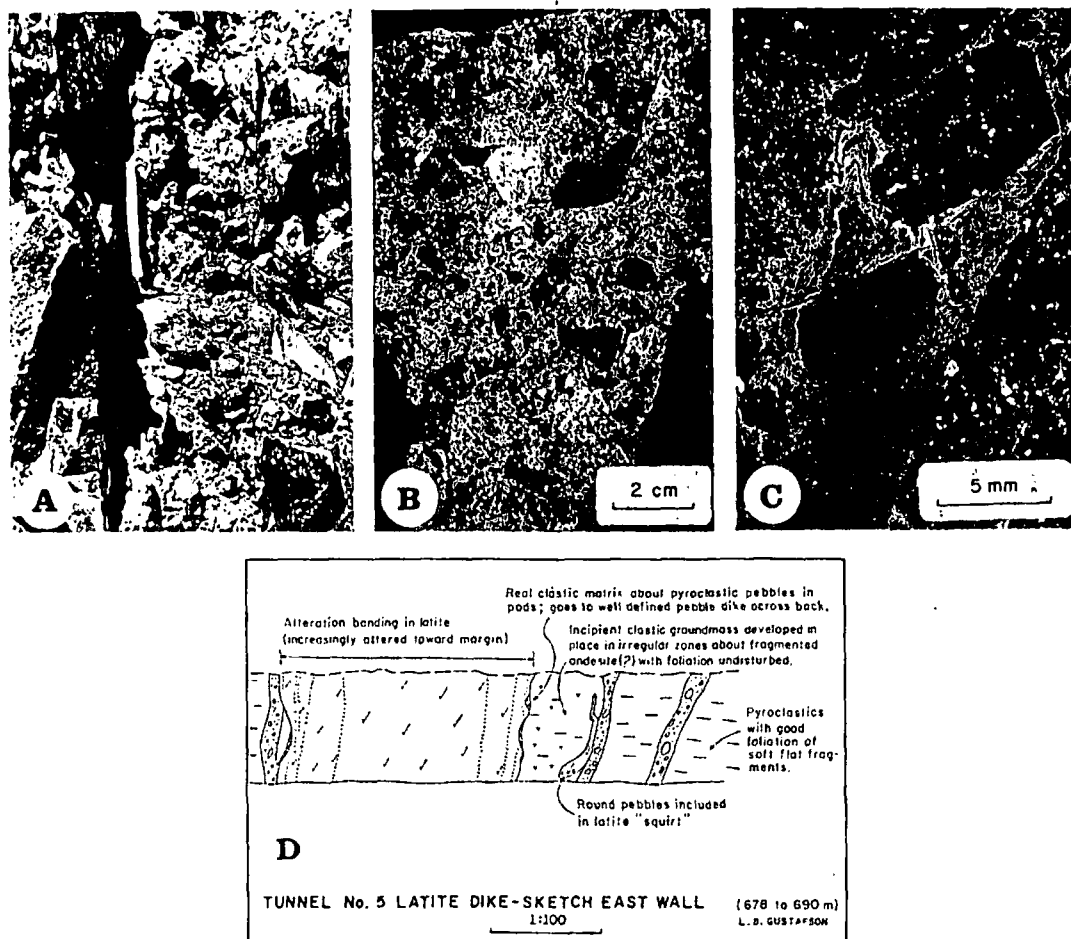


FIG. 12. Pebble breccias and latite dikes.

A, Surface exposure, showing rounded pebbles in sandy clastic matrix. At high elevations, most pebble dikes are altered to advanced argillic assemblages.

B, Sawed specimen of pebble dike from the deepest level. Subangular to round porphyry pebbles are not altered.

C, Photomicrograph of the clastic matrix of a pebble dike showing flow banding.

D, Sketch of a drift wall, showing close spatial association and contradictory age relationships between pebble dikes and latite dikes.

dikes obviously guide very intense sericitic and advanced argillic alteration. A few younger, relatively nonsiliceous pebble dikes lacking advanced argillic alteration cut siliceous and highly altered pebble dikes. This and the fact that the younger and older pebble dikes can be interpreted as belonging to two different radial sets about two different centers, roughly 600 m apart, suggests at least two distinct episodes of pebble-dike formation.

Geochemistry of the intrusive rocks

Some chemical analyses of the least altered available exposures of intrusive rocks at El Salvador are presented in Table 1. In most cases, only single samples of each rock were analyzed. The one intrusive unit, "L" Porphyry, which was sampled to represent the range of textural variants, shows a

wide compositional variation in most elements, illustrating the problem of adequately sampling these rocks. An even more serious sampling problem is the fact that truly fresh samples of the mineralized rocks are not exposed. Unaltered samples can be obtained only of postmineral intrusive rocks or so far away from the center of mineralization that correlation with the mineralized rocks is uncertain.

With these qualifications in mind, we tentatively conclude from these data that the early rhyolites are more siliceous and have higher K_2O/Na_2O ratios than the granodiorite porphyries associated with the main period of mineralization. Later dikes ("A" Porphyry and latite) appear to have still lower silica, higher iron, and possibly higher alumina contents than earlier intrusive rocks. Compared with Daly's and Nockolds' granodiorites (Poldervaart, 1955),

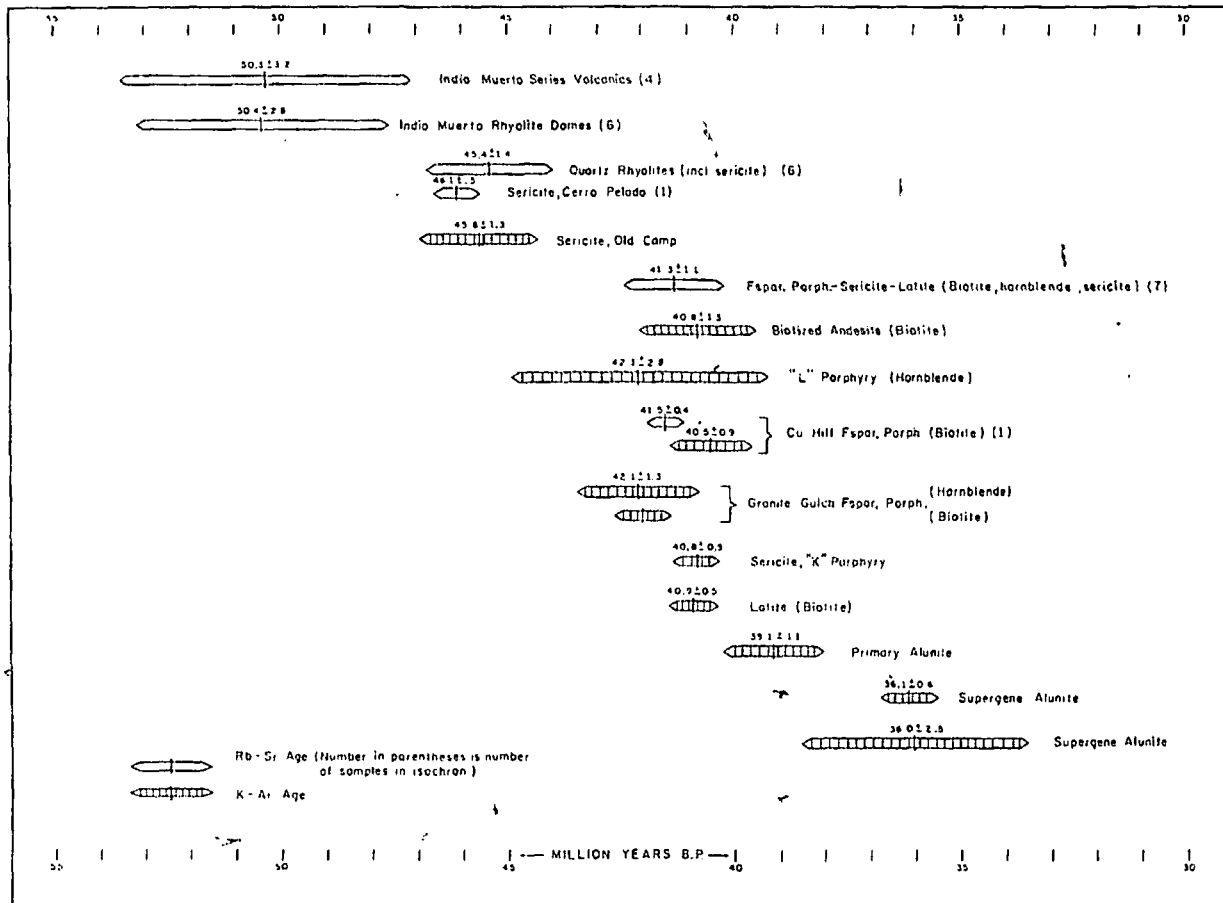


FIG. 13. Selected radiometric age dates, Indio Muerto district.

the freshest El Salvador granodiorites (i.e., "L" Porphyry) are on the low side but within "normal" limits for silica, lower in total iron, and have lower K_2O/Na_2O ratios. Relatively consistent compositional trends within "L" Porphyry correlate with textural variation. Approaching andesite contacts from high-groundmass areas, there is a decrease in SiO_2 and K_2O and an increase in Al_2O_3 , CaO , Na_2O , total Fe, MgO, and TiO_2 . This corresponds to the increase in plagioclase and biotite (and/or hornblende) and decrease in quartz and alkali feldspar. Reaction with the andesitic host rocks is indicated, but insufficient work has been done to define the processes involved.

Radiometric Age Dating

The "absolute" ages of events attending formation of the El Salvador ore deposit have been rather well documented by extensive radiometric dating. In all, 37 independent age determinations have been made by K-Ar and Rb-Sr methods on whole rocks, biotite, hornblende, sericite, alunite, and jarosite. Several of these determinations were duplications by differ-

ent methods and different laboratories on the same specimen. Most of the dates were determined by Christopher Brooks at the Carnegie Institution's Department of Terrestrial Magnetism and at Montreal University. The results presented in Figure 13 are considered to be the most reliable. Determinations considered to be geologically impossible or which have been superseded by more geologically consistent determinations have been discarded and are not shown.

Rubidium-strontium techniques were required to read through later thermal events to define the time gap between the two series of rhyolite domes and the main porphyry series. An age of about 46 m.y. is well established for the quartz rhyolite on Cerro Pelado and Rhyolite Hill and for the sericite alteration in the Cerro Pelado center. Six whole-rock specimens of quartz rhyolite yield an isochron of 45.4 ± 1.4 m.y., with an initial strontium ratio of 0.7040. Included in this isochron are two specimens altered to sericite, indicated by geologic mapping to be closely related in space and apparently also in time to the intrusive event. The most Rb-enriched

of these seri
 46.1 ± 0.5 m
 0.7040 is us
 m.y. on seri
 geologic arg
 intrusion of
 quartz rhyoli
 in these intr
 volcanic even
 low age for t
 mesh) fracti
 The $50.4 \pm$
 Rhyolite dom
 mens of petr
 are included
 suggest that
 significant e
 domes but d
 tive age of tl



FIG.
 A, porph
 "K".
 B, whic
 than
 abund
 C, dissen
 super
 D, "K"
 is mu

of these sericite specimens yields a mineral age of 46.1 ± 0.5 m.y. when an initial strontium ratio of 0.7040 is used. A single K-Ar age of 45.6 ± 1.3 m.y. on sericite from the Old Camp supports the geologic arguments previously presented that the intrusion of quartz porphyry is closely related to the quartz rhyolite volcanic event and that mineralization in these intrusive centers is closely related to the volcanic events. To avoid obtaining an anomalously low age for this specimen, all but the coarsest ($+100$ mesh) fraction of the sericite had to be separated out.

The 50.4 ± 2.8 m.y. age on the early Indio Muerto Rhyolite domes is less well established. Six specimens of petrologically similar but separated masses are included in a single isochron. Geologic relations suggest that the quartz rhyolites were emplaced after significant erosion of the Indio Muerto Rhyolite domes but do not conclusively prove even the relative age of the different rhyolites. The inclusion of

all rhyolites (with and without quartz eyes) in a single isochron yields 45.1 ± 1.1 m.y. The selection of the 50 m.y. age as most probable is a matter of geologic judgment, and the indicated approximately 5 m.y. time gap between the two rhyolite events cannot be considered firmly established. The 50.3 ± 3.2 m.y. isochron on Indio Muerto series volcanics includes four whole-rock samples of rhyolitic flows and ignimbrite from the thick volcanic sequence on the hills southeast of Indio Muerto. The indicated initial strontium ratio of 0.7041 is very close to all other initial strontium ratios in the district.

K-Ar ages in the Turquoise Gulch center for biotites from early-stage alteration to the postmineral latite dikes, for hornblende from three feldspar porphyries, and for alteration sericite all fall close to 41 m.y. Rb-Sr analyses of the same specimens define an isochron at 41.3 ± 1.1 m.y., with an initial strontium ratio of 0.7042. The single biotite sufficiently

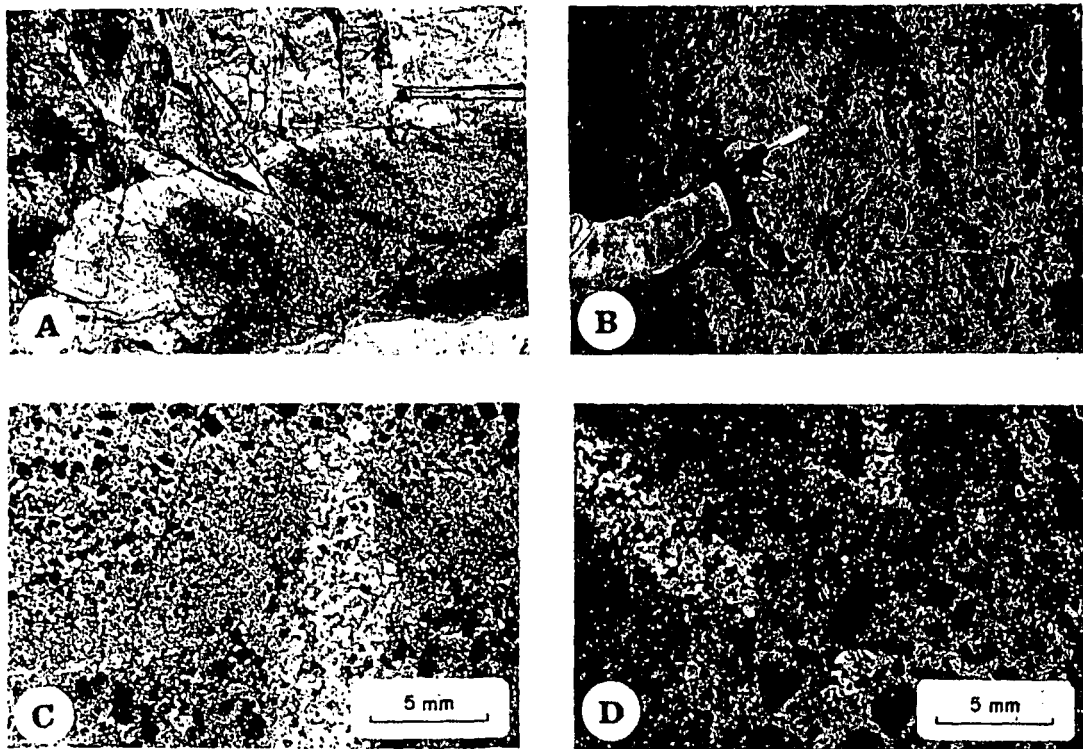


FIG. 14. Relations at intrusive contacts between feldspar porphyries.

A. Contact between "L" Porphyry (below) and "K" Porphyry (above). Younger "L" has a clean porphyry texture, is weakly altered, and contains much less quartz veining and sulfides than the older "K". Bleaching is due to supergene kaolinization, extending only a short distance into "L" Porphyry.

B. Intrusive contact within the "K" Porphyry mass. Older rock (right) contains many quartz veins which are truncated at the contact, although many other quartz veins of this same Early type are younger than the intruding porphyry. Both rocks are strongly altered to K-silicate assemblages and contain abundant chalcopyrite-bornite, although alteration of the older rock is more intense.

C. Thin section of "L" Porphyry (above)—"K" Porphyry contact. Truncated early quartz vein with disseminated chalcopyrite-bornite extends into chilled margin of "L" Porphyry. Feldspars are altered to supergene kaolinite. (Cross-polarized light)

D. Thin section of early quartz veins in "K" Porphyry (above), truncated and included by younger "K" Porphyry. Degree of K-silicate alteration, as indicated by degree of obliteration of porphyry texture, is much stronger in the older rock. Supergene kaolinization of plagioclase. (Cross-polarized light)

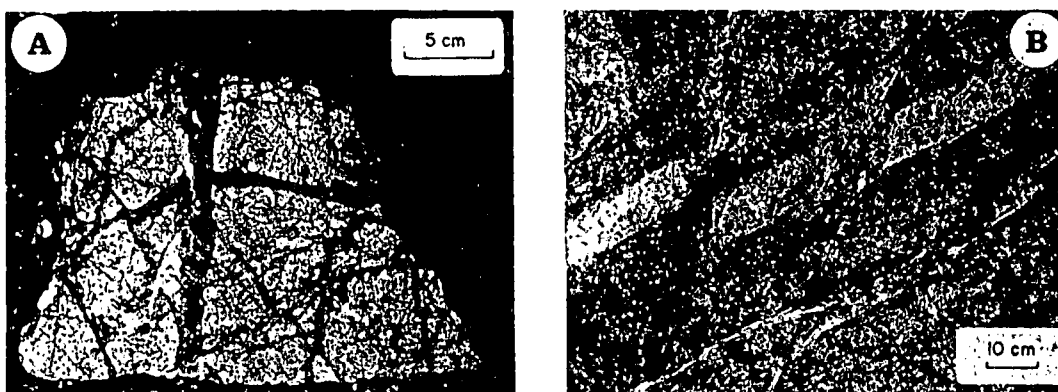


FIG. 15. Vein types at El Salvador.

A. Continuous vertical "B" vein, with relatively coarse quartz and sparse sulfide, cuts less continuous "A" veins, which are dark because of abundant disseminated sulfides and fine granular habit. Rock is "X" Porphyry bleached by supergene kaolinization.

B. Two steep "D" pyrite-chalcocite veins with sericite halos cut a 10-cm "L" Porphyry dike within "K" Porphyry. The veins have characteristically little quartz, and one occupies a small fault. Rock is bleached by supergene kaolinization.

enriched in Rb to provide an independent mineral age is calculated to be 41.5 ± 0.4 m.y. old. It is apparent that the ages of mineralization events of the main Turquoise Gulch area are indistinguishable within the analytical accuracy of the combined dating techniques. All appear to have been compressed within a period of less than one million years. The initial $^{87}\text{Sr}/^{86}\text{Sr}$ ratios for all isochrons, including the group of Indio Muerto volcanics, are remarkably consistent at 0.7041 ± 0.0003 m.y.

Alunite from primary advanced argillic alteration was formed essentially contemporaneous with the intrusion of latite. The 39.1 ± 1.1 K-Ar age on this alunite is therefore slightly anomalous but does indicate the general amenability of alunites to K-Ar dating. The roughly 36 m.y. ages of supergene alunites could probably therefore be considered minimum ages. The main period of supergene oxidation and enrichment probably followed no more than 5 million years after the hypogene event. Attempts to date jarosite in leached capping yielded ages that are much too young. Five samples indicate ages less than 21 m.y., with two indicating ages younger than the 10 to 13 m.y.-old gravels capping the erosion surface which truncates the enrichment blanket. It is apparent that even coarse crystalline jarosite does not retain argon well enough to be useful for K-Ar dating.

Relative Age Relations

Most of our understanding of the evolution of mineralization and porphyry intrusion has stemmed from surface and underground mapping on a 1:500 scale, especially in the areas of intrusive contacts. The underground exposures in closely spaced haulage and grizzly drifts were particularly valuable in ac-

curately working out the detailed three-dimensional geometry. Many kilometers of the back and walls of underground workings were scrubbed with detergent and wire brushes to reveal details. In many places, 1:100-scale notes were also taken to supplement the regular 1:500-scale observations. Mineralogic detail was mapped using a color code.

It has proved to be very important to differentiate primary "background" features from those features clearly related to later throughgoing veins and other structures. Background features include mineralization which is disseminated or occurs on small discontinuous veins and seams, and associated pervasive alteration. The distinction is generally unambiguous in deep central zones where hydrothermal veins with K-feldspar-destructive alteration halos are clearly superimposed on background mineralization characterized by K-silicate alteration assemblages and contrasting sulfide assemblages. However, the distinction is far from straightforward in peripheral and in high-elevation mineralization zones where background mineralization and alteration assemblages are commonly indistinguishable from the structurally controlled assemblages.

The superposition of supergene alteration and mineralization patterns on primary assemblages presents another obstacle to correct interpretation. At El Salvador, we were greatly aided by the exposure of a deep central sulfate zone, completely free of supergene effects, in which to study deeper primary patterns. The sulfate zone, which will be discussed in more detail subsequently, is a zone in which the rock is thoroughly impregnated with anhydrite and into which supergene solutions have not penetrated because of extremely low porosity and permeability.

Detailed
the contact
strong evid
relationship
mineralizat
contact bet
15B show
Porphyry.
the porphy
cation of
(Figs. 14C
strong con
mineralize
phyry, wh
assemblage
chalcopyrit
assemblage
clear that
tion, and
was acco
Porphyry.
veins with
Table 2)
ment, cut
ally within
separate li
range of
quartz vei
demonstra
tion were
porphyry
the empla

E:

The E
were larg
the last r
are chara
and mine
with stal
pyrite-bo
pyrite an
veins and
dor perha
emplaced
ation and

"A" quar

Quartz
scribed a
family of
trusive c
have bee
15A, 16,
assembla
chalcopy

Detailed mapping of underground exposures of the contacts between the porphyries has provided strong evidence of an extremely close time and space relationship between the processes of intrusion and mineralization. Figures 14A and 14C show a major contact between "L" and "K" Porphyries, and Figure 15B shows a dike of "L" Porphyry cutting "K" Porphyry. The intrusive nature and relative ages of the porphyries are clearly demonstrated by the truncation of many early quartz veins at such contacts (Figs. 14C and 14D). At this contact, there is a strong contrast between the nearly fresh, very weakly mineralized "L" Porphyry and the older "K" Porphyry, which has been intensely altered to K-silicate assemblages characterized by alkali feldspar, biotite, chalcocopyrite, and bornite. The change in mineral assemblage is abrupt at the intrusive contact. It is clear that most of the primary alteration, mineralization, and emplacement of quartz veins at this point was accomplished before the intrusion of the "L" Porphyry. Some quartz veins and all later sulfide veins with hydrolytic alteration halos (Fig. 15B and Table 2) as well as supergene alteration and enrichment, cut across such contacts. Other contacts, especially within the "K" Porphyry complex (Fig. 14B), separate lithologically similar porphyries with a wide range of intensity of alteration, mineralization, and quartz veining. Mapping of relative age relations has demonstrated that the early processes of mineralization were imposed upon each successive surge of porphyry magma and its wall rocks before and after the emplacement of the next surge.

Early Alteration and Mineralization

The Early alteration and mineralization, which were largely accomplished before the intrusion of the last major feldspar porphyry ("L" Porphyry), are characterized by distinctive types of quartz veins and mineral assemblages. Alteration assemblages with stable alkali feldspar and biotite and chalcocopyrite-bornite or chalcocopyrite-pyrite with antithetic pyrite and bornite are characteristic of both the quartz veins and background mineralization. At El Salvador perhaps as much as 75 percent of the copper was emplaced during this Early time of K-silicate alteration and low-sulfur sulfide mineralization.

"A" quartz veins

Quartz veins at El Salvador were originally described and classified by Langerfeldt (1960). The family of Early quartz veins, often truncated at intrusive contacts by "X", "K", and "L" Porphyries, have been called "A" veins. As illustrated in Figures 15A, 16, and Table 2, "A" quartz veins are granular assemblages of quartz, perthitic feldspar, anhydrite, chalcocopyrite, and bornite. Pyrite, with chalcocopyrite

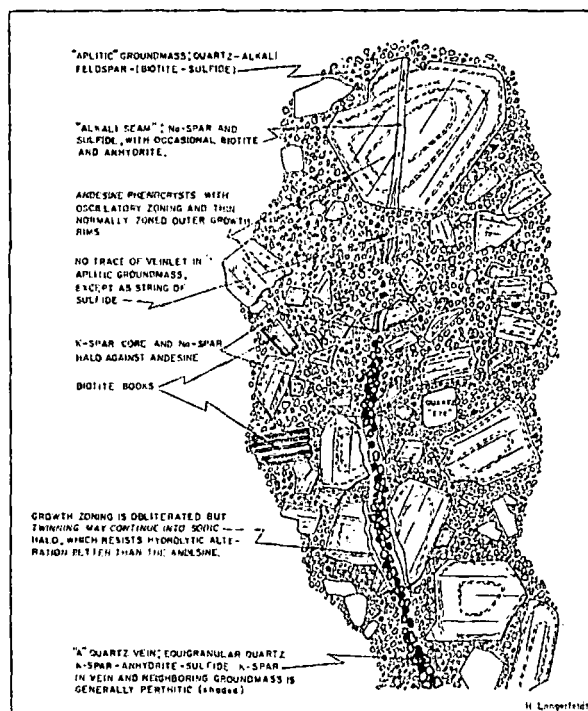


FIG. 16. Composite idealized sketch of an "A" quartz veinlet in feldspar porphyry, showing gradational relationships between "A" veinlets and "alkali seams." No single actual occurrence shows this complete range of variation. After H. Langerfeldt.

but never with bornite, occurs in "A" veins only near the edges of the deposit. Alteration halos about these veins are practically indistinguishable from the strong background K-silicate alteration with which these veins are typically associated. Where they cut less pervasively altered rock, perthitic K-feldspar, anhydrite, chalcocopyrite, and bornite form in halos along with recrystallized quartz, biotite, and accessory apatite and rutile. With the rare exception of K-feldspar-andalusite alteration halos (see below), there is no hydrogen-ion metasomatism about these Early quartz veins. They are cut by all other veins.

The oldest "A" quartz veins are typically very irregular, discontinuous, and segmented. This is not only because they have been subjected to multiple shearing, segmentation, and recrystallization but because many apparently never formed with parallel walls. The fractures occupied by these veins appear to have been formed before the rock was able to sustain continuous brittle fracture. The K-feldspar, sulfides, and anhydrite in "A" veins occur as disseminated grains with the same sizes and shapes as the associated quartz. Successively younger "A" veins tend to have more parallel walls and to occupy more continuous and systematically oriented breaks. A few of these tend to have some internal symmetry, which is lacking in earlier types, with the K-feldspar

TABLE 2. Vein Types at El Salvador

Silicate Assemblage and Texture	Alteration Halo	Age and Structural Style	Sulfide Assemblage and Texture	Fluid Inclusions
<p>"A" Veins Quartz-K-spar-anhydrite-sulfide with rare traces biotite; quartz ranges from 50% to 95%. The K-spar is usually perthitic. The fine equigranular texture of quartz is shared by the other minerals which are evenly disseminated through the vein. No vein symmetry is typical, but banding of K-spar at the edges or center is not uncommon. More or less sutured contacts between quartz and K-spar are common.</p>	<p>Halos of K-spar, usually perthitic, are more or less developed about most veins. These may be very thin and inconspicuous, especially in strong K-silicate altered rock. They are strongest and most obvious about late veins in relatively fresh rock.</p>	<p>"A" quartz veins are the earliest of all veins, invariably cut by "B" quartz veins. Repeated "A" vein formation started prior to the intrusion of "X" Porphyry and persisted after emplacement of the "L" Porphyry complex. The earliest veins are most randomly oriented and discontinuous, commonly segmented and "whispy." Widths usually range from 1 to 25 mm, and strike continuity from centimeters to a few meters.</p>	<p>Disseminated chalcopyrite-bornite, with proportions usually similar to the background sulfide; traces of molybdenite locally.</p>	<p>Extremely abundant; both high-salinity (I) and low-density (II) types.</p>
<p>"B" Veins Quartz-anhydrite-sulfide, with K-spar characteristically absent. The quartz is relatively coarse grained and tends to be elongated perpendicular to the walls, occasionally approaching "cockscorn" texture. Granular quartz, especially in sheared bands, is common. Vein symmetry, of sulfides, anhydrite or granularity along centerlines, margins or irregular parallel bands, is typical but unevenly developed.</p>	<p>Lack of alteration halos is characteristic. Occasionally faint and irregular bleached halos are present, but most are probably due to superimposed veining.</p>	<p>Younger than "A" veins and older than "D" veins. "B" veins cut all intrusive rocks except Latite. They are characteristically regular and continuous, and tend to have flat attitudes. Widths usually range from 5 to 50 mm, and strike continuity from meters to tens of meters.</p>	<p>Molybdenite-chalcopyrite is characteristic. Traces of bornite occur in some, but more commonly minor pyrite occurs in contrast to bornite-chalcopyrite in the walls. Sulfides tend to be coarse grained and occupy banding parallel to the walls or cracks perpendicular to them.</p>	<p>Abundant, both high-salinity (I) and low-density (II) types. In some veins with drusy centerlines, the youngest quartz contains markedly fewer inclusions which tend to be of low salinity (type III).</p>
<p>"D" Veins Sulfide-anhydrite with minor quartz (except where superimposed on "B" veins) and occasional carbonate. The quartz is typically free of inclusions, and tends to show crystal form. Anhydrite locally forms coarse crystalline masses and is commonly banded with the sulfides.</p>	<p>Feldspar-destructive halos are characteristic, but patterns vary and have not been well documented. Sericite or sericite-chlorite halos may or may not have outer kaolinite-calcite halos.</p>	<p>"D" veins cut all "A" and "B" quartz veins, but are almost entirely older than pebble dikes. They are continuous, though locally irregular and "lacing," and occupy systematic structure patterns. Widths usually range from 1 to 75 mm, and strike continuity from meters to tens of meters.</p>	<p>Pyrite is usually predominant, with chalcopyrite, bornite, enargite, tennantite, sphalerite and galena common. Minor molybdenite and many other sulfides occur locally. "Reaction" textures are typical.</p>	<p>Only sparse low-salinity (III) inclusions are seen in quartz, anhydrite and sphalerite.</p>

Note. Textural characteristics and sulfide assemblages given are those of typical veins in the main mineralized center (background chalcopyrite-bornite zone). Gradations between types and zonal variations are seen.

L. R. GUSTAFSON AND J. P. HUNT

concentrat
veinlets.
coarsely g
tern, with
sulfide relic
symmetry
of mineral
The dist
levels is sh
tional "B"
included in
ally in at
Quartz ve
the rock ve
percent in
K-silicate
K-silicate
of Early al
K-feldspar
this assem
very abun
ubiquitous
and Na-fel
mon assoc



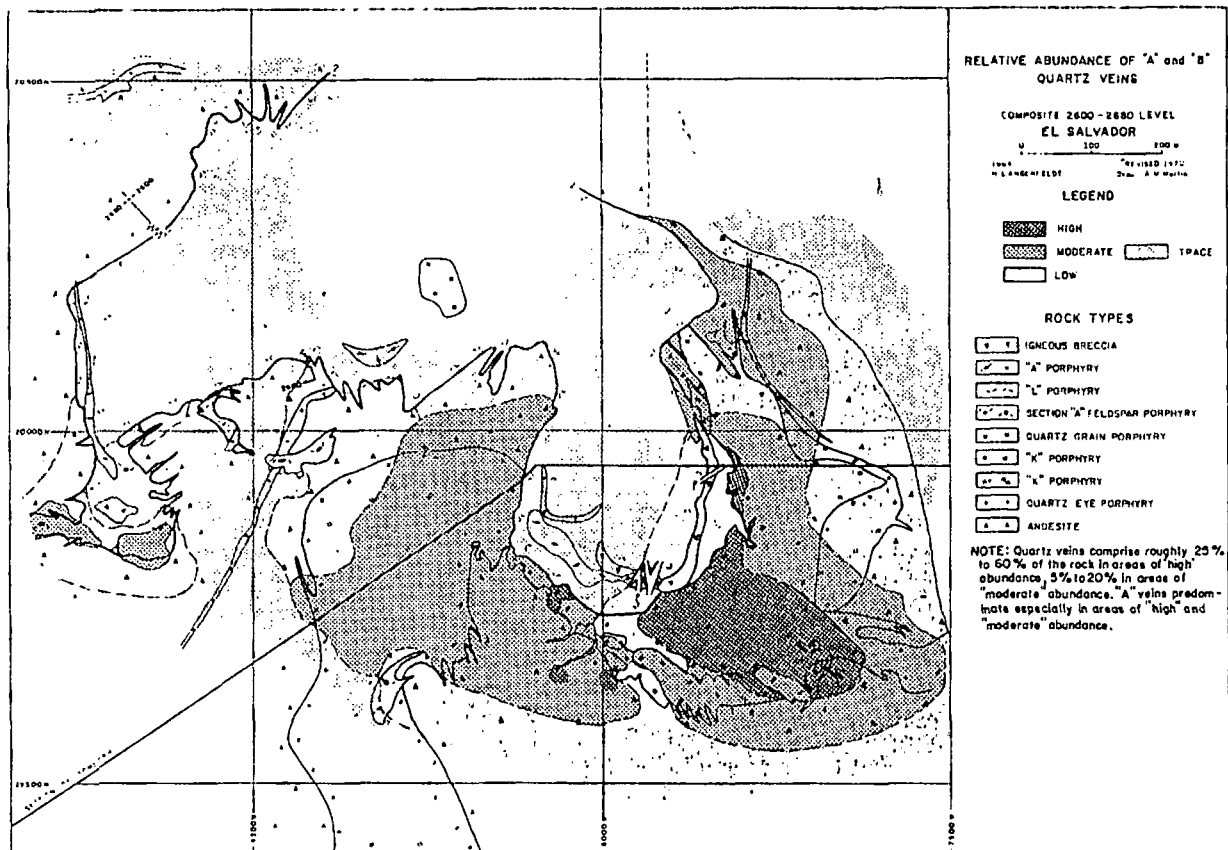


FIG. 17. Relative abundance of "A" and "B" quartz veins at the 2,600- and 2,660-meter levels.

concentrated along center lines or margins of the veinlets. Quartz is more abundant and usually more coarsely granular. There seems to be a zonal pattern, with decreasing proportions of K-feldspar and sulfide relative to quartz and more common internal symmetry upward and outward beyond the center of mineralization.

The distribution of quartz veins on the 2600-2660 levels is shown in Figure 17. Although some Transitional "B" veins (Fig. 15A and Table 2) have been included in this map, "A" veins predominate, especially in areas of high and moderate abundance. Quartz veins make up roughly 25 to 60 percent of the rock volume in areas of high abundance, 5 to 20 percent in areas of moderate abundance.

K-silicate alteration and perthitic groundmass

K-silicate alteration assemblages are characteristic of Early alteration and mineralization at El Salvador. K-feldspar and biotite are the essential minerals in this assemblage, with quartz ubiquitous and usually very abundant. At El Salvador, anhydrite is also ubiquitous (where not removed by supergene action), and Na-feldspar, chlorite, and minor sericite are common associates. Characteristically absent are kao-

linite, pyrophyllite, alunite, zeolites, and montmorillonites. The component minerals are essentially the same as those usually formed in the last stage of magmatic crystallization.

With increasing intensity of K-silicate alteration, there is an increasing degree of replacement of original plagioclase. Phenocrysts and groundmass feldspar are replaced by perthitic alkali feldspar. Replacement of the plagioclase about its rims and along crosscutting cracks and veinlets is commonly zoned. Sodite plagioclase (probably oligoclase) typically separates unreplaced andesine from perthitic K-feldspar. This alteration tends to obliterate the euhedral outlines of the plagioclase phenocrysts (compare altered rock types in Figure 8 with fresh-rock equivalents in Figure 7). Coarsening and development of perthitic feldspar in the groundmass accompany this replacement (Fig. 10B). Development of this perthitic groundmass is locally seen as halos about early quartz veins and veinlets, where it is clearly an alteration feature formed after consolidation of the groundmass.

Strong K-silicate alteration destroys magnetite and hematite-rutile intergrowths after ilmenite. Bulk chemical analyses show that there is a net removal

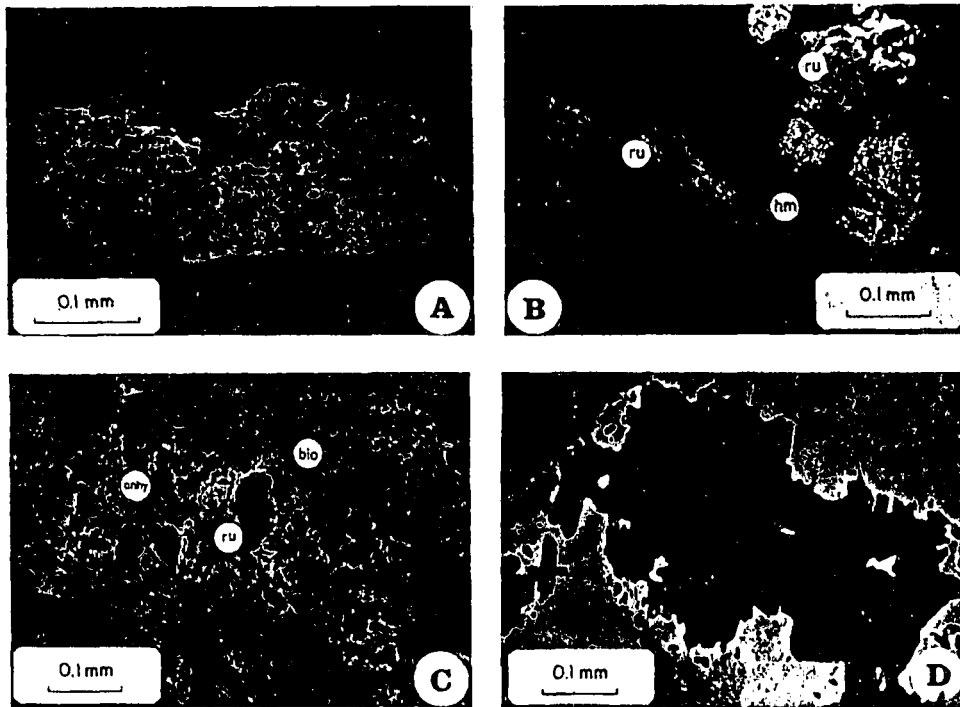


Fig. 18. Textures of Fe-Ti oxides.

A, Intergrowth of hematite-rutile after ilmenite. Incipient oxidation of ilmenite produces hematite-rutile intergrowths oriented along basal or rhombohedral planes of the parent mineral, but more complete separation of phases into this anhedral granular intergrowth apparently represents a common tendency toward textural equilibrium. (Reflected light)

B, Magnetite completely replaced by hematite (white). The octahedral orientation of this marmitic texture is characteristic of supergene oxidation. The rutile (light gray) "sponges" are formed on removal of hematite from hematite-rutile intergrowths. This hypogene alteration of hematite-rutile intergrowths is accompanied by destruction of magnetite, except in a transitional zone from which this specimen was taken. (Reflected light)

C, Granular intergrowth of rutile, anhydrite, and quartz, presumably derived by alteration of sphene. The rock is "X" Porphyry, which contains hematite-rutile after ilmenite and biotite after hornblende. (Transmitted light)

D, Rutile cluster (medium grain) with pyrite (black), presumably derived by sulfidation of hematite-rutile after ilmenite. In other specimens with incomplete replacement of hematite, there are no hematite-pyrite contacts, hematite apparently being dissolved ahead of the front of pyrite precipitation. (Transmitted light)

of iron from the rock rather than a simple accommodation of the iron in biotite and sulfides. The TiO_2 remains as granular rutile (Fig. 18).

Evidence that these same alteration effects are also operative before final consolidation of the porphyry melt has been seen locally at intrusive contacts between surges of "K" Porphyry. Within a zone a few centimeters wide, the following changes are observed within the intruding rock, going from the main mass into a zone of reaction with the older rock. The feldspar porphyry texture becomes obliterated through replacement of plagioclase phenocrysts by perthite and oligoclase. Mafic phenocrysts, biotite books, and biotized hornblendes are resorbed or replaced by perthite-quartz containing inclusions of rutile and oriented residuals of biotite. The "aplitic" groundmass (Fig. 10A) becomes coarser and more ragged and perthitic. As the groundmass gets coarser and more perthitic, clear K-feldspar and

sodic plagioclase disappear. Magnetite and hematite-rutile disappear, leaving only rutile with no evidence of anything replacing them, except probably groundmass silicates. The abundance of Early quartz veins in the rock increases. These veins are typically segmented, and some appear to be the last undigested remnants of the intruded rock.

Biotization of andesite

K-silicate alteration in andesite takes the form of a broad halo of biotization about the porphyry intrusions (Fig. 19B). The basic mineral assemblage is biotite-sodic plagioclase-anhydrite-quartz. Accessory minerals are Fe-Ti oxides, sulfides, minor apatite, and zircon.

At the outer edge of the biotized zone, roughly 500 to 1,000 m from the main intrusive contacts, biotization is not megascopically recognizable, but biotite is present as very fine grained flakes restricted

to the matrix is well preserved.

Closer to intensity of of megascopic product intense biot rock is usually granular assemblage drite, and quartz crystals may with biotite chlorite, and from biotized zones, and vicinity of "

Propylitic al

Weak presence about the m originally no more detail rocks are n constituents of chlorite, calc present as p by structure product dissolved also an abundant in and thermal alteration

Beyond the sulfide mineral magnetite, n growths of locally ilmenite hematite: Near the out seminated chlorite after p Chlorite does contrast to this, most of the biotite-chalcopyrite alteration. F tion halos are pyrite veinlets rutile, and a seminated with

Alteration of

Hornblende only in deep biotized zone placement to

to the matrix of the rock. The original rock texture is well preserved.

Closer to major intrusive contacts, the increasing intensity of biotization is marked by the appearance of megascopically recognizable biotite as an alteration product of intermediate plagioclase. In areas of intense biotization close to intrusive contacts, the rock is usually entirely recrystallized to a fine equigranular assemblage of biotite, Na-plagioclase, anhydrite, and quartz. A few residual plagioclase phenocrysts may remain, but these are usually altered with biotite, anhydrite, and occasionally sericite, chlorite, and calcite. K-feldspar is generally absent from biotized andesite, except in strongly mineralized zones, and is generally restricted to the immediate vicinity of "A" quartz veins.

Propylitic alteration

Weak propylitic alteration forms a green fringe about the mineralized zones at El Salvador, as was originally noted by Swayne and later described in more detail by Eckstrand (1967). The propylitized rocks are mostly andesitic flows and sedimentary rocks of the Cerrillos formation. Characteristic constituents of the propylitic assemblages are epidote, chlorite, calcite, quartz, and plagioclase. They are present as pervasive alteration and are controlled by structures. Calcite is abundant as an alteration product disseminated in the rocks and in veins and is also an abundant and possibly original cementing material in andesitic sediments well beyond any hydrothermal alteration.

Beyond the outer limits of biotization and pyritic sulfide mineralization, iron and titanium oxides are magnetite, more or less altered to hematite, intergrowths of magnetite-rutile, hematite-rutile, and locally ilmenite. Veinlets of epidote-calcite-specular hematite are present with epidote alteration halos. Near the outer limits of the zone of biotization, disseminated chlorite is present with fine-grained epidote after plagioclase grains and in tiny veinlets. Chlorite does not appear to replace biotite, in contrast to this characteristic replacement sequence in most of the biotized zone. Veins of epidote-magnetite-chalcopryrite are associated with the chloritic alteration. Pyritic veins with sericite-chlorite alteration halos are later than epidote-magnetite-chalcopryrite veinlets. Fe-Ti oxides are converted to pyrite-rutile, and a small amount of chalcopryrite is disseminated within the sericitic alteration halos.

Alteration of hornblende and Fe-Ti oxides

Hornblende, ilmenite, and sphene are preserved only in deep levels within "L" Porphyry. Hornblende phenocrysts are present in all stages of replacement to assemblages of biotite-anhydrite-rutile.

Clusters of "shreddy" biotite with rutile and anhydrite occur throughout higher exposures of "L" Porphyry and much of the "X" and "K" Porphyries and suggest original sites of hornblende phenocrysts. In "L" Porphyry in which hornblende is partially altered, ilmenite is seen to be partially replaced by an intergrowth of hematite, and rutile (Fig. 18). This reaction seems to be a simple oxidation reaction: $2 \text{FeTiO}_3 + 1/2 \text{O}_2 \rightarrow \text{Fe}_2\text{O}_3 + 2 \text{TiO}_2$. Sphene is pseudomorphically replaced by an intergrowth of rutile and anhydrite, apparently as a result of the reaction, $\text{CaTiSiO}_5 + \text{SO}_3 \text{ sph.} \rightarrow \text{TiO}_2 + \text{CaSO}_4 + \text{SiO}_2 \text{ sph.}$. Silica released in this reaction does not seem to be fixed in place as quartz. Ilmenite partially replacing sphene in a few specimens is apparently part of an unknown earlier reaction. Of 20 specimens of "L" Porphyry with hornblende, only 2 do not also contain ilmenite. Only two specimens with ilmenite but no hornblende have been seen. Minor sphene is present in several of these specimens but in practically no others. Apparently there are three concomitant reactions: biotization of hornblende, oxidation of ilmenite, and destruction of sphene. Pseudomorphic replacement products of ilmenite and sphene as well as hornblende are seen at higher elevations in the well-mineralized porphyries and "L" Porphyry. These replacements appear to be the earliest (at any given point) and deepest manifestations of K-silicate alteration.

Alkali seams

In weakly mineralized "L" Porphyry, a large proportion of the sulfides are present in alkali seams, small veinlets marked primarily by alteration halos of alkali feldspar where they cut plagioclase phenocrysts (Fig. 16). Only where alkali seams contain appreciable biotite, anhydrite, and (or) sulfide are they usually traceable through the groundmass. Sericite, either within the seam or as a halo about it, is present in those alkali seams that contain pyrite but is usually absent where there is no pyrite. Traces of apatite are occasionally seen in alkali seams in areas of somewhat stronger mineralization, as in "K" Porphyry. A gradation between alkali seams and "A" veins is suggested, although no single specimen displays a complete range of gradation between the two. Extensions of small "A" quartz veins across plagioclase phenocrysts commonly show zoned reaction halos, with K-feldspar separated from the plagioclase by a rim of more sodic plagioclase.

Anhydrite mineralization

Anhydrite is among the earliest and latest products of mineralization and, in fact, spans the entire history of mineralization at El Salvador. The bulk of the early anhydrite is disseminated and is a character-

istic component of "A" quartz veins and K-silicate alteration assemblages. Later anhydrite is dominantly fracture controlled and is a characteristic product of all younger veins. Thus, depending on timing, anhydrite is an associate of a wide variety of mineral assemblages. These include early feldspar and biotite-stable, low-sulfur, chalcopyrite-bornite and chalcopyrite-pyrite suites and later feldspar-destructive, sericite-bearing (and even andalusite-bearing) alteration assemblages with abundant pyrite.

Within the sulfate zone, disseminated anhydrite accounts for more total sulfur than all sulfides combined. The abundance of anhydrite is greatest in andesitic host rocks (5 to 10 percent by volume) and declines in successively younger intrusive rocks (1 to 5 percent by volume). The anhydrite content of wall rocks apparently reflects both the original available calcium content and the intensity and duration of the mineralizing processes to which the rocks were exposed. There is a rough inverse correlation between the abundance of anhydrite and the abundance of residual calcic plagioclase and hornblende. Replacement of plagioclase by alkali feldspar, sericite, and andalusite and replacement of hornblende by biotite are believed to have been the principal anhydrite-fixing reactions.

Anhydrite-impregnated rock, the sulfate zone, has a porosity and permeability of nearly zero and thus forms an effective underground barrier for the movement of ground water (and mine water). With time, however, the upper and outer surfaces of the sulfate zone are attacked by supergene and other ground waters causing first a hydration of primary anhydrite to gypsum and then the dissolution of gypsum, leaching both calcium and sulfate. The supergene removal of anhydrite causes the wall rocks to undergo a significant increase in porosity and decrease in specific gravity, as well as a marked decrease in competency. The present position of the top of the sulfate zone at El Salvador lies below the supergene enrichment blanket and is shown by cross-hatching in Figures 20 and 21.

Disseminated sulfide assemblages and zones

Patterns of sulfide zoning on deep mine levels are illustrated in Figure 19A. These patterns are based on megascopic mapping supported by quantitative as well as qualitative microscopic examination of hundreds of samples. Background assemblages, occurring as disseminations and in small discontinuous fractures, have been carefully separated from assemblages in large throughgoing veins and associated alteration halos. The distinction is important in that the background assemblages define well-developed zonal patterns. The assemblages in younger veins and halos, although containing certain elements

of their own zonal patterns, in general contrast with background assemblages and do not reflect the major zoning. At El Salvador, the background mineralization contains between two-thirds and three-quarters of the total copper of the deposit.

The central chalcopyrite-bornite zone is characterized by an absence of pyrite in the background assemblage, pyrite being present only in younger veins and their halos. The proportion of bornite increases from nil at the outer edge of the zone to greater than 50 percent at the center. Minor primary "chalcocite" is locally present with the bornite near the center. Sulfides constitute from 0.5 to 2.0 percent by volume of the rock, and the copper grade ranges between 0.3% and 1.0% Cu by weight. The trace abundance of gold and silver in the deposit correlates well with the primary abundance of copper. Values greater than 0.005 oz/t Au and 0.050 oz/t Ag are restricted almost exclusively to the central chalcopyrite-bornite zone.

Surrounding the chalcopyrite-bornite zone is a chalcopyrite-pyrite zone from which bornite is absent. The proportion of pyrite in the assemblage increases outward from nil to 75 percent at the outer margin of the zone. Pyrite proportions continue to increase outward through the outer pyrite zone. Total sulfide ranges from 0.75 to 2.5 percent by volume in the chalcopyrite-pyrite zone and varies widely from 0.5 to greater than 6 percent in the pyritic fringe. Primary grades in the chalcopyrite-pyrite zone range from 0.3% to 1.0% Cu by weight and are generally less than 0.2% Cu in the pyritic zone. Where pyrite is more than a small proportion of the total sulfide, it is invariably associated with sericitic alteration, which is clearly superimposed on older K-silicate alteration.

A low-sulfide zone, generally containing less than 0.25 percent total sulfide by volume and usually containing abundant primary Fe-Ti oxides (magnetite and ilmenite or hematite-rutile), is restricted to the late porphyries. Background sulfides are generally too sparse to define consistent sulfide assemblages. Locally, such as at higher elevations in the area where the "L" Porphyry has removed a portion of the central ore zone (Fig. 20A), more abundant sulfides (usually 0.25 to 0.50 percent by volume) define consistent low-intensity chalcopyrite-bornite and chalcopyrite-pyrite zones.

Alteration zoning

The patterns of alteration assemblages associated with the sulfide zones on the 2600 level are shown in Figure 19B. The sulfate zone (stippled on Fig. 19B) includes several of the major alteration zones. The present top of the sulfate zone lies less than 75 m above the level but once extended upward, prob-



FIG. 19. Sulfide and alteration zoning, 2600 level. A, Sulfide zoning. B, Alteration zoning.

20300 N

20000 N






19950





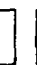
19500 N

19000 N

Section of Isometric

ALTERATION ZONING - 2800 LEVEL

-  Symbol 1: A box with a diagonal line from top-left to bottom-right.
-  Symbol 2: A box with a stippled pattern.
-  Symbol 3: A box with a horizontal line.
-  Symbol 4: A box with a vertical line.
-  Symbol 5: A box with a diagonal line from top-right to bottom-left.

-  Symbol 6: A box with a stippled pattern.
-  Symbol 7: A box with a horizontal line.
-  Symbol 8: A box with a vertical line.
-  Symbol 9: A box with a diagonal line from top-left to bottom-right.
-  Symbol 10: A box with a diagonal line from top-right to bottom-left.

Legend: Symbols 1-5 represent alteration zones defined by the presence or absence of specific alteration minerals. Symbols 6-10 represent alteration zones defined by the presence or absence of specific alteration minerals and the presence or absence of specific alteration minerals.

1. Alteration zone defined by the presence of chlorite and the absence of kaolinite and illite.

2. Alteration zone defined by the presence of kaolinite and the absence of chlorite and illite.

3. Alteration zone defined by the presence of illite and the absence of chlorite and kaolinite.

4. Alteration zone defined by the presence of chlorite and illite and the absence of kaolinite.

5. Alteration zone defined by the presence of kaolinite and illite and the absence of chlorite.

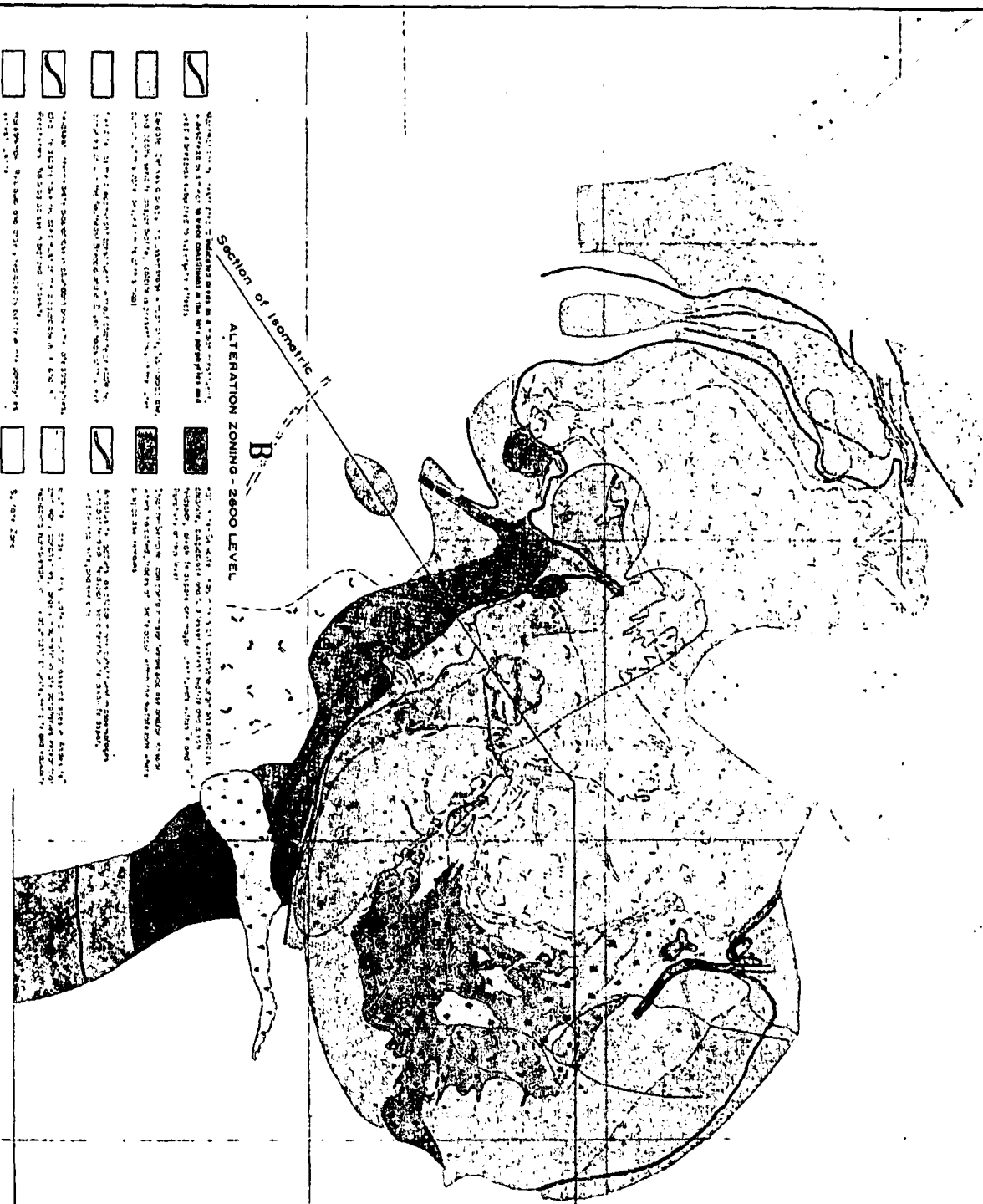
6. Alteration zone defined by the presence of chlorite and kaolinite and the absence of illite.

7. Alteration zone defined by the presence of kaolinite and chlorite and the absence of illite.

8. Alteration zone defined by the presence of illite and chlorite and the absence of kaolinite.

9. Alteration zone defined by the presence of chlorite and illite and the absence of kaolinite.

10. Alteration zone defined by the presence of kaolinite and illite and the absence of chlorite.



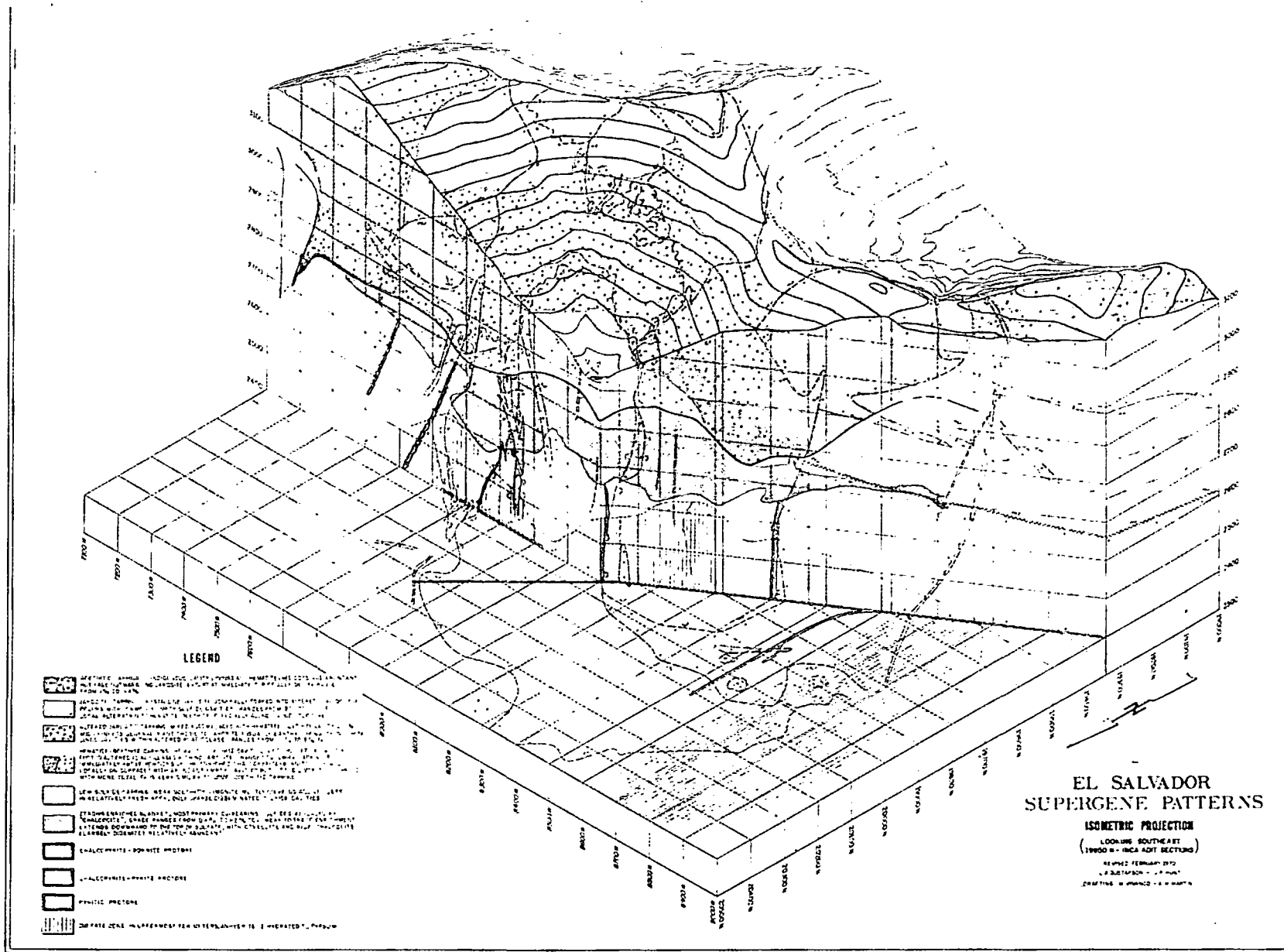


FIG. 21. Supergene patterns— isometric projection.

ably at least to the present surface, as indicated by tiny relict grains of anhydrite preserved within vein quartz.

Central mineralized zones contain K-silicate alteration assemblages. Hornblende phenocrysts have been replaced by biotite, intermediate plagioclase phenocrysts have been more or less replaced by sodic plagioclase and K-feldspar, but biotite phenocrysts usually remain unaltered in all but the most intense alteration assemblages. Sphene has been altered to rutile plus anhydrite, while the original magnetite-ilmenite assemblage has been altered to either magnetite plus hematite-rutile intergrowths or, with the subtraction of iron, simply rutile.

A broad halo of biotized andesites surround the porphyry intrusions. Intense recrystallization of the andesites to an assemblage of sodic plagioclase-biotite-quartz-anhydrite completely obliterates original textural and stratigraphic features close to the contacts. As shown in Figure 19, in most of these rocks, K-silicate assemblages correlated with chalcopyrite-bornite and chalcopyrite-pyrite zones with relatively low pyrite proportions. Incipient K-silicate alteration in "L" Porphyries is accompanied by only very low intensity sulfide mineralization.

A chlorite-sericite alteration zone lies outside the present K-silicate zone. Chlorite and sericite pseudomorphically replace the biotite and alkali feldspar formed as part of a prior K-silicate assemblage, which originally extended across most of the present chlorite-sericite alteration zone but with intensity decreasing outward. With increasing intensity of alteration, sericite replaces chlorite and feldspars, starting with original calcic plagioclase, then sodic plagioclase, and finally K-feldspar. The resulting assemblage is quartz-sericite-chlorite-anhydrite-sulfide. There is a generally good correlation between the appearance of major sericite and of pyrite at the inner edge of the chlorite-sericite alteration zone at the 2600 level. At lower elevations, the inner edge of major sericite lies within the pyrite zone, while at higher elevations it encroaches into the bornite-chalcopyrite zone.

The gray area in Figure 19B represents a zone in which kaolinite has replaced chlorite, feldspar, and locally, biotite. The kaolinite is generally associated with secondary enrichment of the sulfides, does not occur within the sulfate zone, and is almost entirely of supergene origin. Montmorillonite replacing plagioclase and biotite as a major constituent occurs in only a few places and probably is also of supergene origin.

Propylitic alteration, defined by the occurrence of epidote with chlorite (Fig. 19B), forms a broad halo about the orebody and includes the weak outer portion of the pyritic fringe. Chlorite is more or less abundant, as is calcite where not removed by super-

gene action. Within the propylitic zone are veinlets containing magnetite, epidote, and chalcopyrite, and farther out beyond the limit of sulfides, hematite, epidote, and calcite. Propylitic and K-silicate alteration assemblages are probably contemporaneous and zonally related.

Transitional Mineralization and Alteration

Pyritic and K-feldspar-destructive mineralization-alteration followed the consolidation of most of the last major porphyry complex ("L" Porphyry). Prior to the full development of this high-sulfur and strongly hydrolytic environment, there was a Transitional stage of mineralization characterized by "B"-type quartz veins, abundant molybdenite, and tourmaline.

"B" quartz veins

Quartz veins younger than "A" veins and older than late pyritic veins (Fig. 15 and Table 2) are called "B" veins at El Salvador. They are characteristically continuous planar structures with parallel walls and usually some form of internal banding. They commonly have flat dips and range up to 10 cm in width. They are further characterized by molybdenite and coarse-grained quartz and a lack of K-feldspar and hydrolytic alteration minerals either in the vein or in halos. They cut all rock types except latite, the only exceptions being rare occurrences of late "L"-type porphyry and aplite cutting "B" veins in the northeast part of the "L" Porphyry mass.

Within the group clearly defined by a combination of characteristics (Table 2), we see variations in quartz texture and in the nature of the internal vein symmetry. "B" veins occasionally show a vuggy center filled with anhydrite in the sulfate zone. These vuggy centers are lined by coarse crystals of the last quartz deposited in the veins.

Whereas "A" quartz veins contain sulfides similar to those in the surrounding background assemblage, "B" veins, especially in the deep central zones of the deposit, tend to contain sulfides different from the background. Abundant molybdenite is most striking and characteristic. Traces of bornite are rare in "B" veins, while chalcopyrite and minor pyrite are more characteristic. Abundant pyrite is present in "B" veins only within the pyritic fringe of the deposit or where the veins have been cut by younger pyrite-rich veins. Reopening of "B" vein structures and filling with later veins are common and probably responsible for most if not all of the weak hydrolytic alteration halos seen on some "B" veins.

Molybdenum mineralization

The distribution of molybdenite at El Salvador is closely tied to "B" quartz veins and the Transitional

mineralizing environment they represent. Most of the molybdenite in the deposit probably occurs within the "B" quartz veins. It is also abundant as "smears" in late joints with no other associated sulfide or gangue minerals and without any alteration halos. Minor amounts of molybdenite also occur with Early disseminated sulfides and in Late pyritic assemblages. Only in areas of abundant "B" quartz veins and associated better grade molybdenite mineralization are these other occurrences of significant abundance.

Molybdenum grades in the deposit range from less than 0.005% Mo to greater than 0.05% Mo, averaging about 0.02% Mo by weight. The pattern of distribution is not very regular but appears to form three centers possibly lying along an arcuate zone. Highest molybdenum values occur within areas of abundant chalcopyrite-bornite and chalcopyrite-pyrite zones. Even stronger evidence of a Transitional age than the association with "B" quartz veining is the fact that the zone of better grade molybdenum mineralization cuts across the contact between "L" Porphyry and older rocks. Molybdenum values greater than 0.02 percent tend to close over lower values in "L" Porphyry somewhere above the 2,700-m elevation. This pattern may possibly be interpretable as a crude, inverted cup.

Tourmaline

Although geometrically independent of "B" quartz veining, the distribution of tourmaline appears to be closely associated in time with the Transitional stage of mineralization.

Tourmaline occurs in a variety of thin veinlets and in tourmaline breccias. Tourmaline veins, studied by Heatwole (1973), seem to vary between two extreme types. One type, apparently the earliest, cuts plagioclase (oligoclase) as well as K-feldspar with no alteration. This type contains chalcopyrite-bornite without pyrite. The proportion of sulfide is usually small, and minor quartz may or may not occur in the vein. The other type, which contains pyrite with or without chalcopyrite, is bordered by conspicuous sericite-pyrite alteration halos. K-feldspar, as well as plagioclase and biotite, is destroyed in the halo to which pyrite is added and bornite removed. Intermediate types with weak sericite-carbonate halos and abundant residual K-feldspar and plagioclase have been seen. Many tourmaline veins appear to have neither sulfide nor alteration halos.

Tourmaline veins commonly cut early "A" quartz veins, but definitive age relations with later types of veining are not abundant. "B" veins commonly contain tourmaline. Where crosscutting age relations can be demonstrated, the tourmaline is generally younger. Molybdenite is almost never closely as-

sociated with tourmaline veins. Later pyritic veins rarely contain either abundant molybdenite or tourmaline.

Tourmaline breccias are early pebble breccias with rounded fragments whose elastic matrix has been cemented with tourmaline and quartz. Tourmaline breccias may either cut or be cut by "B" quartz veins. They are invariably cut by Late hydrothermal "D" veins. They contain more or less pyrite with sericitic alteration, are low in copper, and do not contain molybdenite.

Disseminated tourmaline, with and without associated sericitic alteration, is abundant at El Salvador. Vertical zoning is strong. On the 2400 level tourmaline veins are rare and there are no disseminations of tourmaline rosettes. Tourmaline in veins and disseminations increases upward toward the surface, 400 to 600 m above, where both tourmaline veins and disseminated tourmaline are abundant and widespread. The relative age of disseminated tourmaline is not known, but its abundance generally correlates with abundance of tourmaline veining. Both forms appear to span the period from "B" quartz veins to "D" sulfide veins and may therefore be in part contemporaneous.

Andalusite and corundum

An assemblage of andalusite with K-feldspar is locally abundant at relatively deep levels at El Salvador as on the 2600 level. This assemblage is classified with the Transitional period of mineralization-alteration because of gross geometric arguments and chemical inferences, although evidence of its age relative to "B" veins is lacking. Andalusite assemblages are spatially related to the "L" Porphyry-mass and locally crosscut it.

Figures 19B and 20B show the deepest occurrences of andalusite in "X" Porphyry and andesite to the west of the southeast lobe of "L" Porphyry and in quartz porphyry dikes northeast and northwest of the "L" Porphyry contact. The occurrences in "X" Porphyry and andesite lie within the sulfate zone in rock that has been strongly affected by K-silicate alteration and that contains both chalcopyrite-bornite and chalcopyrite-pyrite. The andalusite occurs along small, discontinuous, and commonly poorly defined veins and halos. These are most commonly streaks of alkali feldspar replacement of plagioclase, which appear dark because of the associated biotite and sericite. Some are also apparently halos about certain "A"-family quartz veins, of a type which probably formed late in the "A" vein group. A dike of "L" Porphyry cutting across this area appears to contain no andalusite. Although no definitive age relations have been found, the strong contrast between the unaltered dike and its strongly altered walls

would suggest that the andalusite assemblages were formed prior to or possibly contemporaneous with the intrusion of the dike.

Essential minerals of the assemblage formed during this stage of alteration appear to be K-feldspar, Na-plagioclase, andalusite, and anhydrite with biotite or sericite. Judging by optical properties, the plagioclase appears to be oligoclase and the K-feldspar non-perthitic orthoclase. Quartz is ubiquitous and abundant, but only rarely is it in contact with andalusite. Some residual calcic plagioclase (andesine) is usually present but not in contact with the andalusite. Most commonly, andalusite-bearing assemblages have clearly been developed by the replacement of plagioclase phenocrysts, but in other areas there has apparently been more pervasive recrystallization of the whole rock.

The kaolinite associated with andalusite in quartz porphyry occurrences is probably a supergene replacement of alkali feldspar, chlorite, or biotite, which had been formed with the andalusite. A quartz porphyry dike at 2,400-m elevation (Fig. 20B) contains traces of andalusite with alkali feldspar, quartz, sericite, chlorite, and anhydrite. Both sodic and potassic alkali feldspar are present, along with chalcocopyrite-pyrite and rutile. This is the deepest known occurrence of andalusite at El Salvador.

Corundum in trace quantities is seen in several specimens of andalusite. In about half of these, the corundum is closely associated with andalusite, commonly in contact with it. In others, corundum with no andalusite occurs within crystals of alkali feldspar or within biotitic streaks containing only minor alkali feldspar. A close association between the formation of corundum and the alteration of biotite to a very pale green pleochroic mica, probably phlogopite, is strongly suggested in several specimens. No corundum-quartz contacts have been seen.

Late Mineralization and Alteration

Late mineralization and alteration are characterized by abundant pyrite and strong hydrolytic (K-feldspar and biotite-destructive) alteration. Pyrite-quartz veins, pyritic veinlets with sericitic alteration halos, peripheral zones of disseminated pyrite and pervasive sericitization, and upper level high-sulfur and sericitic to advanced argillic assemblages containing pyrite-bornite are the major products of this Late environment.

"D" Veins

The sulfide veins and veinlets that cut all Early and Transitional veins as well as all rock types except latite are known as "D" veins (Fig. 15B and Table 2).

Width of the "D" veins ranges from less than a millimeter to more than 20 cm. They characteristically occupy continuous, systematically oriented fractures. They contain high proportions of pyrite, with lesser amounts of chalcocopyrite, bornite, enargite, tennantite, sphalerite, and galena. Quartz is usually minor, tends to show crystal forms, and is low in fluid inclusions. Anhydrite is present in most "D" veins, where not removed by supergene action. Dolomite is a fairly common minor constituent.

Simple sericitic or sericite-chlorite alteration halos surround many "D" veins, particularly the smaller veins. Other veins commonly have zoned alteration halos, with outer kaolinite or kaolinite-calcite halos separating the sericite from fresh rock. K-feldspar is usually destroyed in the sericite zone but may or may not persist in the outer alteration halos. Iron from both oxides and silicates is usually fixed as pyrite in the alteration halos, and anhydrite forms in most alteration halos.

In the deepest exposures in the mine, pyrite is usually the dominant or only sulfide in "D" veins. Pyrite and only traces of chalcocopyrite occur in the alteration halos. Where "D" veins cut fresh and unmineralized late porphyries, the chalcocopyrite traces may represent a slight addition of copper, particularly at the outer portions of the halos. However, in similar veins cutting strongly mineralized rock, especially chalcocopyrite-bornite assemblages, sericite-pyrite halos commonly represent a complete reworking of the sulfide assemblage and an inward flushing of copper out of the vein halo. In such cases, chalcocopyrite increases outward from the vein within the halo and bornite appears only beyond the outer limit of pyrite. Other veins, seen only at higher elevations, add pyrite to their halos without destroying bornite and chalcocopyrite. In these, pyrite occurs not only as a sulfidization of oxide and silicate iron but also as inclusions within original chalcocopyrite-bornite grains. This type of halo has not been noted about barren pyrite veins; only about those with significant copper. Some of these veins contain a pyrite chalcocopyrite-bornite assemblage, but unfortunately most have been seen in zones of strong supergene enrichment so that the original sulfide minerals are difficult to determine.

Tennantite in "D" veins is largely restricted to lower levels of the mine (below 2600 level), while parallel veins directly above contain abundant enargite. Assemblages of pyrite-bornite-tennantite are rare, and enargite has not been observed in contact with chalcocopyrite. Sphalerite and galena occur together and commonly with copper minerals in "D" veins throughout the deposit to the deepest levels of exposure. No zoning of lead and zinc relative to copper has been noted. Relatively rare occurrences of stibnite, realgar, arsenopyrite, and marcasite

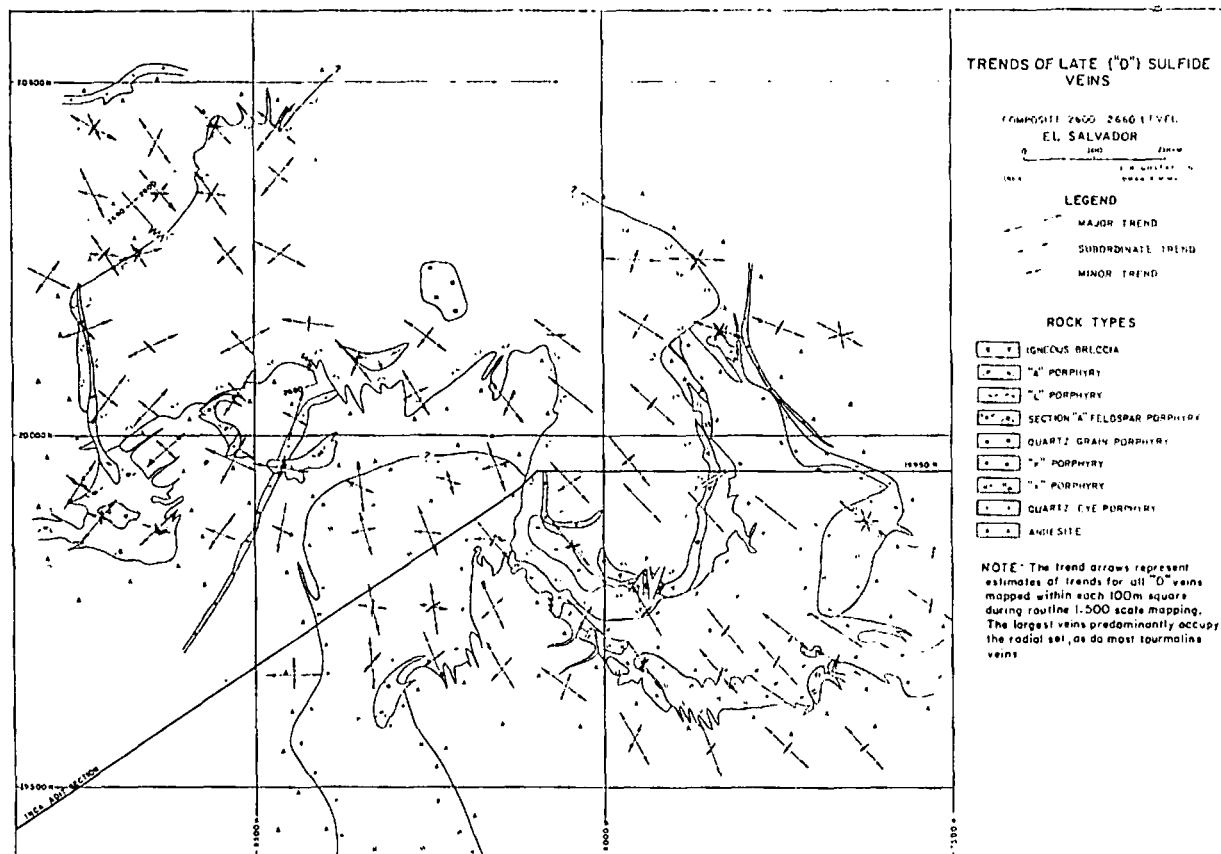


FIG. 22. Trends of Late "D" sulfide veins, 2600 and 2660 levels.

are found in "D" veins containing sphalerite and galena.

The proportion of sulfides other than pyrite in "D" veins tends to increase upward. With this increase in other sulfides, there is an increase in the apparent degree of replacement of pyrite by these sulfides. The elevation at which "D" veins begin to contain significant copper-bearing sulfides is quite variable. Some sort of wall-rock control may be important, as "D" veins in "L" Porphyry are barren pyrite well above the elevation at which they contain significant copper in "K" Porphyry.

Consistent and mappable "D" vein trends are apparent underground and have been recorded in the routine 1:500-scale geologic mapping. Larger veins were mapped as individual structures, and many more smaller veins were mapped schematically to show their general abundance and orientation trends. An imperfect but definite radial pattern is present, centered roughly at 20,300 N, 8300 W (Fig. 22). A conjugate radial-circumferential set and other minor trends are much more strongly developed by the small veins than by the large veins. The radial set is emphasized by the larger veins. This pattern persists throughout all the levels of exposure in the mine.

Large tourmaline veins generally conform closely to the radial component of the sulfide vein pattern.

Peripheral sericitic and pyritic assemblages

Peripheral background alteration zones surround the central sulfide zones (Fig. 20) and are characterized by abundant sericite and pyrite. At lowermost elevations, preserved in the sulfate zone, the characteristic assemblage in the peripheral zone is sericite-chlorite-quartz-anhydrite-pyrite. Residual alkali feldspar and biotite are most abundant in the inner portions, where chalcocopyrite is also most abundant. Rutile is the only iron-titanium oxide in areas of strong sericite-chlorite alteration (Fig. 23). In the inner portions of the peripheral zone, there is textural evidence of chlorite replacing biotite and of sericite replacing feldspars, suggesting superposition on earlier K-silicate alteration. At the outer limits of the peripheral zone, sericite-chlorite-pyrite assemblages fade out in propylitic assemblages, which, as described above, are older at the point of overlap.

There is a good general correlation between the abundance of pyrite and the intensity of sericite-chlorite alteration, both on a zonal scale and locally about structures. Both the strongest sericite-chlorite

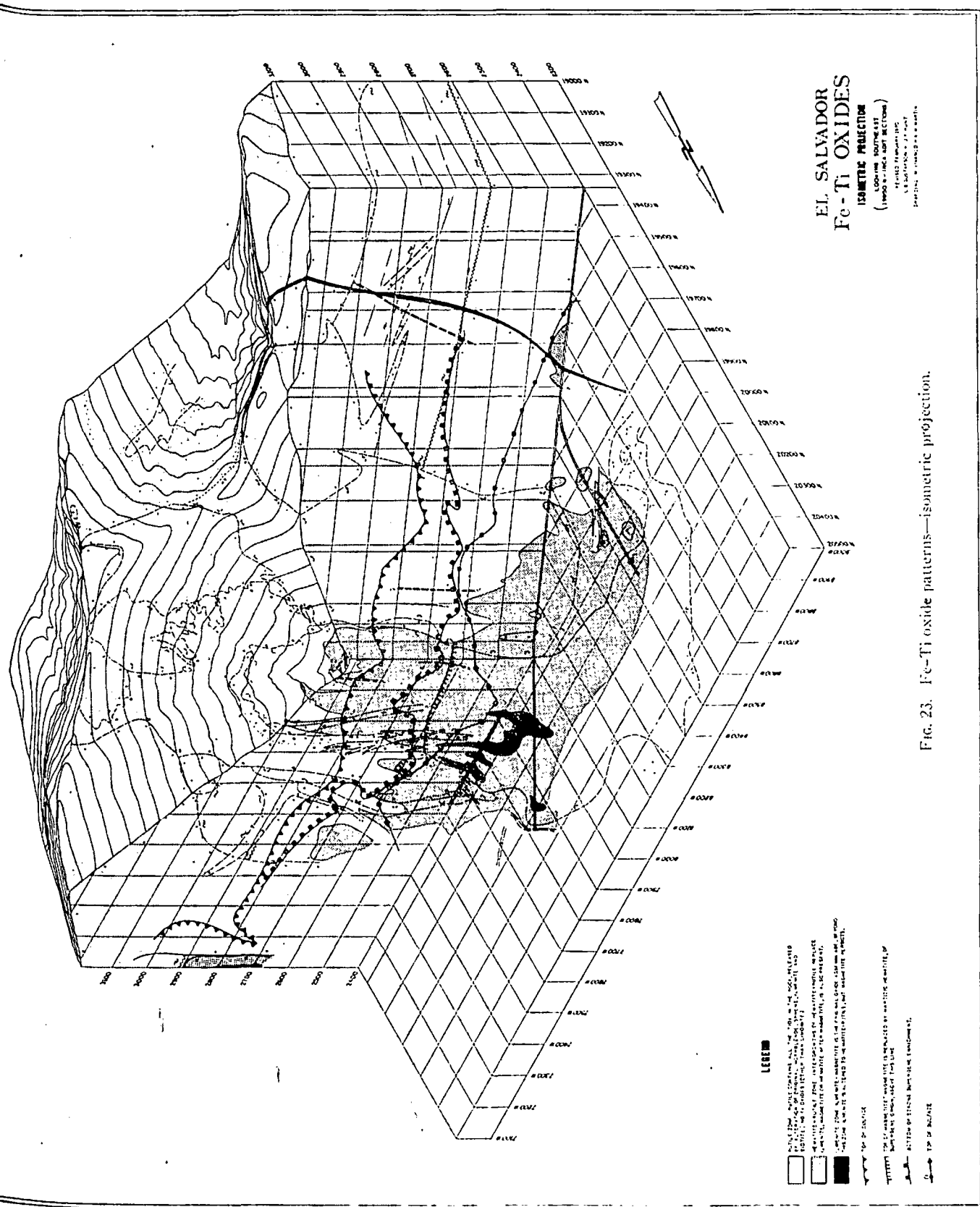


Fig. 23. Fe-Ti oxide patterns—*isometric projection.*

(D) SULFIDE
S
-2860 LEVEL
/ADOR
2000
L. B. SUBSTANTIAL
DRAWN BY W. J. ...

DR TREND
ORDINATE TREND
IR TREND

(PES
DIA

DISPAR PORPHYRY
PORPHYRY

ORPHRY

dots represent
all "D" veins
in square
scale mapping.
dominantly occupy
most tourmaline

closely to
tern.

is

surround
character-
lowermost
the char-
is sericite-
alkali
the inner
abundant.
areas of
) In the
is text-
and of
erposition
iter limits
pyrite as-
es, which,
overlap.
between the
sericite-
and locally
c-chlorite

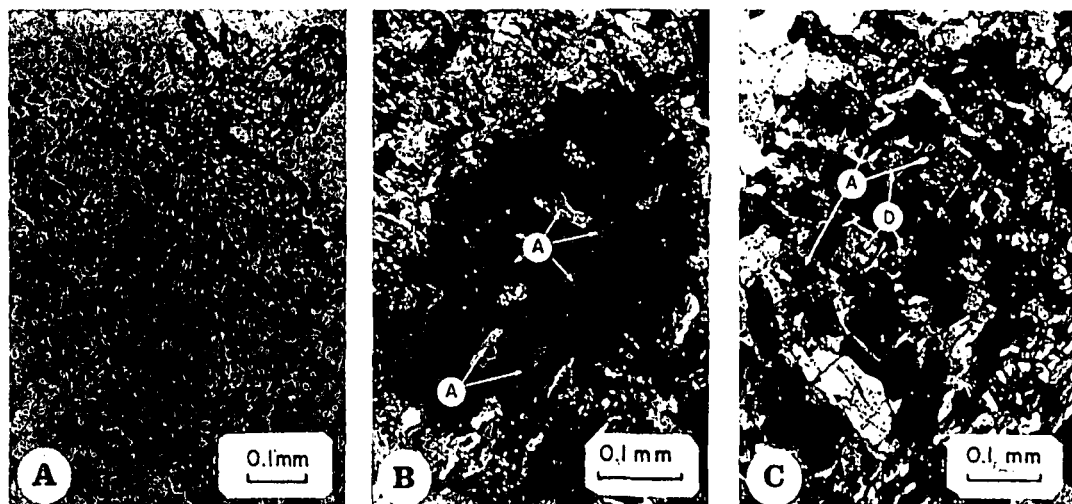


FIG. 24. Textural evidence of sequence in andalusite assemblages.

A, Typical habit of unaltered andalusite in andalusite-sericite-quartz assemblage. Andalusite replaces plagioclase, K-feldspar, and biotite, along with sericite, which commonly fringes the andalusite. In underlying andalusite-K-feldspar assemblages, the andalusite occurs mostly as small anhedral grains, usually within alkali feldspar replacing plagioclase. (Plane polarized light)

B, Pseudomorphic replacement of andalusite by low-index amorphous material. Remnant andalusite (A) and intergranular sericite emphasize the pseudomorphic texture. (Cross-polarized light)

C, Pseudomorphic replacement of andalusite (A) by diaspore (D) with intergranular white mica rims. Pyrophyllite accompanies diaspore, apparently directly replacing sericite. (Cross-polarized light)

Photographs by O. R. Eckstrand.

alteration and maximum pyrite intensity are seen in the central portion of the peripheral zone. There is an increased structural control of pyrite as lacing veinlets with sericite-chlorite alteration halos in the outer half of the zone where minor chalcopyrite is disseminated in the rock rather than on veinlets.

Despite extensive search during detail mapping, no structures with pyritic mineralization and sericitic alteration have been found that are older than "B" quartz veins. Although age relations involving the discontinuous lacing veinlets in the pyritic zone are commonly obscure, many of these structures have been seen that clearly crosscut "B" veins. Age relations between well-defined "D" veins and the lacing pyritic veinlets that comprise the background mineralization in the zone are usually ambiguous. Although some larger and more continuous veins retain obvious "D" vein characteristics and contrast with the small lacing veinlets which never have zoned alteration halos, it is impossible to make consistent distinctions between these types of mineralization. We suspect that they are contemporaneous and part of the same mineralization-alteration stage.

Minor calcite is associated with the usually weak sericitic "dusting" of plagioclase and alteration of biotite to chlorite superimposed on K-silicate assemblages in the upper part of the sulfate zone.

Upper level alteration zones

A striking vertical zonation of alteration and mineralization is present at El Salvador (Fig. 20B).

Inside the peripheral sericite zone, lower level alteration assemblages are dominated by feldspar and biotite. At upper levels above the enrichment blanket, alteration assemblages are dominated by sericite and andalusite.

The andalusite-sericite assemblage contains abundant quartz but, at most, minor to trace amounts of pyrophyllite, diaspore, or alunite. Accessories include pyritic sulfides (or their oxidized limonitic equivalents), zircon, and rutile. Inclusions of relict anhydrite locked within andalusite crystals are convincing evidence that the andalusite was formed within the former upward extent of the sulfate zone. In this zone, the andalusite characteristically occurs as clusters of lath-shaped crystals (Fig. 24) and is generally more coarsely crystalline than it is in the K-feldspar-andalusite "root" zones below, where incipient crystallization as small isolated anhedral grains is more common. In some specimens, particularly of quartz porphyry, andalusite makes up as much as 40 percent of the rock volume. Where the rock texture is discernible, andalusite appears most commonly in altered plagioclase phenocrysts. Sericite occurs fringing the andalusite and as a replacement of all rock silicates except quartz. Sericite-andalusite assemblages, like K-silicate alteration assemblages, produce a recrystallization of the rock texture which tends to obliterate original porphyry textures. In contrast, most sericitic alteration assemblages tend to preserve original rock texture, although commonly rendering it hard to discern megascopically.

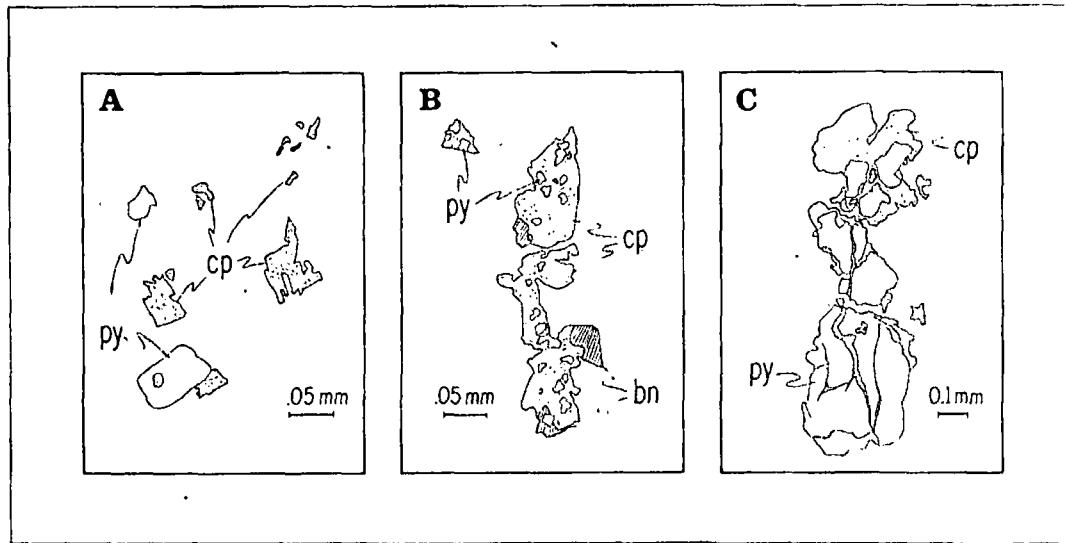


FIG. 25. Sulfide textures.

A, "Separate or tangent" texture, typical of chalcopyrite-pyrite assemblages on deep levels. Chalcopyrite and pyrite occur usually as separate grains and when in contact, seldom rim or vein one another.

B, "Inclusion" texture, a type of "reaction" texture typical of pyrite-chalcopyrite-bornite assemblages on upper levels. Pyrite is usually confined to larger grains of chalcopyrite-bornite. At least in some halos about "D" veinlets within the chalcopyrite-bornite zone, the pyrite is formed by the reaction chalcopyrite + bornite + S \rightarrow pyrite + bornite + chalcopyrite.

C, "Reaction" texture, typical of "D" veins and pyritic assemblages on upper levels. "Chalcocite" replacing chalcopyrite and bornite in this texture commonly gives the erroneous impression that it is replacing pyrite.

Sericite-andalusite assemblages appear to be gradual, both zonally and paragenetically, with underlying K-feldspar-andalusite assemblages. Both the proportion of sericite and the abundance of andalusite appear to increase progressively upward. It is impossible to say unequivocally whether sericite in the upper exposures was formed contemporaneously with the andalusite or whether it replaced K-feldspar in K-feldspar-andalusite assemblages. Although this latter retrograde reaction is clearly evidenced at lower elevations, we favor contemporaneity at higher elevations.

Andalusite reaches its deepest levels around the edges of "L" Porphyry (Fig. 20B). Andalusite also occurs within igneous breccia dikes cutting "L" Porphyry. Late "A" Porphyry dikes in "K" Porphyry also have been seen to contain sericite-andalusite alteration. In pre-"L" Porphyry exposures that are directly above strong K-silicate alteration and contain abundant "A" quartz, the original K-silicate alteration assemblages are replaced by sericite-andalusite assemblages. It is probable that most andalusite was formed after the intrusion of "L" Porphyry.

Upper level sulfide zones

Direct evidence for sulfide zoning at higher elevations is largely based on the study of relict sulfides in the leached capping above the enrichment blanket. We have found that at higher magnification (600 \times)

very small (0.005 to 0.1 mm) relict sulfide grains can be identified in nearly all specimens of leached capping. These grains are usually locked in quartz, which protects them from supergene oxidation, leaching, and enrichment. Point counting of the relict sulfides at El Salvador has allowed us to detect and reconstruct the original primary sulfide patterns that existed at high levels prior to supergene leaching and enrichment.

The deep sulfide patterns with antithetic pyrite and bornite, formed by Early mineralization, are abruptly truncated between the 2,700- and 2,900-m elevations by a group of high-sulfur sulfide patterns formed by Late mineralization. A very extensive pyrite-bornite zone caps all deep zones. It contains contact assemblages of pyrite and bornite with variable amounts of chalcopyrite or "chalcocite." The pyrite-bornite-"chalcocite" assemblage tends to be zonally above and is possibly younger than the pyrite-bornite-chalcopyrite assemblage, although these subpatterns are not well defined. In the "roots" of the pyrite-bornite zone, pyrite first appears in the assemblage as inclusions within chalcopyrite-bornite grains. A very close spatial association of pyrite with the other sulfides forms textures that have been classed as reaction textures (Fig. 25). The pyrite tends to occur only in contact with other sulfides rather than separately as it does in lower level assemblages with chalcopyrite. The distribution of pyrite in the "roots"

is clearly related to the proximity of small veinlets containing pyrite with chalcopyrite and bornite and commonly also sphalerite. These veinlets are not major structures or even well-defined "D" veinlets. Many do not appear to have strong or well-defined hydrolytic alteration halos and are the type of lacing veinlets that would contain only chalcopyrite and bornite in deeper zones. A few "roots" of the pyrite-bornite zone extend below the 2600 level within "K" Porphyry.

These sulfide patterns reflect in only a very general way the patterns of rock alteration. Although pyrite-bornite assemblages are mostly associated with sericitic or advanced argillic alteration, the "roots" seen in the sulfide zone reach down into assemblages characterized by alkali feldspar, sericite, and chlorite. At lowest elevations, there are a few occurrences of pyrite and bornite in K-feldspar-biotite alteration.

The occurrence of disseminated enargite with pyrite appears to be the result of late hydrothermal reworking of chalcopyrite-pyrite and pyritic fringe assemblages at high elevations (Fig. 20A). The pyrite-enargite subzone does not extend into the present leached capping, where the transition of pyrite-chalcopyrite assemblages directly into pyrite-bornite-chalcopyrite assemblages is seen in the relict sulfide grains. Enargite is very rarely preserved as relict sulfides, and we therefore do not know its true original extent. A reasonable interpretation seems to be that the relatively young enargite mineralization was not accompanied by significant precipitation or recrystallization of quartz, in contrast with sulfides from earlier mineralization. Only sulfide grains trapped in quartz, analogous to secondary fluid inclusions which they resemble in shape, are preserved as relicts. Therefore, we believe that the mineralization associated with quartz was protected not only from supergene oxidation and leaching but also from late hydrothermal reworking. In a few places at the high outer fringe of the ore zone, in what is now pyritic waste, corresponding relict sulfides include bornite and chalcopyrite with pyrite. The inference is that locally the outer and upper portions of the original copper sulfide zones were converted to pyritic waste during advanced argillic alteration of the rock.

The pyrite-sphalerite subzone marks the appearance of very minor sphalerite as part of the background mineralization on tiny cracks and seams. In the main mineralization zones, sphalerite is only seen in definite "D" veins. Interestingly, it appears in the background assemblage in a normal peripheral position. The purple line in Fig. 20A encloses occurrences of relatively abundant covellite in relict sulfides. Although some of this covellite has a matted multicrystalline habit typical of supergene covellite, euhedral single crystal blades are common

and are suspected of being primary, although we have never seen this habit in the sulfide zone. We speculate that a pyrite-covellite assemblage could have formed with upward increasing sulfur activity as an uppermost primary sulfide zone.

Advanced argillic assemblages

The red line in Figure 20B, for the most part within the present leached capping, encloses advanced argillic assemblages containing pyrophyllite and a variety of associated minerals, such as diaspore, primary alunite, amorphous material, andalusite, sericite, and local corundum. Kaolinite is not present. In almost all occurrences, advanced argillic assemblages appear to be superimposed upon sericitic or sericite-andalusite assemblages rather than formed directly from fresh or K-silicate-altered rock (Eckstrand, 1966). Andalusite and probable sericite are partially replaced by diaspore and pyrophyllite in these assemblages. Andalusite is generally unaltered in areas with little or no pyrophyllite. There is clear textural evidence of the replacement of andalusite by amorphous material and by diaspore (Fig. 24). The evidence for replacement of sericite by pyrophyllite and locally by alunite is not conclusive. There is a general inverse correlation between the abundance of sericite and that of pyrophyllite or coarse-grained alunite. Pyrophyllite and alunite have the same habit as sericite in the altered rocks. Small mica crystals filling a vug in one specimen proved to be a mixture of both sericite and pyrophyllite.

Diaspore occurs as an alteration product of andalusite and only in rocks with abundant pyrophyllite. Where present, coarse-grained micaceous alunite may be seen in any and all sites in which sericite occurs in sericitic assemblages. Alunite is particularly abundant in rhyolitic intrusive and pyroclastic rocks. Where alunite is the major constituent, there is usually abundant pyrophyllite and diaspore, yet some sericite-alunite assemblages with little pyrophyllite are found. No systematic patterns for the distribution of alunite have been detected.

Corundum has been seen in surface outcrops of rhyolitic rock in only a few restricted localities. Its habit is irregular, generally like that of diaspore after andalusite with which it is associated, and the grains are very cloudy with a parallel parting generally well developed. It is seen only near the outer limit of andalusite occurrences and is presumably formed as an alteration product of andalusite or diaspore, although the textures are not diagnostic. Quartz, which is abundant in these rocks, is separated from corundum only by a murky microscopic rim about the corundum grains.

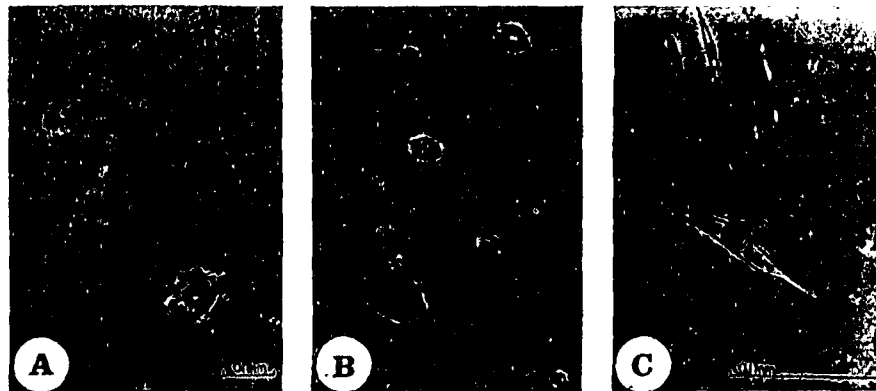


FIG. 26. Types of fluid inclusions at El Salvador.

A, Type I: characterized by a moderate-size bubble (b), a colorless isotropic cube of halite (h), and one or more opaque phases (o). Only rarely is a second cube, presumably sylvite, seen. The largest opaque occasionally displays red internal reflection and tends to have a triangular outline. It is probably hematite. Other minute solid phases have not been identified, but a rare second triangular opaque may be chalcopyrite. (Plane polarized light)

B, Type II: characterized by a large bubble (b), usually 40 to 80 percent by volume, and a single opaque solid (o). The opaque is probably hematite. Both types I and II inclusions invariably occur together as secondary or pseudo-secondary inclusions in Early and Transitional quartz veins. (Plane polarized light)

C, Type III: characterized by a small to moderate bubble and no solid phases. These are seen in quartz, anhydrite, and sphalerite of Late "D" veins, but types I and II inclusions do not occur in these veins. (Plane polarized light)

That advanced argillic alteration was formed later than practically all alteration and mineralization at lower elevations is proved by the fact that many near-surface pebble dikes are the loci of the most intense sericite-diaspore alteration. These same pebble dikes crosscut Late "D" veins at depth but had to have become inactive before delicate crystals of diaspore and pyrophyllite grew in the matrix between pebbles. However, advanced argillic alteration seems to have ceased before the final formation of the last sericitic pebble dikes, described previously, that cut pebble dikes with strong advanced argillic assemblages.

Fluid Inclusions

Three distinct types of fluid inclusions in El Salvador rocks are illustrated in Figure 26. Type I inclusions are found in "A" and "B" quartz veins but never in "D" veins. They contain a very high salinity fluid and are invariably and intimately associated with type II inclusions, which contain a very low density fluid. Type III inclusions contain relatively low salinity fluids and are found in all age veins, including "D" veins where they are the only type of fluid inclusion, occurring within quartz, anhydrite, and sphalerite. Fluid inclusions are relatively sparse in "D" vein quartz, but types I and II inclusions are *never* seen in "D" veins.

Fluid inclusions with characteristics intermediate between types II and III are also present. They are less common than the three main types in most rocks

and do not seem to occur in a systematic position within the orebody.

On the heating stage, both types I and II fluid inclusions homogenized over a temperature range between 360°C to greater than 600°C, even within a single healed fracture. The heating behavior of a single inclusion, which contained both halite and sylvite, confirms estimates from volumetric considerations that type I fluids contain 35% to 40% NaCl and less than 12% KCl. Attempts to freeze the fluid in types I and II inclusions were unsuccessful, but the salinity in type II inclusion fluid is presumed to be low. The immediate collapse of the bubble released on crushing type I inclusions in oil indicates a very small vapor pressure. The behavior of the bubble released from type II fluid inclusions crushed in Hb40 oil (Roedder, 1970) suggests a CO₂ content of roughly 1/8 to 8 atmospheres at room temperature. Although only rough calculation is possible, this probably means an aqueous fluid low pH (less than 4) and less than 4% CO₂ by weight in the inclusions.

Type III inclusions (from two specimens) homogenized between 175°C and 310°C. Their freezing behavior indicates an "equivalent NaCl" content of 5 to 20 percent, but the CaCl₂ content of the solution is not known. Attempts to determine the CO₂ content of type III inclusions from "D" veins containing carbonate were unsuccessful. The single specimen containing type II-III inclusions that was examined was from a drusy quartz-pyrite vein,

which probably represents a relatively old "D" vein type. Homogenization temperatures range from 300°C to slightly greater than 350°C, freezing temperatures suggest "equivalent NaCl" of 12 to 15 percent, and crushing behavior indicates 1 to 30 atmospheres partial pressures of CO₂.

The evidence from fluid inclusions indicates a change in the character of the fluids trapped before the end of the time of formation of "B" veins and those trapped in "D" veins. This change can be seen within a single "B" vein in which clean crystalline quartz is formed as an overgrowth on the typical granular-columnar "B" vein quartz to form a vuggy center line. Growth zones are marked by abrupt stepwise decreases in abundance of types I and II fluid inclusions. The youngest growth zone near the central vug contains only type III inclusions.

It is impossible to determine time breaks or sequence of trapping of types I and II fluid inclusions within the earlier times of formation of "A" veins and "B" veins. In each type of vein, both types of secondary or pseudo-secondary inclusions are found within any given healed fracture. The temperatures of homogenization of both types within any small area of a single specimen appear to vary over a wide range. Fluid inclusions in "B" veins are practically as abundant as they are in "A" veins in any given area of the deposit. Apparently fluids were trapped over a range of temperature and time, but it is not certain that preserved fluid inclusions represent anything trapped earlier than "B" vein time.

Supergene Effects

The patterns formed by the supergene processes of oxidation, leaching, and secondary enrichment of primary sulfides have been presented in Figure 21.

Supergene enrichment

The El Salvador mine was developed to exploit the secondary enrichment blanket beneath Turquoise Gulch. Although the enriched ores are described as part of a "chalcocite" blanket, they are in fact composed of a group of copper sulfide minerals replacing primary sulfides. The principal secondary sulfide assemblages are chalcocite-djurleite and djurleite-digenite. Covellite is locally a minor constituent, especially in djurleite-digenite assemblages and in areas of weak or incipient enrichment below the main enrichment blanket. Cuprite and native copper are rare but also locally present.

Practically all supergene sulfides were formed as direct replacements of chalcopyrite or bornite. Although some have been formed as coatings on pyrite, we have seen no evidence to indicate extensive replacement of pyrite. Thick coatings and veining of pyrite by "chalcocite" are seen in some areas, but

close inspection indicates that the textures are inherited from primary chalcopyrite or chalcopyrite-bornite which replaced pyrite. Similar textures are seen in the protore below (Fig. 25C).

The upper surface of the enrichment blanket is for the most part a sharply defined boundary between leached capping and secondarily enriched sulfides ("top of sulfides"). The enrichment blanket ranges in thickness from a few meters to as much as 300 meters. In general, the thickest enrichment column formed in areas of richer primary mineralization. The bottom of enrichment is gradual and in many places defined only by arbitrary grade limits imposed by mining. The bottom of strong enrichment lies a few meters to more than 300 meters above the present top of the sulfate zone.

Supergene alteration

Supergene waters have not penetrated the present sulfate zone. This has allowed us to distinguish supergene from primary alteration assemblages. The absence of kaolinite in the sulfate zone, except for that clearly related to "D" vein halos, and of fine-grained alunite and montmorillonite clays indicates that they are all supergene products.

The zone of kaolinite-sericite alteration, shown in Figure 20B, lying between the top of the sulfate zone and the base of pervasive sericitic alteration, is the zone of strongest supergene effects. With increasing intensity from bottom to top within this zone, kaolinite replaces calcic plagioclase and chlorite, then sodic plagioclase and biotite, and finally K-feldspar. The accompanying sericite occurs exactly as it does throughout the sericite zone above and is thought to be all of hypogene origin. Fine-grained, low-birefringent alunite, texturally distinct from the coarse alunite of the advanced argillite assemblages, is locally abundant, especially in kaolinitic, moderately pyritic andesites with strong sulfide enrichment. Veins of fine-grained alunite are rather common throughout the supergene zone. Amorphous clay ("allophane") is locally abundant in the zone of supergene enrichment, especially in alunite-bearing andesites.

Kaolinite is conspicuously absent from the high-level sericitic assemblages that characterize siliceous rocks above the Hornitos unconformity. There is no evidence that primary sericite has anywhere been altered to supergene kaolinite, even in zones of most intense supergene activity. However, andalusite in high-level assemblages, where it has not been altered to diaspore during superimposed advanced argillite alteration, is more or less altered to amorphous material. It is most probable that this amorphous material was also formed by supergene alteration.

Traces of montmorillonite are widespread in the zone between the top of the sulfate zone and the

bottom of strong kaolinite alteration, but it is only locally abundant. It occurs as an alteration of intermediate plagioclase and as small veins or coatings of open fractures. It is most strongly developed along late faults and pebble dikes cutting relatively fresh rock and along the margins of latite dikes, where it is usually nontronite.

Magnetite is oxidized to hematite by supergene alteration. This oxidation extends below the base of strong supergene enrichment but stops well above the top of the sulfate zone (Fig. 23). The slightly magnetic hematite that is formed has a characteristic texture reflecting replacement along octahedral zones in the parent magnetite. This texture contrasts with that of the trace hematite seen deep within the sulfate zone. This trace hematite evidently was formed by hypogene oxidation of magnetite as single crystal rims on magnetite rather than as octahedral intergrowths.

Supergene kaolinitic alteration tends to reduce the porosity and permeability introduced by the leaching of sulfates from the rock. Kaolinite, alunite, and amorphous clay tend to fill the open spaces and produce rock which is soft but relatively tough and shock resistant.

Apparently very late oxidation effects are seen penetrating the zone of relatively high permeability at the base of the supergene enrichment. It is here and not at the top of the enrichment blanket that native copper and cuprite are locally abundant replacing supergene "chalcocite."

Leached capping

Most of the important characteristics of the limonite zones are summarized in the legend of Figure 21. In the fringing goethitic zone, most of the limonite is in lacing veinlets. Dissemination increases inward, especially in the volcanics and quartz porphyry, as does the abundance of hematite. Most of this limonite is indigenous rather than transported, in that it lines sulfide cavities.

In the more central jarosite zone, jarosite forms abundant disseminations as well as veinlets, especially in porphyry. Jarosite is characteristically disseminated in the sites of original plagioclase phenocrysts now altered to sericite assemblages. Crystalline jarosite is usually the only limonite mineral in the jarosite zone except locally where hematite-goethite is abundant. In one tunnel, pyritic sulfide waste alternates with jarositic limonite cut by occasional veinlets and halos with hematite-goethite. There is no difference in sulfide or silicate mineralogy to account for the localization of the hematite-goethite. The large central zone designated "altered jarositic capping" is a mixed zone dominated by hematite-goethite with more or less earthy jarosite. It contains areas of

jarositic capping as well as capping with abundant sulfide cavities but very sparse limonite. Exposed only in drill core and underlying jarositic and altered jarositic capping on surface are an outer zone of goethite-hematite and an inner zone with mostly empty sulfide cavities and minor hematite-goethite. Limonite in these zones is largely indigenous within sulfide cavities and is not found disseminated in plagioclase sites as is some of the hematite-goethite in the "altered jarositic" capping above. No jarosite occurs in this lower leached capping, although a zone of jarosite, less than one meter thick, is seen at the immediate top of pyritic sulfide on the eastern fringe.

There is evidence of at least two stages of limonite development. Only rare occurrences show jarosite partially replaced by hematite-goethite. However, the habit of hematite-goethite disseminated in plagioclase sites suggests replacement of jarosite. At El Salvador, this characteristic habit of jarosite is only very rarely duplicated by pyrite in plagioclase sites. Most convincing is the penetration by a diamond drill hole of a residual sulfide block within the jarosite zone. Surrounding the residual, which contains pyrite-"chalcocite," is a shell a few meters thick of hematite-goethite. This shell is similar to the lower capping below and typical of what one would expect to be derived from pyrite-"chalcocite" ore following "classic" leached capping interpretation (e.g., Tunell, 1930). Both this shell and the lower capping immediately above the top of sulfide apparently represent a second-stage oxidation of sulfide which had previously produced a jarositic capping during an earlier period of oxidation. Presumably, the alteration of jarosite to hematite-goethite occurred at this time.

Copper is reduced to low background levels (mostly less than 0.05% Cu) in nonreactive capping altered to sericite or advanced argillic assemblages. Comparison of many assays immediately above and below the top of sulfide confirms that molybdenum and gold are relatively immobile during supergene leaching and enrichment. Silver tends to be leached from the oxide capping, but not nearly as efficiently as copper. Iron, on the other hand, tends to be slightly enriched in the leached capping relative to the underlying sulfide zone. Although there is local redistribution of iron by supergene processes, the overall iron content of the leached capping appears to reflect fairly well the iron content of the rocks before oxidation.

Interpretations

Volcanic events and depth of emplacement

The formation of porphyry copper mineralization in the Turquoise Gulch area culminated a long vol-

canic history in the Indio Muerto district. The granodioritic porphyry complex with which the mineralization is associated was intruded into a volcanic center which had produced two previous periods of felsic volcanism roughly 9 m.y. and 4 m.y. prior to the main ore-forming event. The early rhyolite domes were formed during a period of volcanism that had apparently built up a thick volcanic pile in the region. The geometries of the quartz rhyolite and quartz porphyry intrusions indicate a shallow, near-surface emplacement following possibly significant erosion of the early volcanic pile. Minor copper and molybdenum mineralization was associated with the volcanic centers of this second volcanic stage. We do not know how large a volcanic edifice was built during this second volcanic event or how much erosion preceded the intrusion of the main porphyry sequence. It seems improbable that much more than 1 to 2 km of cover above the present topography were present when the porphyries were intruded, but we do not have a precise measure of this thickness.

The 0.704 value of initial $^{87}\text{Sr}/^{86}\text{Sr}$ in all rocks analyzed is more similar to values in oceanic crust and island arcs than to values in thick silic crust, such as that which apparently underlies El Salvador (Munizaga et al., 1973; Lomnitz, 1962). This indicates that the porphyry melts did not assimilate a significant amount of this crust during their passage through it, although incorporation of overlying Tertiary volcanics cannot be excluded.

Early intrusion, alteration, and mineralization

Most of the copper at El Salvador was emplaced during the Early period of alteration-mineralization that accompanied the emplacement of the first two major intrusions ("X" and "K" Porphyries). The formation of K-silicate alteration assemblages, "A" quartz veins, and chalcopyrite-bornite mineralization occurred repeatedly, each time closely related in time and space to multiple individual intrusive surges within each of the intrusive units. The irregular discontinuous structure of the very early quartz veins suggests fracturing of a plastic rather than a brittle rock. The silicates, sulfides, and anhydrite in these Early assemblages are integral parts of the Early veins and their halos and must have been formed very shortly after consolidation of the porphyry melt. These same alteration assemblages and textures have also been locally seen forming thin reaction zones within the intruding rock at intrusive contacts, apparently by alteration of phenocrysts within a still unconsolidated melt. The pressure and temperature of this Early type of alteration-mineralization were very close to that of the final crystallization of the melt itself. As illustrated in Figure 27, the inferred

pressures in the intruding viscous melt at an estimated depth of about 2 km were somewhat greater than lithostatic. As the depth is not precisely known, overpressures much greater than lithostatic are not necessarily inferred, but pressures much greater than hydrostatic are clearly required.

Obviously, some kind of aqueous fluid was required to accomplish bulk transport of metals and other elements deposited or removed during Early mineralization and alteration. Possible sources of this fluid are the melt itself or meteoric water from surrounding host rocks. Meteoric water, driven by hydrostatic pressure of cooler, denser water in the outer part of a convective system, such as that envisioned by White (1968), is not a likely source for the simple reason that it could not get into the high-pressure region where Early mineralization at El Salvador was accomplished. This is not to say that some meteoric water may not have entered by diffusion or by bulk transport into the outer or upper portions of the K-silicate-altered zone before the end of Early mineralization or that this might not be a more important process in other deposits. It is very significant that not all of the several and otherwise similar porphyry intrusions were accompanied by K-silicate alteration and copper mineralization. Therefore, something more than just heat for driving meteoric convective systems must have been involved to explain why neither the early rhyolites and quartz porphyry nor the late "L" and "A" Porphyry intrusions into this area accomplished important Early-type mineralization and alteration. At least some water capable of transporting very large quantities of dissolved elements (Burnham, 1967) must have been released from the crystallizing porphyry melt and underlying magma chamber. Even though we do not know the mass of this magma, its water content, or many of the other factors necessary for quantitative evaluation, it seems to us that magmatic water is the major component of the Early mineralizing fluids.

We have observed that K-silicate alteration appears to be contemporaneous with propylitic fringe mineralization and zonally related to it, while both are older than sericitic and pyritic assemblages. Therefore, we believe that prior to the intrusion of the last major ("L") porphyry, a central zone of K-silicate alteration and chalcopyrite-bornite mineralization (possibly a composite pattern built around successive intrusive surges) was surrounded by a broad zone of weak propylitic alteration into which it graded with decreasing abundance of sulfides and proportion of bornite. At that time, there were no more than sparse pyrite and little or no sericitic or argillic alteration at present levels of exposure. During the waning stages of Early mineralization, the last major

porphyry stock ("L" Porphyry) was intruded, destroying the northwesterly quarter of the preexisting Early pattern of mineralization. Some of the copper, sulfide, potassium, and volatiles assimilated by the "L" Porphyry magma at lower levels moved upward and finally settled in the cooler portions of the "L" Porphyry intrusion itself, as shown by the increase in intensity of mineralization upward within this porphyry stock. Strongly telescoped patterns of mineralization and alteration about the margins of "L" Porphyry also suggest lateral remobilization and the influence of the thermal and chemical regime of the "L" Porphyry mass during subsequent cooling.

Hydrogen and oxygen isotopic evidence (Sheppard and Gustafson, in prep.) supports these interpretations. Solutions responsible for Early K-silicate alteration appear to have equilibrated isotopically at magmatic temperature with a large reservoir of igneous silicates. We have no evidence to indicate whether the fringing propylitic alteration was accomplished by magmatic or meteoric solutions, but Taylor's (1974) studies in the western Cascades suggest by analogy that meteoric water is more probable.

Possibly as much as 10^9 tons of oxidized sulfur were fixed as anhydrite during this Early stage of alteration-mineralization. The arguments presented above as well as the isotopic evidence make it most unlikely that the oxygen required was introduced with oxygenated ground water. Although it is conceivable that oxidized sulfur was introduced with the porphyry melt from a very deep source, it is more probable that sulfur was oxidized at shallow levels during mineralization. The likely mechanism is the dissociation of magmatic water in response to leakage of highly mobile hydrogen gas from the magmatic system. The accompanying production of hydrogen ions from reactions such as $H_2S + 2O_2 \rightarrow SO_4^{2-} + 2H^+$ probably contributed to extensive hydrogen metasomatism in higher and cooler parts of the deposit. The probable deuterium enrichment in the remaining fluids may be responsible for the calculated δD shift in the hydrothermal fluids (Sheppard and Gustafson, in prep.).

Transitional mineralization

As consolidation and cooling of the intrusive complex progressed, the structural and chemical character of the accompanying mineralization shifted. Randomly oriented, discontinuous, irregular veining gave way to continuous veins with systematic orientations and internal symmetry. At about this time, a set of flat vein structures appeared, suggesting a vertical release of pressures throughout the intrusive complex.

The nature of the fluids associated with this Transitional time of mineralization may be reflected in the fluid inclusions trapped in "A" and "B" quartz veins. These appear to have been boiling saline fluids trapped at temperatures ranging from about 350°C to greater than 600°C. Corresponding pressures along the liquid vapor curve for 40% NaCl brine range roughly from 200 to greater than 900 bars. This liquid-vapor curve approximates the pressure-temperature environment of Transitional mineralization (Fig. 27), although KCl in the brine would lower the indicated pressure somewhat (R. Fournier, pers. commun., 1973).

The evidence indicates a progressive change in physical conditions during the Transitional period. This change is interpreted as marking the first significant inflow of ground water into the cooling intrusive center. This inflow was made possible by the cessation of magmatic activity and attendant decreases in pressure and temperature. Contraction of the vertically elongate intrusive column on cooling may well have lowered pressures below lithostatic and produced flat fractures with local and probably transient hydrostatic pressures. Rates of influx probably fluctuated greatly, but the rate of cooling of the intrusive center would have increased. The ranges of temperatures and pressures of filling of fluid inclusions in "B" veins apparently reflect this period of declining and probably fluctuating pressures and temperatures. During the Transitional period, conditions shifted from near-magmatic temperatures and lithostatic pressures dominated by aqueous fluids derived from the magma to Late environments under hydrostatic pressures and relatively low temperatures dominated by meteoric waters. The shift in isotopic composition of the fluids responsible for Transitional and Late mineralization (Sheppard and Gustafson, in prep.) is compatible with this interpretation. However, the composition of meteoric water at El Salvador before the uplift of the Andes was probably not sufficiently light isotopically to be unambiguously identified as meteoric. The observed isotopic shift suggests further modification of this water through evaporation, exchange with rock silicates, and possible hydrogen leakage. Quantification of the relative abundance of magmatic and meteoric-hydrothermal water at different times during mineralization at El Salvador is not possible.

Late mineralization and alteration

After the intrusive complex had sufficiently cooled, probably below about 350°C, meteoric waters worked inward along fractures and reacted with previously mineralized wall rock to produce pyritic mineralization and K-feldspar-destructive alteration ("D" veins and the peripheral zone of

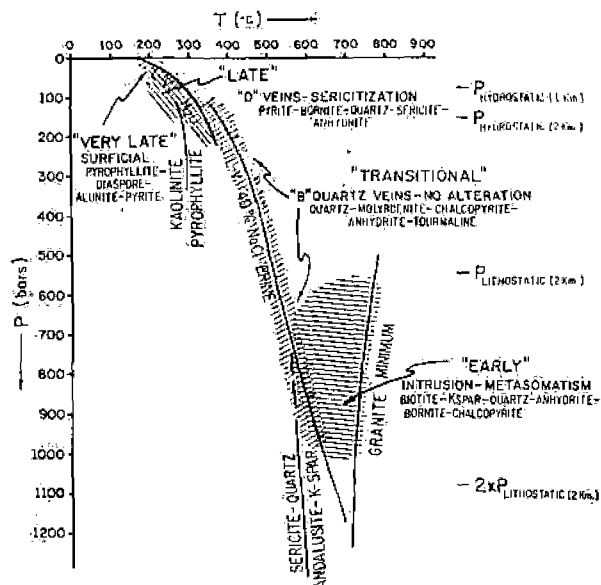


FIG. 27. Pressure-temperature environments of intrusion and Early, Transitional, and Late mineralization-alteration at El Salvador. Lithostatic and hydrostatic pressures are noted for 2 km, the approximate depth of present exposures at the time of formation.

sericitic alteration). This water was probably part of a large, deep convective system driven by the heat from the intrusive center. A final magmatic surge localized in the northeastern lobe of the "L" Porphyry stock apparently opened a radial-concentric pattern of fractures for Late ("D") vein mineralization. Mineralization during this Late period is much more obviously controlled by throughgoing fractures than during the Early period. This is probably due to the brittle nature of the cooled porphyry stocks as well as to the reduced permeabilities of the rocks resulting from earlier anhydrite and other alteration and mineralization. Relatively unfractured Late vein quartz contrasts with intensely fractured quartz in older veins, reflecting a marked decrease in the intense local stresses that attended intrusion of the porphyries.

Upper and peripheral zones of Late alteration and mineralization were progressively formed by inward and downward encroachment of meteoric waters reworking earlier mineralization. Late patterns of alteration and mineralization were strongly influenced by the "L" Porphyry mass, which was the principal source of heat during Late mineralization.

The Hornitos unconformity also influenced the pattern of Late alteration and mineralization (Fig. 20). There is much more pervasive development of disseminated pyritic sulfides and associated hydrolytic alteration above the general level of the Hornitos unconformity than at lower elevations in both the porphyries and volcanics. This is appar-

ently due both to higher lateral permeabilities and to more reactive and alkali-rich volcanic glass in the siliceous pyroclastics than in the underlying andesites. The quartz porphyry dikes also appear to have been permeable zones utilized by inflowing waters circulating at depth around the cooling "L" Porphyry stock.

The patterns of high-sulfur assemblages (pyrite-bornite, pyrite-"chalcocite," and pyrite-covellite) at high levels correspond only generally with patterns of strong sericitic alteration. Roots of these sulfide assemblages extend below into the K-feldspar-bearing assemblages. The textures of pyritic assemblages (Fig. 25) are interpreted as resulting from a reworking of Early assemblages by addition of sulfur. This, probably occurred with little or no addition of copper, although in some areas a significant increase in the protore grade can be inferred passing upward from pyrite-chalcopyrite into pyrite-bornite-chalcopyrite assemblages with reaction textures.

During the relatively early part of the Late mineralization, lower level sericite-chlorite-pyrite fringe mineralization was probably overlain by a zone of sericite with or without andalusite, with pyrite-bornite-chalcopyrite (or "chalcocite"). We believe that this upper zone cut across the "L" Porphyry intrusive complex above the present erosion level of Turquoise Gulch and draped downward around it. Still later, solfataric hot-spring activity caused advanced argillic alteration, reworking of sulfides, removal of copper, and formation of additional pyritic waste. The local formation of corundum through leaching of silica from andalusite sites is evidence for the presence of a shallow convective system, because inward-moving and warming water would have a tendency to become undersaturated and to leach silica from the siliceous rocks. The absence of kaolinite and the abundance of pyrophyllite in the advanced argillic assemblages are noteworthy and suggest a relatively high temperature and high silica activity in the very late hot-spring environment. The widespread occurrence of a diaspore-pyrophyllite-quartz assemblage, which apparently is not an equilibrium assemblage (Henley, 1969), suggests very local control of silica activity in the rock and probably low pressure.

The Late vein environment (Fig. 27) is a natural extension of the evolutionary trend initiated when meteoric waters began to encroach on the mineralized center during Transitional time. Important from the standpoint of hypogene alteration is the fact that K^+/H^+ values along the P-T path (Fig. 27) began in the vicinity of the K-feldspar-andalusite boundary. Although total KCl/HCl relations are not shown, this implies a significant reservoir of total acidity as unionized HCl in the brines at high-tem-

perature to be consumed by alteration with falling temperature (Meyer and Hemley, 1967). The fact that abundant quartz was deposited but practically no wall-rock alteration was accomplished during Transitional "B" vein formation suggests rapid dumping of silica in response to very rapid decrease in temperature and pressure rather than continued solution flow along the vein structures. Pressure probably fluctuated between lithostatic and hydrostatic as waning magmatic forces and thermal stresses were active, and temperature responded to sporadic inflow of cooler meteoric water and thermal effects of boiling brine solutions. Widespread sericitic alteration about "D" veins began with the continued influx of meteoric water but probably with continuing supply of volatile magmatic constituents and some oxidation of H_2S . Fluid inclusions trapped during this time have relatively low salinity.

As relatively cool meteoric water encroached inward and downward on the mineralized zone, it probably dissolved Early-formed anhydrite in upper and peripheral parts of the orebody, contributing to the pervasive replacement of Early assemblages by Late assemblages. Pyrite and anhydrite were deposited in halos of deep "D" veins where there is also evidence of extraction of copper. This and an apparent shift to isotopically heavy sulfur in Late assemblages (Field and Gustafson, in prep.) supports speculation that a process of dissolution of Early mineralization at levels below present exposure may have been the source of most of the sulfur (and presumably also the copper) emplaced during Late mineralization.

Mechanism of formation of pebble dikes

Langerfeldt (1964a) suggested a mechanism of fluidization for the origin of pebble dikes at El Salvador. The probable existence of an overlying hot-spring system at El Salvador during the time of pebble-dike formation suggests that the medium of fluidization was ground water. The pebble dikes were probably formed when fluidizing steam columns in fractures were generated when latite magma rising in fractures encountered ground water. Because the thermal gradient in the hot-spring system was already close to the boiling curve, boiling even around "blind" dikes at depth was able to expel steam from the fractures to the surface. Pressure in individual fractures was thereby lowered well below liquid hydrostatic and well below the boiling point for the temperature of the wall rocks. Spontaneous boiling of water from the walls promoted spread of the upward fluidizing flow of steam in the interconnected fractures. Fluidization was sustained as long as the thermal gradient and the rate of outflow of steam were high enough to

prevent condensation and suppression by build-up of hydrostatic pressure. The effect was probably a short-lived geyser field at the surface of what is now Turquoise Gulch. This may have occurred in two distinct periods, producing the two radial sets of pebble dikes of different ages. Each radial set may reflect a separate advance of latite magma causing doming and tensional opening of shallow fractures.

It is noteworthy that pebble dikes, although extremely common in porphyry copper deposits, have not been reported in volcanic hot-springs areas, such as Yellowstone Park. Perhaps this is partly due to poor exposure and they have been overlooked. On the other hand, the absence of pebble dikes may indicate that the waning or terminal stage of volcanism and magmatic activity has not yet been reached.

Supergene processes

Supergene oxidation and leaching of copper from the surficial zone and its deposition in an enrichment blanket were responsible for the formation of the commercial orebody. Secondary Cu-S minerals extensively replaced chalcopyrite and bornite but coated pyrite with little or no replacement.

The early jarositic capping over the orebody must have been formed under different physical and chemical conditions than those under which the underlying jarosite-free capping was formed. Both cappings represent oxidation of the same sulfides in the same generally nonreactive gangue assemblage. The lower capping is interpreted in the usual way as a product of an attack by an oxidizing, acid, relatively cold ground water on mineralized rock. The upper jarositic capping may have been formed earlier and at higher temperature during the waning stages of the acid geothermal hot-spring system above the cooling intrusions. During the formation of each capping, downward copper enrichment probably occurred. The present enrichment blanket is in effect a composite of both supergene environments.

Chemical gains and losses

Hundreds of thousands of analyses for copper and thousands of analyses for selected elements (Mo, Au, Ag, Fe, S, K, Na, and others) as well as several dozen whole-rock analyses were made. Although various empirical chemical patterns have emerged, we cannot give quantitative estimates for the chemical gains and losses during alteration and mineralization because fresh rocks are not available for comparison. Even the andesites in the mine area are so obscured by alteration that correlation of individual units with unaltered equivalents outside the mine area is impossible. Moreover, in addition

to significant original chemical variation in both intrusive rocks and andesitic host rocks, there are many complexities introduced by the sequence of alteration assemblages that we have detected and described.

Quantitative estimates of chemical grains can therefore be made only for those elements that were probably entirely added to the rocks during mineralization. Thus, for example, it is reasonable to estimate that mineralization in the Turquoise Gulch center alone introduced 10^7 tons of Cu, 10^8 tons of Mo, and between 10^8 and 10^9 tons of S, depending on assumptions about the original extent of the anhydrite zone. Comparison between fresh and altered rocks shows changes on the order of 10^{-2} g/cc, or 10^7 tons per km^3 , for most elements. However, for most major elements it is difficult to determine whether the net chemical changes represent a gain or a loss when the whole deposit is considered. For example, the total volume of porphyry and andesite affected by strong K-silicate alteration was approximately 6 km^3 . Approximately 20 km^3 of andesite and porphyry were altered to sericitic assemblages. Thus, possible losses in FeO and MgO and gains in Na_2O , K_2O , and probably SiO_2 during K-silicate alteration could be on the order of 10^8 tons for each element. However, several times as much rock was affected by later base-leaching alteration processes (hydrogen-ion metasomatism), which could easily reverse chemical changes resulting from Early alteration and mineralization. Chemical gains and losses must therefore be characterized in an appropriate time frame with the evolution of the mineral assemblages. For example, sodium and then potassium were progressively removed as sericitic and then advanced argillic assemblages were superimposed. Calcium appears to have been largely fixed as anhydrite in K-silicate and sericitic alteration but was removed by supergene solutions and probably also during advanced argillic alteration. Magnesium was apparently removed in each successive alteration assemblage. Iron was reduced by supergene kaolinization of biotite and chlorite and by "chalcocite" replacement of chalcopyrite and bornite. Copper was extracted from Early assemblages in deep "D" vein halos and emplaced higher in the veins. A dissolution of anhydrite and sulfides from still deeper Early assemblages may have been the source of most of the sulfur fixed as Late pyrite-anhydrite.

Genetic model—variations on a theme

Porphyry copper deposits from many parts of the world display many features similar to those at El Salvador. Very similar rock textures, types of veining, patterns of alteration-mineralization assem-

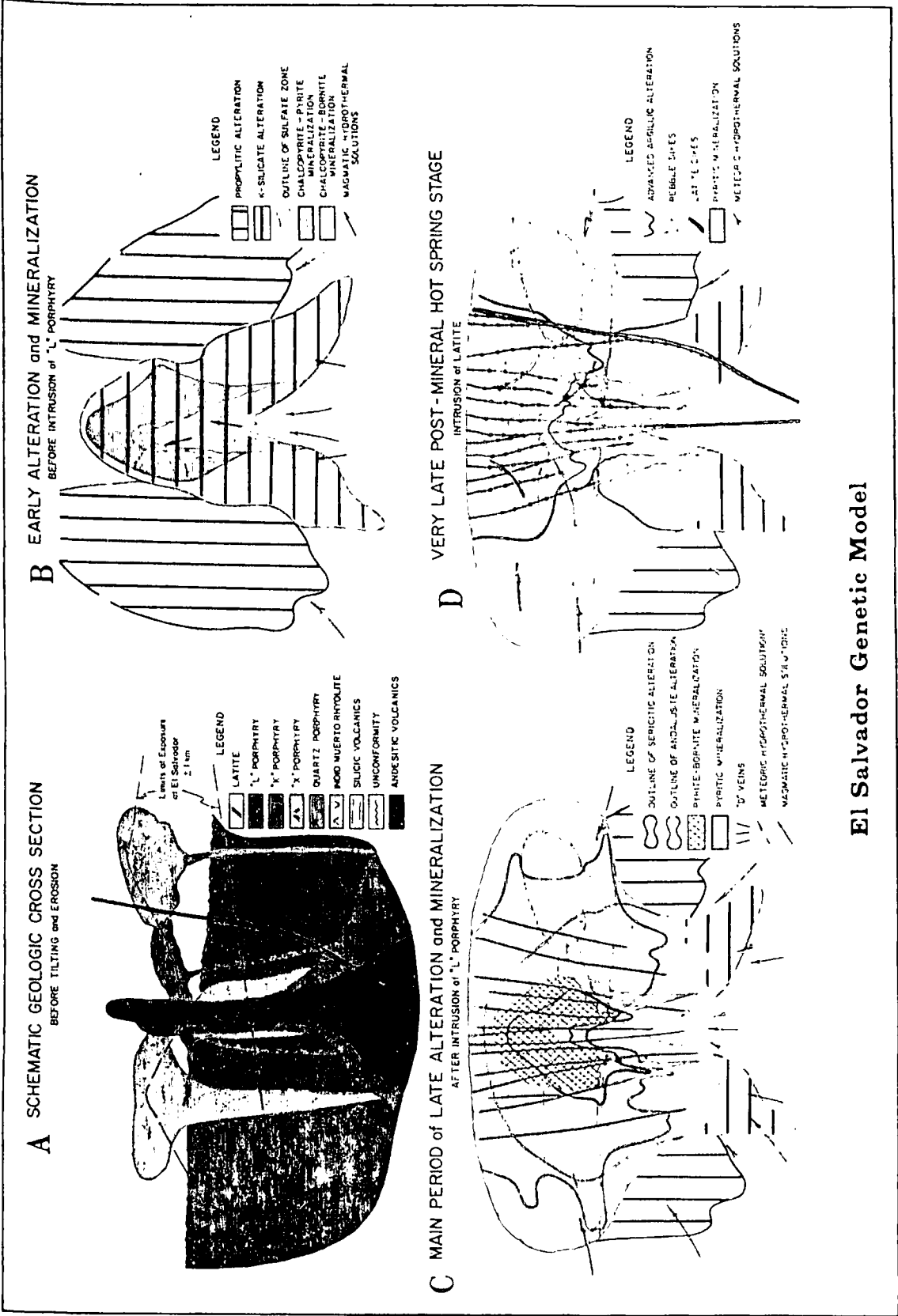
blages, and the same general evolutionary trend can be seen in many deposits. Yet each deposit is unique in detail. We suggest that these differences result principally from differences in the degree of development of Early vs. Late types of mineralization and alteration and in the degree of distortion of geometric patterns relative to those we have described for El Salvador. In some deposits, Late assemblages may be more weakly developed than Early assemblages (e.g., Yerington, Atlas-Latopan). In others, the central K-silicate zone may contain very low concentrations of sulfides while the ore is largely confined to the fringing sericitic and relatively pyritic zone (e.g., San Manuel). In still other examples, the Early mineralization may extend well beyond or above any exposure of a large porphyry mass (e.g., Ray), or Late pyritic and sericitic assemblages may be superimposed across the central part of an exposed pattern where evidence for Early alteration and mineralization may be masked or almost lacking (e.g., Cananea). Calcium may be partly fixed as carbonate as well as anhydrite or instead of it in the alteration assemblages of some deposits (e.g., Ajo, Bingham). Late intrusive activity or pebble breccias may remove much of the Early pattern in still others (e.g., El Teniente). Present levels of exposure also influence how much of the true patterns are observed.

Many other variations exist, but we suggest that they are only "variations on a theme." We see essentially similar processes and evolutionary trends at work in each case. The essential elements are (1) relatively shallow emplacement of a usually complex series of porphyritic stocks and dikes in and above the cupola zone of an underlying large batholithic body, (2) metasomatic introduction of copper and other metals, sulfur, alkalis, and hydrogen ions from the solidifying melt into both the porphyries and the country rock, usually during only part of the intrusive process, and (3) the interaction of ground water with the cooling mineralized center. The inevitable evolutionary trends at the site of mineralization following each main intrusive stage are decreasing temperature and pressure, transition from alkali to hydrogen-ion metasomatism, and increasing sulfide-ion activity in the mineralizing fluids. The major variables relate to the geometries and time factors of the intrusive process and include differences in depth of emplacement, degree of availability of ground water, size and timing of successive magma advances, and abundance of metals and mineralizing elements in the fluids evolved from the melt.

The deeper the emplacement of a mineralizing porphyry or the drier the country rock due to prior intrusive history or aridity of climate or other hy-

By trend
 deposit
 these differ-
 s in the
 types of
 degree of
 to those
 some de-
 kly devel-
 Yerington,
 K-silicate
 of sulfides,
 ing sericitic
 (uel). In-
 ation may
 of a large
 and seric-
 across the
 evidence
 may be
 Calcium
 as anhy-
 nblages of
 intrusive
 ch of the
 (eniente).
 ow much

uggest that
 We see
 ury trends
 nents are
 usually
 dikes in
 ing larger
 uction of
 and hydro-
 both the
 during
 the inter-
 mineral-
 trends at
 main in-
 and pres-
 ion meta-
 y in the
 relate to
 intrusive
 emplace-
 ater, size
 nces, and
 nents in
 neralizing
 e to prior
 other hy-



El Salvador Genetic Model

Fig. 28. El Salvador genetic model.

drologic factors, the slower the porphyry will be to cool, the less telescoped the temperature gradients and mineralization patterns about it, and the weaker the Late effects caused by reworking with ground water. The more massive the mineralized porphyry units and the more closely timed the intrusive surges, the less chance for cooling of individual porphyry units. This allows the evolution to Transitional or Late mineralization before reintroduction of Early features about the second surge and produces a composite evolutionary sequence. The less copper in the parent magma, the less chance of producing economic concentrations in any stage of alteration-mineralization. We urge caution to those who apply a "typical" porphyry copper model to the solution of major geologic problems and especially to those who are responsible for wisely investing their corporation's exploration funds!

The series of diagrams in Figure 28 attempts to portray our ideas of the evolution of the El Salvador orebody in graphic form. In these diagrams we have extrapolated well below and above the roughly 1 km of vertical exposure present at El Salvador to show an inferred cupola of a batholithic mass and a kilometer or more of overlying volcanic cover. Diagram A showing only the present rock pattern serves as a "base map" for the following three sequential diagrams.

Diagram B shows the development of a simple, though probably composite pattern of Early mineralization and alteration about the "X" and "K" Porphyry bodies formed before intrusion of "L" Porphyry and the influx of a significant amount of meteoric water. Although we have inferred the formation of sericite-pyrite at very high elevations during this stage, we have no direct evidence here. Early sericite-pyrite is probably not essential, particularly in deposits with little or no oxidation of sulfur to form anhydrite.

In diagram C we show the subsequent effect of intrusion of "L" Porphyry causing upward remobilization of Early assemblages and influencing the upward and downward encroaching ground-water system during Late mineralization. Pyrite-bornite-sericite assemblages are pervasive at higher elevations but restricted to "D" vein structures below. The peripheral zone of pyritic and sericitic mineralization decreases in intensity both downward and outward.

Diagram D shows the postmineral formation of rubble dikes, triggered by the intrusion of late dikes. This occurred during the further encroachment of an acid geothermal hot-spring system driven by the residual heat of the porphyry center and shallow convection in the upper siliceous volcanic pile.

Reworking of primary assemblages by supergene

oxidation and leaching of near-surface rocks with formation of the sulfide enrichment blanket and kaolinitic alteration below has already been illustrated on Figure 21 and can be visualized as the fourth and last step to the sequence illustrated in Figure 28.

Acknowledgments

Although the authors assume full responsibility for the interpretations and conclusions presented here, we gratefully acknowledge the very important contributions of many other Anaconda geologists. As is the case in many discoveries, many persons share the credit for the discovery of the El Salvador orebody. However, Vincent D. Perry and William H. Swayne deserves special recognition. Perry was the first to recognize the significance of the Turquoise Gulch mineralization and as part of Anaconda's top management vigorously supported all stages of subsequent exploration and development of the orebody. Swayne's aggressive, systematic, and intelligent detailed mapping of the prospect and direction of the drilling program was a major factor in the success of the project. Swayne's determination and confidence in completing the fifth and crucial discovery hole was especially important. Moreover most of Swayne's mapping and interpretations have withstood remarkably well the close scrutiny of more than 20 subsequent geologists.

Frank Trask Jr. deserves special credit for his highly constructive leadership of the resident geological department during the period when much of the present research was done. The work of Hans Langerfeldt, Roger Eckstrand, Alvaro Souviron, David Heatwole, Julian Hemley, Nick Davis, and Howell Williams also was especially important to our understanding of the El Salvador deposit. Charles Meyer's pioneering ideas on porphyry copper were a constant stimulation during our work at El Salvador. He has provided particularly useful advice and comment during the preparation of this manuscript, as did Julian Hemley.

Simon M. F. Sheppard, Cyrus W. Field, and Christopher Brooks contributed isotopic analyses of selected suites of specimens from El Salvador. Edwin Koedder and the U.S. Geological Survey provided laboratory facilities and assistance for the study (by Gustafson) of a group of fluid inclusions.

We also acknowledge with gratitude the contribution of Anaconda's top management, who continuously supported our efforts over the decade during which this work was carried out and have permitted its publication. The added cost of printing colored illustrations was underwritten by the Society of Economic Geologists Foundation, Inc.

L. B. G.

AUSTRALIAN NATIONAL UNIVERSITY
CANBERRA, A.C.T., AUSTRALIA

J. P. H.

SCRIPPS INSTITUTION OF OCEANOGRAPHY
LA JOLLA, CALIFORNIA 92037
December 10, 1974; February 20, 1975

FOR REPRINTS, WRITE:

THE ANACONDA COMPANY
GENERAL MINING DIVISION
P.O. Box 27007
TUCSON, ARIZONA 85726

REFERENCES

- Burnham, C. W., 1967, Hydrothermal fluids at the magmatic stage, in Barnes, H. L., ed., *Geochemistry of hydrothermal ore deposits*: New York, Holt, Rinehart and Winston, Inc., p. 34-76.
- Clark, A. H., Cooke, R. V., Mortimer, C., and Sillitoe, R. H., 1967, Relationships between supergene mineral alteration and geomorphology, southern Atacama Desert, Chile—an interim report: *Am. Inst. Mining Metall. Petroleum Engineers Trans.*, v. 76, p. B89-96.
- Craig, H., 1963, The isotopic geochemistry of water and carbon in geothermal areas: in Tongiorgi, E., ed., *Nuclear geology of geothermal areas*, Spoleto: Pisa, Consiglio Nazionale della Ricerca, Laboratorio de Geologia Nucleare, p. 17-53.
- Dickinson, W. R., 1970, Relations of andesites, granites, and derivative sandstones to arch-trench tectonics: *Rev. Geophysics Space Physics*, v. 8, p. 813-860.
- Eckstrand, O. R., 1966, High level alteration: unpub. company rept., Andes Copper Mining Company.
- 1967, Ventilation adit—alteration and mineralization: unpub. company rept., Andes Copper Mining Company.
- Garcia, F., 1961, Map of the area west of the Salar de Pedernales, Chile [unpub.]: Empresa Nacional de Petróleo.
- Gustafson, L. B., and Hunt, J. P., 1971, Evolution of mineralization at El Salvador, Chile [abs.]: *Econ. Geol.*, v. 66, p. 1266-1267.
- Heatwole, David A., 1973, Occurrence and distribution of tourmaline in the El Salvador orebody, El Salvador, Chile: Unpub. company rept., The Anaconda Company.
- Hemley, J. J., 1969, High Al assemblages in porphyry copper deposits: Paper delivered at Penrose Conference on Porphyry Copper Deposits, Tucson, 1969.
- Hunt, J. P., 1964, Sulfide zoning at El Salvador, Chile: Paper delivered at the S.E.G. Symposium on the Geochemistry of Ore-forming Fluids, Princeton; reported by E. Roedder, *Econ. Geol.*, 1965, v. 60, p. 1398.
- 1969, Anhydrite and gypsum mineralization in porphyry copper deposits: Paper delivered at Penrose Conference on Porphyry Copper Deposits, Tucson, 1969.
- Langerfeldt, Hans, 1960, Quartz vein mapping: Unpub. company rept., Andes Copper Mining Company.
- 1964a, Pebble dikes at El Salvador: unpub. company rept., Andes Copper Mining Company.
- 1964b, Quartz vein project—progress report: unpub. company rept., Andes Copper Mining Company.
- Lomnitz, C., 1962, On Andean structure: *Jour. Geophys. Research*, v. 67, p. 351-363.
- Lowell, J. D., and Guilbert, J. M., 1970, Lateral and vertical alteration-mineralization zoning in porphyry ore deposits: *Econ. Geol.*, v. 65, p. 378-408.
- Meyer, C., and Hemley, J. J., 1967, Wall rock alteration, in Barnes, H. L., ed., *Geochemistry of hydrothermal ore deposits*: New York, Holt, Rinehart and Winston, Inc., p. 166-235.
- Munizaga, F., Aguirre, L., and Herve, F., 1972, Rb/Sr ages of rocks from the Chilean metamorphic basement: *Earth Planet. Sci. Letters*, v. 18, p. 87-92.
- Perry, V. D., 1960, History of El Salvador development: *Mining Eng.*, v. 12, p. 339-382.
- Poldervaart, A., 1955, Chemistry of the earth's crust: *Geol. Soc. America Spec. Paper* 62, p. 119-144.
- Roedder, E., 1967, Fluid inclusions as samples of ore fluids, in Barnes, H. L., ed., *Geochemistry of hydrothermal ore deposits*: New York, Holt, Rinehart and Winston, Inc., p. 515-574.
- 1970, Application of an improved crushing microscope stage to studies of the gases in fluid inclusions: *Schweiz. mineralog. petrog. Mitt.*, v. 50, p. 41-58.
- Ruiz, F. C., Aguirre, L., Corvalan, J., Klohn, C., Klohn, E., and Levi, B., 1965, Geología y yacimientos metalíferos de Chile: *Inst. Invest. Geol. Santiago, Chile*, 385 p.
- Segerstrom, K., 1963, Matureland of northern Chile and its relationship to ore deposits: *Geol. Soc. America Bull.*, v. 74, p. 513-518.
- 1967, Geology and ore deposits of central Atacama province, Chile: *Geol. Soc. America Bull.*, v. 78, p. 305-318.
- Sheppard, S. M. F., Nielsen, R. L., and Taylor, H. P., Jr., 1971, Hydrogen and oxygen isotope ratios in minerals from porphyry copper deposits: *Econ. Geol.*, v. 66, p. 515-542.
- Sillitoe, R. H., Mortimer, C., and Clark, A. H., 1968, A chronology of landform evolution and supergene mineral alteration, southern Atacama Desert, Chile: *Am. Inst. Mining Metall. Petroleum Engineers Trans.*, v. 77, p. B166-B169.
- Swaync, W. H., and Trask, F., 1960, Geology of El Salvador: *Mining Eng.*, v. 12, p. 344-348.
- Taylor, H. P., Jr., 1974, The application of oxygen and hydrogen isotope studies to problems of hydrothermal alteration and ore deposition: *Econ. Geol.*, v. 69, p. 843-883.
- Tunell, G., 1930, Oxidation of disseminated copper ores in altered porphyry: Unpub. Ph.D. thesis, Harvard University.
- White, D. E., 1968, Environments of generation of some base metal ore deposits: *Econ. Geol.*, v. 63, p. 301-335.
- Muffler, L. J. P., and Truesdell, A. H., 1971 Vapor-dominated hydrothermal systems compared with hot-water systems: *Econ. Geol.*, v. 66, p. 75-97.

Sulfur Isotopes in the Porphyry Copper Deposit
at El Salvador, Chile

CYRUS W. FIELD AND LEWIS B. GUSTAFSON

Abstract

Sulfur isotope analyses have been performed on 64 monomineralic concentrates from 37 samples that are representative of mineralization in time and space at El Salvador. The hypogene sulfates (mean +10.7‰; range +7.3 to +17.0‰) are enriched in ^{34}S relative to supergene sulfates (-0.7‰; -4.6 to +3.6‰) and to hypogene sulfides (-3.0‰; -10.1 to -0.3‰). Coexisting hypogene sulfides are increasingly depleted in ^{34}S in the order molybdenite, pyrite, chalcopyrite, and bornite. The isotopic data suggest that sulfur in the supergene sulfates was largely derived from the oxidation of hypogene sulfides and that supergene "chalcocite" probably replaced hypogene chalcopyrite or bornite, but not pyrite. Isotopic temperature estimates from sulfate-sulfide fractionation pairs range from 400° to 570°C and are only in crude agreement with temperatures (<300° to >600°C) indicated by other geologic evidence. Those estimated from pyrite-chalcopyrite fractionation pairs (95° to 185°C) are much too low. Fractionation between 13 coexisting hypogene sulfate-sulfide assemblages (21 mineral pairs) defines a rather narrow band in f_{O_2} -pH-T space and suggests that f_{O_2} and pH acted as internally controlled variables throughout mineralization. Mass balance estimates of $\delta^{34}\text{S}_{\Sigma_s}$ indicate a value of about +6 per mil for the sulfate zone and a value probably significantly heavier than 0 per mil for the entire deposit as presently exposed. The $\delta^{34}\text{S}$ per mil values of coexisting hypogene sulfate and sulfide pairs approximate linear trends when plotted against their respective delta (Δ) values. These trends suggest that Early anhydrite-chalcopyrite-bornite assemblages were formed from a sulfur reservoir having $\delta^{34}\text{S}_{\Sigma_s}$ of approximately +1.6 per mil whereas Late anhydrite-pyrite-chalcopyrite assemblages formed from a reservoir +6.8 per mil $\delta^{34}\text{S}_{\Sigma_s}$. Speculative interpretation suggests that Late sulfur was derived either from remobilization of Early assemblages below the deepest levels of exposure or from volcanic wall rocks surrounding the deposit, rather than from continued emanations from the underlying magma chamber that was the source of Early mineralization. However, at least one totally different interpretation of these data is possible. Recent experimental work by Ohmoto and Rye (1975, written and oral commun.) indicates that our $\delta^{34}\text{S}$ per mil values for pyrite may require a correction factor, which would reduce both Early and Late sulfate-sulfide assemblages to approximately single linear trends. This would imply that the underlying magma chamber continued to be the predominant source of sulfur ($\delta^{34}\text{S}_{\Sigma_s} \cong +2\%$) throughout the entire sequence of alteration-mineralization. The isotopic data do not show any consistent trends of ^{34}S depletion with either paragenesis or zoning that would suggest a restricted reservoir of sulfur in the hydrothermal system. More questions than answers are provided by these data.

Introduction

THE comprehensive study of the porphyry copper deposit at El Salvador, Chile, by Gustafson and Hunt (1975) has revealed the systematic evolution of mineralization and alteration that culminated a long history of volcanism and plutonism in the Indio Muerto district. A variety of geologic arguments were presented to support the contention that Early mineralization was accomplished very close in space and time to the final consolidation of certain porphyry magmas and by hydrothermal fluids that were derived from the magmas. The transition to Late mineralization took place as convecting meteoric waters collapsed inward and reacted with the cooling

and mineralized intrusive complex. Inferences as to the pressure, temperature, and chemical conditions at various stages of this evolutionary process have been presented by Gustafson and Hunt (1975). Stable isotope investigations have been undertaken to supplement and perhaps to quantify these interpretations. Many of the minerals used in this sulfur isotope investigation are from samples also studied for hydrogen and oxygen isotopic variations by Sheppard and Gustafson (1976).

Data have been published for the distribution of sulfur isotopes in many ore deposits. In most cases only sulfide minerals were analyzed and interpretations have been largely concerned with fractionation

effects between sulfide minerals, isotopic trends and zonations, and the question of whether or not the sulfur was of "magmatic" hydrothermal or of "biogenic" sedimentary origin. Relatively few studies have been directed to the porphyry-type deposits or their related fissure and replacement deposits (Field, 1966a, 1973; Field and Moore, 1971; Lange and Cheney, 1971; and Petersen, 1972). Moreover, the limited availability of appropriate experimental calibration curves has restricted the application of sulfide-sulfide fractionation effects to temperature estimates in porphyry-type environments. Our interpretations of the El Salvador data have benefited enormously by the recent contributions of Sakai (1968) and Ohmoto (1972) who have demonstrated from theory the potential systematic isotopic variations between sulfate and sulfide minerals as a function of acidity (pH), oxygen fugacity (f_{O_2}), and temperature (T). The study of mixed sulfide assemblages containing sulfate minerals at El Salvador provides additional fractionation pairs for geothermometry and for internal checks on isotopic equilibrium. In addition, the overall patterns of isotopic fractionation between coexisting sulfate and sulfide minerals, considered in time and space, offer the possibility of placing some constraints on mass balances of sulfur and on the isotopic composition of total sulfur ($\delta^{34}S_{\Sigma S}$) in the hydrothermal system.

Sample Selection and Presentation

The principal objective of the sampling program (conducted by L.B.G.) was to obtain sulfate-sulfide assemblages representative of the major mineralization types within the mine and with respect to both their zonal and paragenetic distributions. The reader is referred to the article by Gustafson and Hunt (1975) for a description of the geology of the El Salvador deposit and for an explanation of the terminology used herein.

Detailed information concerning the location, geology, paragenesis, and mineralogy of each sample is given in Appendix 1. The order of samples listed in Appendix 1 is repeated, where applicable, in Figure 1 and Tables 1 and 3 for various groupings of the sulfur isotope data. This order generally represents the paragenetic sequence from Early, through Transitional, to Late mineralization events. Because the Late events collapsed inward and downward on the Early events, the tabulated sequence represents at best a crude three-dimensional progression from deep central to shallow peripheral zones of mineralization. However, this sequence is only generally followed as various samples containing minerals of supergene origin are listed above pyrite-bearing samples formed during the Late period of hypogene mineralization.

Early disseminated "background" mineralization in the deep central zone contains the assemblage chalcopyrite-bornite-anhydrite as represented by samples (ES: 1910R, 8230R, and 2699R) of host rocks subjected to K-silicate alteration. Host rocks altered to sericite-chlorite contain the Late assemblage pyrite-chalcopyrite-anhydrite in samples (ES: 8237 and 1116) from the deep intermediate zone and pyrite-anhydrite in samples (ES: 8238 and 1173) from the deep peripheral pyritic fringe zone.

Vein mineralization is represented by samples of the Early "A" veins (ES: 1910V and 8230V), the Transitional "B" veins (ES: 2699V and 7536V), and the Late "D" veins (ES: 7525V and 7576V, and its sericitic halo 7576H). All of these vein samples are from the deep central zone and they contain hypogene sulfate-sulfide assemblages. Upward and outward beyond the top of the sulfate zone the anhydrite has been removed by hydration and dissolution (Gustafson and Hunt, 1975). Thus, other samples from above the top of the sulfate zone do not contain primary hypogene sulfate-sulfide assemblages. Samples of sulfate not associated with sulfides include gypsum (Gyp-2) from the hydrated capping at the top of the sulfate zone and selenite gypsum (Gyp-1) and jarosite (ES-7466) from the leached capping of the peripheral and intermediate zones, respectively.

Samples ES-1855, DDH 65, DDH 599, and ES-1809 are from locations within or immediately below the zone of supergene sulfide enrichment. The alunite-bearing samples were selected to determine whether or not the isotopic data supported the geologic evidence indicating that coarsely crystalline alunites (ES: 5827 and 6573) of the advanced argillic assemblage are hypogene whereas finely crystalline varieties (ES: 7486V, 1450, and 8233) associated with secondary enrichment are of supergene origin. Mineral pairs from two of these samples, alunite-pyrite of ES-7486V and alunite-jarosite of ES-5827, do not represent contemporaneous or equilibrium assemblages. Samples ES: 1855 and 1809 and DDH 65 contain supergene "chalcocite" (quotation marks are used for any mixture of chalcocite, digenite, and djurleite).

Eleven samples containing pyrite and listed at the end of the tabulations (App. 1, Fig. 1, and Table 1) were collected from the outer and uppermost parts of the sulfide zone as presently exposed, where nearly all of the remaining sulfur resides in pyrite. Representation among these samples includes the outer pyritic fringe of the propylitic alteration zone at relatively low elevations (DDH 570 and ES: 5470 and 5472); the main pyritic fringe at the highest elevations of exposure (ES: 5709, 5715, 2511, and 3196); and pyritic waste-rock overlying chalcopyrite-

pyrite protore at high elevations in the intermediate zone (ES: 2079, 2087, and 3977). The latter three samples represent a very late event of pyritic mineralization that appears to have flushed out earlier higher grades of copper metallization. Sample DDH 129A is from high-level pyritic ore that overlies the central zone of mineralization.

Sample Preparation, Analysis, and Data Presentation

Sulfur isotope analyses have been obtained on 64 concentrates of sulfate (anhydrite 13, gypsum 4, alunite 5, and jarosite 2) and sulfide (molybdenite 1, pyrite 23, chalcopyrite 9, bornite 4, and "chalcocite" 3) minerals separated from 37 rock samples. Mineral separations using standard methods of concentration were performed by Judy Montoya of the Anaconda Geology Laboratory. Where necessary, concentrates of the sulfide minerals were leached in cold dilute hydrochloric acid to remove crystalline intergrowths of sulfate. Prior to subsequent preparation for isotopic analyses, the purity of all concentrates was further checked by examination with the binocular microscope and, for many, by X-ray diffractometer analyses. With the exception of pyrite and "chalcocite" from two samples as described below, the concentrates were essentially monomineralic and purities were 95 percent to, more commonly, 99 percent or better. However, the purity of pyrite and "chalcocite" concentrates from two samples (ES-1855 and DDH 65) ranged from 80 to 90 percent. The isotopic data for these four concentrates represent "adjusted" values derived from algebraic equations using the raw analytical data and estimates of contamination from both microscopic examination and yields of sulfur dioxide during subsequent preparations for mass spectrometer analysis.

Sulfate and sulfide mineral concentrates were prepared and isotopically analyzed by standard procedures. The majority of mineral concentrate preparations, prior to isotopic analyses, were conducted at Oregon State University (by C.W.F.). Sulfate-sulfur of anhydrite, gypsum, alunite, and jarosite concentrates was reduced to hydrogen sulfide in a boiling solution of hydrochloric-hydriodic-hypophosphorous acid as described by Thode and others (1961). Silver sulfide, derived from the reduction of sulfate minerals, and most of the sulfide minerals were oxidized to sulfur dioxide gas using a modification of the nitrogen-oxygen combustion method developed by Sakai and Yamamoto (1966). Eleven sulfide concentrates were oxidized to sulfur dioxide gas by the cupric oxide combustion method at the Isotope Geology Branch of the U. S. Geological Survey, Denver, Colorado. Measured recoveries of sul-

fur from the reduction of sulfate minerals and the combustion of sulfides was at least 90 percent and usually greater. Sulfur isotope analyses of the sulfur dioxide gases were performed both at the University of Utah, under contract with Professor M. L. Jensen of the Laboratory of Isotope Geology, and in Denver where facilities of the U. S. Geological Survey were used under the direction of Dr. Robert O. Rye.

The isotopic data are presented in terms of conventional per mil deviations ($\delta^{34}\text{S}$) as obtained from the relationship

$$\delta^{34}\text{S}\text{‰} = \left(\frac{R_x}{R_s} - 1 \right) \cdot 10^3$$

where R_x and R_s represent the measured and assumed $^{34}\text{S}/^{32}\text{S}$ ratios of the sample and standard, respectively. Positive and negative per mil deviations indicate enrichment and depletion of ^{34}S in the sample relative to the meteoritic standard for sulfur isotope analyses (0 per mil by definition). The standard deviation of the analytical error is slightly less than ± 0.2 per mil as determined from multiple preparations and analyses of the O.S.U. secondary standard. Analyses of this standard at both the University of Utah and the U. S. Geological Survey (Denver) agree by less than 0.1 per mil and thus affirm the equivalency of data between the two laboratories. This inference is supported by three analyses of pyrite in sample ES-5470, based on the two different methods of sulfide preparation and mass spectrometer analyses cited above, that provided remarkably uniform values of -10.06 , -10.13 , and -10.11 per mil respectively. Although the tabulated per mil values are given to the hundredth place as calculated from the instrumental record, they and the derived delta values as discussed in the text are rounded to the nearest tenth for consistency with the measured analytical error.

Isotopic differences between two coexisting sulfur-bearing mineral phases may originate from temperature-dependent fractionation effects of isotopic exchange equilibria. For the purposes of geothermometry, the isotopic difference between two minerals (A and B) is normally expressed as a delta (Δ_{A-B}) value that is derived from the measured $\delta^{34}\text{S}$ per mil values. The equation

$$\Delta_{A-B} = \delta^{34}\text{S}_{A\text{‰}} - \delta^{34}\text{S}_{B\text{‰}} - 1,000 \ln \alpha \quad (2)$$

relates the delta (Δ_{A-B}) value, or difference between the measured $\delta^{34}\text{S}$ per mil values, to the fractionation factor (α). Provided variations of the fractionation factor with temperature are known either from theory or experiment, the delta value may thus serve as an estimate of the temperature of mineral deposition.

TABLE 1. Analytical Data Given as $\delta^{34}\text{S}$ Per-Mil Values for Mineral Concentrates of the El Salvador Sample Suite

Cursory geologic description of samples listed in approximate order of district zonation and (or) paragenesis.

Sample	Description	Sulfide $\delta^{34}\text{S}$ ‰	Sulfate $\delta^{34}\text{S}$ ‰
ES-1910R	Andesite; central, 2,400 m; wall rock of "A" vein; K-silicate	Cp -3.56	Ah +7.64
ES-1910V	"A" vein	Bn -4.21 Cp -5.25	Ah +9.09
ES-8230R	"K" porphyry; central, 2,400 m; wall rock of "A" vein; K-silicate	Bn -5.71 Cp -3.20	Ah +7.31
ES-8230V	"A" vein	Bn -4.79 Cp -3.08	Ah +9.38
ES-2699R	"X" porphyry; central, 2,400 m; wall rock of "B" vein; K-silicate	Bn -4.76 Cp -3.94	Ah +9.69
ES-2699V	"B" vein		Ah +10.09
ES-7536V	Andesite; central, 2,400 m; "B" vein; K-silicate	Mo -0.82 Py -1.66	Ah +9.90
ES-8237	Andesite; intermediate, 2,400 m; sericite-chlorite	Cp -4.65 Py -0.79	Ah +9.88
ES-1116	"X" porphyry; intermediate, 2,400 m; sericite-chlorite	Cp -4.14 Py -2.11	Ah +10.65
ES-8238	Andesite; peripheral, 2,400 m; sericite-chlorite	Cp -5.21 Py -1.56	Ah +10.05
ES-1173	Andesite; peripheral, 2,400 m; sericite-chlorite	Py -1.21	Ah +10.54
ES-7525V	"L" porphyry; central, 2,400 m; "D" vein	Py -3.13	Ah +11.77
ES-7576H	"L" porphyry; central, 2,400 m; halo of "D" vein	Py -5.05	Cp +11.40
ES-7576V	"D" vein	Py -4.06	Ah +12.39 Cp +11.01
ES-7486V	Pyroclastic; peripheral, 2,875 m; "D" vein with finely crystalline supergene alunite	Py -3.52	Al +3.33
ES-1855	Andesite; peripheral, 2,710 m; enriched ore with "chalcocite" replacing chalcopyrite	Py -1.19 Cc -3.59	
DDH 65-182m	Andesite; intermediate, 2,630 m; enriched ore with "chalcocite" replacing chalcopyrite	Py -0.34 Cc -4.14	
DDH 599-24m	Andesite; intermediate, 2,570 m; protore below DDH 65	Py -1.08 Cp -3.23	
ES-1809	Andesite; central, 2,710 m; enriched ore with "chal- cocite" replacing chalcopyrite-bornite	Cc -4.35	
ES-5827	Rhyolite; peripheral, 3,250 m; capping with coarsely crystalline hypogene alunite; advanced argillic		Al +17.00 Jr -1.58
ES-6573	Pebble dike; intermediate, 2,990 m; capping, coarsely crystalline hypogene alunite; advanced argillic		Al +14.80
ES-1450	Pebble dike; central, 3,100 m; capping with vein of finely crystalline supergene alunite		Al +3.64
ES-8233	"X" porphyry; central, 2,710 m; vein of finely crystalline supergene alunite		Al -1.48
ES-7466	Leached capping; intermediate, 2,875 m; jarosite		Jr -3.34
Gyp-2	Hydrated upper sulfate zone; central, 2,600 m; gypsum vein		Cp +10.51
Gyp-1	Leached capping; peripheral, 2,600 m; gypsum vein		Cp -4.63
DDH 570-84m	Andesite; peripheral, 2,550 m; propylitic waste rock	Py -1.23	
ES-5470	Pyroclastic; peripheral, 2,660 m; unaltered, waste	Py -10.10	
ES-5472	Pyroclastic; peripheral, 2,660 m; sericite, waste	Py -3.94	
ES-5709	Pyroclastic; peripheral, 2,930 m; sericite, waste	Py -1.05	
ES-5715	Pyroclastic; peripheral, 2,930 m; sericite, waste	Py -1.83	
ES-2541	Pyroclastic; peripheral, 2,875 m; sericite, waste	Py -1.77	
ES-3196	Rhyolite; peripheral, 2,930 m; sericite, waste	Py -2.20	
ES-2079	Pyroclastic; intermediate, 2,930 m; advanced argillic, waste	Py -1.58	
ES-2087	Quartz porphyry; intermediate, 2,930 m; advanced argillic, waste	Py -1.54	
ES-3977	Pyroclastic; intermediate, 2,875 m; advanced argillic, waste	Py -1.37	
DDH 129A-105m	Andesite; central, 2,840 m; sericite-kaolin, enriched ore	Py -1.49	

Results and Interpretations

Isotopic data for the 64 sulfur-bearing mineral concentrates of the El Salvador suite are listed in Table 1. The distribution of all $\delta^{34}\text{S}$ per mil values, with horizontal lines connecting values for coexist-

ing mineral phases of a single sample, is graphically summarized in Figure 1. Means and ranges of the isotopic data are given in Table 2 for various mineralogic, genetic, zonal, and paragenetic groupings of the samples. The mean $\delta^{34}\text{S}$ composition of 18 hypo-

TABLE 2. Means and Ranges of $\delta^{34}\text{S}$ Per Mil Values for Sulfate and Sulfide Minerals Grouped with respect to origin (hypogene versus supergene), mineralogy, orebody zonation, and paragenesis.

Grouping	n	Mean $\delta^{34}\text{S}$ ‰	Range $\delta^{34}\text{S}$ ‰	
Sulfates—all	24	+7.9	-4.6	+17.0
Hypogene	18	+10.7	+7.3	+17.0
Supergene	6	-0.7	-4.6	+3.6
Hypogene sulfates				
Central	12	+10.0	+7.3	+12.4
Intermediate	3	+11.8	+9.9	+14.8
Peripheral	3	+12.5	+10.1	+17.0
Anhydrite	13	+9.9	+7.3	+12.4
Central	9	+9.7	+7.3	+12.4
Intermediate	2	+10.3	+9.9	+10.7
Peripheral	2	+10.3	+10.1	+10.5
Early K-silicate	3	+8.2	+7.3	+9.7
Early "A" veins	2	+9.2	+9.1	+9.4
Transitional "B" veins	2	+10.0	+9.9	+10.1
Late sericite-chlorite	4	+10.3	+9.9	+10.7
Late "D" veins	2	+12.1	+11.8	+12.4
Gypsum—Late "D" veins	2	+11.2	+11.0	+11.4
Sulfides—all	40	-3.1	-10.1	-0.3
Hypogene	37	-3.0	-10.1	-0.3
Supergene	3	-4.0	-4.4	-3.6
Molybdenite	1	-0.8		
Pyrite	23	-2.3	-10.1	-0.3
Chalcopyrite	9	-4.0	-5.3	-3.1
Bornite	4	-4.9	-5.7	-4.2
Chalcocite (supergene)	3	-4.0	-4.4	-3.6
Pyrite				
Central	5	-3.1	-5.1	-1.5
Intermediate	7	-1.3	-2.1	-0.3
Peripheral	11	-2.7	-10.1	-1.1
Transitional "B" veins	1	-1.7		
Late sericite-chlorite	5	-1.4	-2.1	-0.8
Late "D" veins	4	-3.9	-5.1	-3.1
Pyritic "fringe"	11	-2.6	-10.1	-1.1
Chalcopyrite				
Early K-silicate	3	-3.6	-3.9	-3.2
Early "A" veins	2	-4.2	-5.3	-3.1
Transitional "B" veins	1	-4.7		
Late sericite-chlorite	3	-4.2	-5.2	-3.2

to retrograde effects and to the relatively small sample representation that emphasizes the temporal evolution, rather than the spatial distribution, of mineralization at El Salvador.

Hypogene and supergene sulfate minerals

The distinction between sulfates of hypogene and supergene origin was based on geologic, mineralogic, and textural criteria established during field investigations. In accordance with equilibrium fractionation theory, the hypogene sulfates are distinctly and variably enriched in ^{34}S relative to associated hypogene sulfides (Fig. 1 and Tables 1 and 2). Temperature-dependent fractionation is suggested by the data for hypogene sulfates that show near-surface alunite (range +14.8 to +17.0‰) to be distinctly enriched in ^{34}S relative to deeper anhydrite (range +7.3 to +12.4‰). In contrast, gypsum (range +10.5 to +11.4‰) is compositionally similar to anhydrite from which it was derived by late-stage hy-

dration. The mean values for anhydrite (Table 2) exhibit small increments of progressive ^{34}S enrichment for groupings with respect to both district zonation (+9.7, +10.3, and +10.3‰ for central, intermediate, and peripheral zones respectively) and to paragenesis (+8.2, +9.2, +10.0, +10.3, and +12.1‰ for Early disseminated, "A" vein, "B" vein, Late sericite-chlorite, and "D" vein occurrences respectively).

Perhaps the simplest and most straightforward interpretation of the sulfur isotope data is in the distinction between sulfates of hypogene and supergene origin. Isotope fractionation theory predicts that hypogene sulfate, equilibrated with sulfide, should be distinctly enriched in ^{34}S relative to the sulfide and to any supergene sulfate derived from the quantitative unidirectional oxidation of sulfide-sulfur (Field, 1966b; Jensen et al., 1971; and Field and Lombardi, 1972). Consistent with this rationale, values for coarsely crystalline hypogene alunite in samples ES-5827 (+17.0‰) and ES-6573 (+14.8‰) are markedly enriched in ^{34}S relative to those for the finely crystalline or "earthy" supergene varieties in samples ES-7486 (+3.3‰), ES-1450 (+3.6‰), and ES-8233 (-1.5‰). The isotopically light alunite in sample ES-8233 (-1.5‰), gypsum in sample Gyp-1 (-4.6‰) and jarosites in samples ES-5827 and ES-7466 (-1.6 and -3.3‰) appear to have derived their sulfur through oxidation and redeposition of sulfide-sulfur in the leached capping. We attribute the isotopically intermediate values of alunites from samples ES-7486 and ES-1450 (+3.3 and +3.6‰) to mixing and redeposition of both hypogene sulfate and sulfide sources of sulfur in the supergene environment. However, these intermediate values might also originate through low-temperature disproportionation reactions accompanying the surficial oxidation of sulfides that have been proposed by Granger and Warren (1969). The isotopically heavy gypsum of sample Gyp-2 (+10.5‰), from the uppermost capping of the sulfate zone, formed simply by supergene hydration of hypogene anhydrite, as did gypsum in the "D" vein (+11.0‰) and halo (+11.4‰) of sample ES-7576.

Jarosite in both samples ES: 5827 and 7466 contains light sulfur (-1.6 and -3.3‰, respectively). Coarsely crystalline alunite and jarosite in a few samples similar to ES-5827 are intergrown in optical continuity. This texture, and other geologic inferences, once supported the speculation that jarosite, as well as alunite, might have formed in equilibrium with pyrite-covellite in a very late stage and shallow hot-spring environment that was transitional between hypogene and "classic" supergene environments (Gustafson and Hunt, 1975). The isotopic evidence, however, indicates that the jarosite, unlike

the alunite, has not undergone fractionation relative to any sulfide mineral. Jarosite has derived its light sulfur from the oxidation of ^{34}S -depleted sulfides and was formed later than the hypogene alunite (+17.0‰) with which it is associated.

Hypogene and supergene sulfide minerals

Both individual $\delta^{34}\text{S}$ per mil values for coexisting sulfide assemblages (Table 1) and mean values for these minerals of the hypogene suite (Table 2) exhibit without exception a preferred order of increasing ^{34}S depletion in the sequence molybdenite (-0.8‰), pyrite (-2.3‰), chalcopyrite (-4.0‰), and bornite (-4.9‰). This order is attributed to a primary fractionation effect involving isotopic equilibria and it is readily evident from comparisons of tabulated (Tables 1 and 2) and plotted (Fig. 1) data for the coexisting assemblages.

The hypogene sulfides show weak and imperfect isotopic trends for mineral groupings based on paragenetic occurrence (Table 2). For example, mean $\delta^{34}\text{S}$ per mil values for pyrite of "B" vein, Late sericite-chlorite, "D" vein, and pyritic "fringe" assemblages are -1.7, -1.4, -3.9, and -2.6 per mil, respectively. Mean values for chalcopyrite of Early disseminated, "A" vein, "B" vein, and Late sericite-chlorite assemblages are -3.6, -4.2, -4.7, and -4.2 per mil, respectively. It must be emphasized that for many paragenetic groupings the sample populations are small and that the ranges of the per mil values overlap. The apparent lack of isotopic trends with respect to the district zonation of hypogene sulfide minerals is probably related both to the limited sample representation and to the inward collapse and superposition of late mineralization events upon earlier ones.

At El Salvador, as is the case for many deposits that are characterized by appreciable secondary enrichment, it is difficult to determine whether or not pyrite, or other hypogene sulfides, served as the dominant host for the supergene sulfides. Geologists of the Anaconda Company have concluded, on the basis of extensive microscopic examinations, that the great bulk of the supergene sulfides replace primary Cu-Fe sulfides and not pyrite. Moreover, the textures displayed by supergene "chalcocite", and presumably indicative of pyrite replacement, are simply those inherited from their nonpyrite hypogene precursors.

Sulfide concentrates from four samples located within and beneath the zone of secondary enrichment have been analyzed to determine whether or not the supergene "chalcocite" is isotopically distinctive relative to the hypogene sulfides and as an attempt to identify isotopically the primary host mineral. Comparison of the data for the three supergene sulfides

(ES: 1855 and 1809 and DDH 65) to that for the hypogene sulfides, especially protore in DDH 500 that directly underlies DDH 65, shows the "chalcocite" to be isotopically more similar to chalcopyrite and bornite than to pyrite (see Fig. 1, Tables 1 and 2). Supergene "chalcocite" (mean -4.0‰ is depleted in ^{34}S relative to the majority of pyrites analyzed from this suite. Although this isotopic effect is consistent with predictions based on theory (Sakai, 1968; Bachinski, 1969) it is unlikely to have formed by sulfide-sulfide equilibria at the low temperatures that prevail in supergene environments. Thus, in spite of small sample populations, the isotopic evidence is consistent with the microscopic observations which suggest that "chalcocite" replaced chalcopyrite or bornite.

Isotopic equilibrium and geothermometry

The temperature dependency of isotopic fractionation between coexisting phases is well documented and is a potentially useful method of geothermometry. For sulfur-bearing minerals the fractionation effect at constant temperature is largest between sulfate-sulfide pairs, with ^{34}S preferentially concentrated in the sulfate, and is smallest but measurable between many sulfide-sulfide pairs (Sakai, 1968; Bachinski, 1969; Kajiwaru and Krouse, 1971; Czamanske and Rye, 1974; and references cited therein). For most investigations the fractionation factor (α), which is a measure of the isotopic separation between two coexisting minerals, is more conveniently expressed as a delta (Δ) value that is readily derived from the measured $\delta^{34}\text{S}$ per mil values of the mineral pair (see Eq. 2). However, the application of delta values (or fractionation factors) to geothermometry necessitates a knowledge of their variation with temperature, which is obtained either indirectly from calculations based on theory or preferably from direct experimental calibrations. With the exception of the pyrite-chalcopyrite curve derived experimentally by Kajiwaru and Krouse (1971) and the sulfate-pyrite curve predicted from theory by Sakai (1968) and Ohmoto (1972), precise fractionation effects between minerals common to porphyry-type deposits are largely unknown although they may be qualitatively estimated from thermochemical data as suggested by Bachinski (1969).

The validity of isotopic temperature estimates is predicated on the existence of equilibrium between coexisting mineral phases at the time of deposition, the preservation of this isotopic equilibrium thereafter, and the accuracy of the calibration curves by which the calculated delta values are reduced to temperatures. The coexisting mineral assemblages that we have analyzed were free of any evidence of superimposed Late events, although even in the best

TABLE 3. Delta (Δ) Values of Sulfate-Sulfide and Sulfide-Sulfide Mineral Pairs Including isotopic temperature ($^{\circ}\text{C}$) estimates (after data of Sakai, 1968, and Kajiwara and Krouse, 1971) for coexisting hypogene assemblages of El Salvador, grouped according to mineralogy.

Sample	Description	$\Delta_{\text{Gyp-Py}}$	$\Delta_{\text{Anhy-Py}}$	$\Delta_{\text{Anhy-Cp}}$	$\Delta_{\text{Anhy-Bn}}$	$\Delta_{\text{Py-Cp}}$	$\Delta_{\text{Cp-Bn}}$
ES-1910R	Early K-silicate			11.2 (550 $^{\circ}$)	11.9		0.7
ES-1910V	Early "A" vein			14.3 (465 $^{\circ}$)	14.8		0.5
ES-8230R	Early K-silicate			10.5 (570 $^{\circ}$)	12.1		1.6
ES-8230V	Early "A" vein			12.5 (510 $^{\circ}$)	14.1		1.7
ES-2699R	Early K-silicate			13.6 (485 $^{\circ}$)			
ES-7536V	Transitional "B" vein		11.6 (520 $^{\circ}$)	14.6 (460 $^{\circ}$)		3.0 (115 $^{\circ}$)	
ES-8237	Late sericite-chlorite		10.7 (545 $^{\circ}$)	14.0 (475 $^{\circ}$)		3.4 (95 $^{\circ}$)	
ES-1116	Late sericite-chlorite		12.8 (485 $^{\circ}$)	15.9 (435 $^{\circ}$)		3.1 (110 $^{\circ}$)	
ES-8238	Late sericite-chlorite		11.6 (515 $^{\circ}$)				
ES-1173	Late sericite-chlorite		11.8 (510 $^{\circ}$)				
ES-7525V	Late "D" vein		14.9 (435 $^{\circ}$)				
ES-7576H	Late "D" vein halo	16.5 (400 $^{\circ}$)					
ES-7576V	Late "D" vein	15.1 (430 $^{\circ}$)	16.5 (400 $^{\circ}$)				
DDH 599	Late sericite-chlorite					2.2 (185 $^{\circ}$)	

samples some recrystallization of Early anhydrite occurred during subsequent mineralization. Only rarely are the Early high-salinity and low-density fluid inclusions preserved (Gustafson and Hunt, 1975). Late assemblages represent a metasomatism and recrystallization of Early assemblages. As previously noted, the isotopic data show without exception relative ^{34}S enrichments among coexisting minerals (Fig. 1, Tables 1 and 2) that are entirely consistent with those established from theory or experiment (Sakai, 1968; Bachinski, 1969; Kajiwara and Krouse, 1971). The delta values given for various sulfate-sulfide pairs from samples listed in Table 3 show a general but imperfect tendency to increase among the Early to Late and the central to peripheral assemblages. These trends are consistent with isotopic fractionation effects that accompanied decreasing temperatures during the paragenetic and zonal evolution of metallization-alteration. Thus, the isotopic and geologic evidence collectively support our contention that least an approach to equilibrium was attained in our samples over the time and space of hypogene mineralization at El Salvador.

Isotopic temperatures (see Table 3, parentheses) have been determined from the delta values for appropriate mineral pairs by utilizing the theoretical fractionation curve for sulfate-pyrite (Sakai, 1968) and the experimental fractionation curve for pyrite-chalcocopyrite (Kajiwara and Krouse, 1971). Temperatures range from about 460 $^{\circ}$ to 570 $^{\circ}\text{C}$ for anhydrite-chalcocopyrite pairs of the Early K-silicate, "A" vein, and Transitional "B" vein assemblages, and from 400 $^{\circ}$ to 545 $^{\circ}\text{C}$ for gypsum-pyrite and anhydrite-pyrite pairs of the Late sericite-chlorite and "D" vein assemblages.

Isotopic temperatures of the Early assemblages (465 $^{\circ}$ to 570 $^{\circ}\text{C}$) are within the 350 $^{\circ}$ to >650 $^{\circ}\text{C}$ range indicated by fluid inclusion and other geologic

evidence (Gustafson and Hunt, 1975). The single sample from our suite that has also yielded an apparently valid oxygen isotopic temperature is ES-2699R. Isotopic fractionation among quartz, plagioclase, and biotite indicates a minimum temperature of about 525 $^{\circ}\text{C}$ (Sheppard and Gustafson, 1976) compared to that of about 485 $^{\circ}\text{C}$ from anhydrite-chalcocopyrite fractionation (Table 3).

Temperatures of 400 $^{\circ}$ to 515 $^{\circ}\text{C}$ obtained from gypsum-pyrite and anhydrite-pyrite pairs of Late "D" vein and peripheral sericite-chlorite assemblages are not much different from those obtained for the Early assemblages, and they are considerably higher than the values of less than 350 $^{\circ}\text{C}$ inferred by Gustafson and Hunt (1975). Moreover, there is substantial disagreement with the isotopic geothermometry based on pyrite-chalcocopyrite pairs from these same samples. Although the anhydrite-sulfide temperatures appear to be too high, the 95 $^{\circ}$ to 185 $^{\circ}\text{C}$ range calculated from four pyrite-chalcocopyrite pairs utilizing the experimentally derived fractionation curve reported by Kajiwara and Krouse (1971) appears to be too low. Lastly, data for the group of 11 pyrite samples (Table 1 and Fig. 1, bottom) suggest further evidence of disequilibrium. With one exception, their compositions (-3.9 to -1.1‰) are remarkably uniform and relatively enriched in ^{34}S for sulfides deposited at relatively low temperatures in the outer and upper parts of the pyritic "fringe" and beyond the sulfate zone as presently exposed.

Although several of the foregoing problems will be considered at greater length, the causes of these anomalous trends and high and low temperature estimates are uncertain. Isotopic disequilibrium is probably the dominant factor, but further experimental work is needed on the various common mineral pairs of sulfate-sulfide and sulfide-sulfide systems.

Implications as to f_{O_2} and pH

Recent papers by Sakai (1968) and Ohmoto (1972) have demonstrated a need for caution in applying the widely stated generalizations that sulfides derived from a deep-seated source necessarily have isotopic compositions close to that of meteoritic sulfur ($\delta^{34}\text{S} = 0\text{‰}$), and that wide variations from this value are diagnostic of biogenic fractionation. As elegantly developed by Ohmoto (1972), the $\delta^{34}\text{S}$ per mil values of individual sulfate or sulfide minerals are indicative of source, or the composition of total sulfur ($\delta^{34}\text{S}_{\Sigma\text{S}}$) in the system, only when other parameters such as T, f_{O_2} , and pH are known, as these control the types and abundances of the various sulfur species in solution. The 13 samples for which we have isotopic analyses of sulfate-sulfide pairs represent the wide range of depositional conditions in time and space at El Salvador; from early to late and from center to periphery. Early assemblages were formed at pressures and temperatures close to those that prevailed during final consolidation of the porphyry magmas and in equilibrium with fluids that were in equilibrium with the magmas. The Late assemblages were formed at much lower pressures and temperatures and in equilibrium with fluids that were largely heated meteoric waters then reacting with the cooling, mineralized, and altered intrusive center.

Although chemical parameters such as f_{O_2} and pH presumably varied considerably throughout the mineralization episode in both time and space, the observed mineral assemblages are not sufficiently restrictive to define these variables with certainty. However, the f_{O_2} -pH region defined by isotopic assemblages of sulfate (+5 to +15‰) and sulfide (-5 to -1‰) minerals of the El Salvador suite is given in Figure 2A. The illustration is adapted from Ohmoto (1972; fig. 5, p. 559) and uses his predicted isotopic contours for sulfate and pyrite with changing f_{O_2} and pH at 250°C and other assumptions (including $\delta^{34}\text{S}_{\Sigma\text{S}} = 0\text{‰}$) cited therein. The f_{O_2} -pH region permitted by our isotopic data forms a relatively narrow band across the diagram. At higher temperatures, the isotopically equivalent band remains almost as narrow but shifts to regions of higher f_{O_2} . This isotopic effect is shown in Figure 2B for temperatures ranging from 150° to 350°C. Again, the illustration is adapted from Ohmoto (1972; figs. 4, 5, 6, and 7) and the narrow band is derived from the data for El Salvador pyrites (-10 to 0‰) assuming a pH range from 2 to 6. Although thermochemical data are not yet adequate to compute the stability field across the ranges of temperature and pressure appropriate to our mineral assemblages, it is clear that the isotopic data define a rather narrow region in f_{O_2} -pH-T space. They do not scatter across

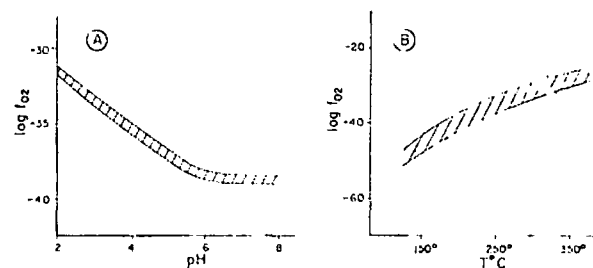


FIG. 2. Apparent regions of (A) f_{O_2} -pH for coexisting sulfate-sulfide assemblages at 250°C as defined by the ranges of $\delta^{34}\text{S}$ per mil values (sulfates +5 to +15‰; sulfides -5 to -1‰) after Ohmoto (1972, fig. 5), and (B) f_{O_2} -T as defined by the range of $\delta^{34}\text{S}$ per mil values for pyrite (-10 to 0‰) over the pH range from 2 to 6 and after Ohmoto (1972, figs. 4, 5, 6, and 7) in part.

the diagrams as might be expected if acidity, oxygen fugacity, and temperature had been independent or externally controlled variables during the evolution of mineralization at El Salvador. On the contrary, our data indicate that two of these variables (presumably f_{O_2} and pH) were internally controlled or buffered. Because the hydrothermal system was saturated with respect to both anhydrite and some Cu-Fe sulfide throughout its evolution, this condition may have served as the effective buffering control. However, many other controlling reactions are possible and particularly those involving iron-bearing oxides and silicates. Presumably the actual mechanisms of buffering and mineral reaction were very complex as in the multicomponent systems considered by Helgeson (1970).

Reservoir and composition of total sulfur

The occurrence of sulfate-sulfide assemblages throughout the mineralization sequence at El Salvador renders the deposit well suited to the study of two common assumptions. These are (1) the compositional similarity of "magmatic" hydrothermal sulfur to meteoritic sulfur (0‰ by definition) and (2) the concept of an "infinite" sulfur reservoir in hydrothermal systems.

On the basis of theoretical predictions developed by Sakai (1968) and Ohmoto (1972), the systematics of sulfate-sulfide fractionation in porphyry-type environments can be summarized as in Figure 3. For any population of coexisting sulfate-sulfide assemblages formed under equilibrium conditions and over a range of temperatures, fractionation trends portrayed by the graphical distribution of the sulfate and sulfide $\delta^{34}\text{S}$ per mil values versus their respective delta values will plot as two straight lines provided the hydrothermal reservoir for sulfur was of infinite supply and maintained a constant isotopic composition and a constant proportion of oxidized to reduced species of sulfur throughout mineralization. Because

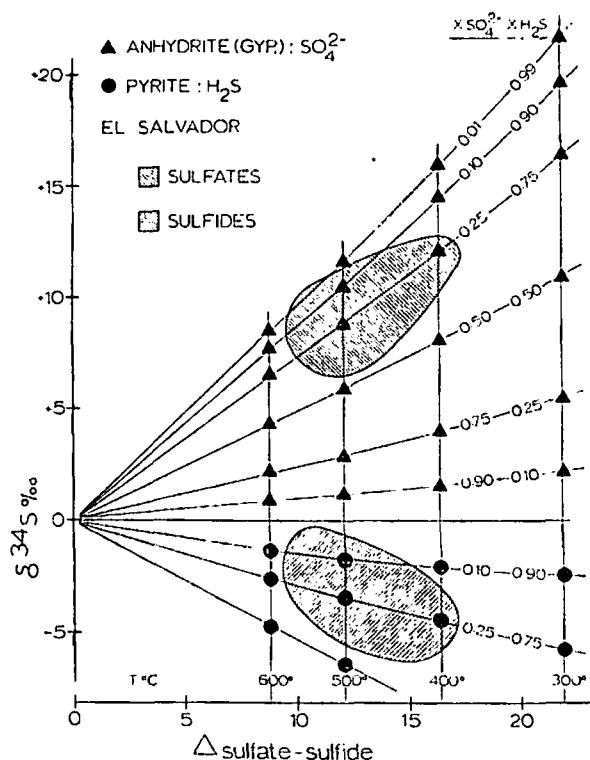


FIG. 3. Theoretical variations in the $\delta^{34}\text{S}$ per mil values of coexisting anhydrite and pyrite in response to changing T and ratios of aqueous SO_4^{2-} to H_2S . Isotopic trends and temperatures determined from sulfate-sulfide fractionations calculated by Sakai (1968), composition of $\delta^{34}\text{S}_{\Sigma\text{S}}$ assumed to be 0 per mil, and shaded areas representing isotopic realms defined by El Salvador sulfates and sulfides.

of the temperature dependency of the isotopic fractionation, extrapolation of the two lines to infinitely high temperature leads to their convergence at the 0 delta value. The point of convergence at high temperature ($\Delta = 0$) theoretically marks the isotopic composition of total sulfur ($\delta^{34}\text{S}_{\Sigma\text{S}}$) in the system. Isotopic variations between coexisting anhydrite and pyrite are shown in Figure 3 as a function of differing temperatures and mole fractions of aqueous oxidized (SO_4^{2-}) and reduced (H_2S) sulfur species in a hydrothermal system for which $\delta^{34}\text{S}_{\Sigma\text{S}}$ is assumed to be 0 per mil. The shaded areas mark the measured isotopic realms of coexisting sulfates and sulfides from El Salvador. Although fractionation effects between the coexisting sulfate and sulfide minerals are relatively large, those between the sulfur-bearing minerals and their aqueous precursors are presumably negligible for the sulfates and very small (less than 1‰) for the sulfides according to Sakai (1968). As emphasized by both Sakai (1968) and Ohmoto (1972), the isotopic composition of sulfate and sulfide minerals depends not only on temperature and $\delta^{34}\text{S}_{\Sigma\text{S}}$ of the system, but also on f_{O_2} and pH which control the mole fractions of aqueous

sulfate and sulfide species in the solution. As illustrated in Figure 3, a mineral exhibits isotopic similarity to $\delta^{34}\text{S}_{\Sigma\text{S}}$ of the system only as its aqueous precursor becomes the dominant sulfur species in the system.

The $\delta^{34}\text{S}$ per mil values of coexisting sulfate-sulfide assemblages from El Salvador (Table 1) are plotted with respect to their delta values (Table 3) in Figure 4. Various symbols representing the data points indicate different paragenetic-alteration occurrences of the samples. For many of the samples two sulfide or sulfate minerals were analyzed, and these samples are represented by two points in both the sulfate and sulfide regions. Data points for pyrite-bearing assemblages from the Late "D" veins and fringing zone of sericite-chlorite alteration exhibit remarkably good linearity. However, those for bornite-chalcopyrite assemblages of the Early background K-silicate and "A" vein occurrences of the deep central zone show considerably more scatter.

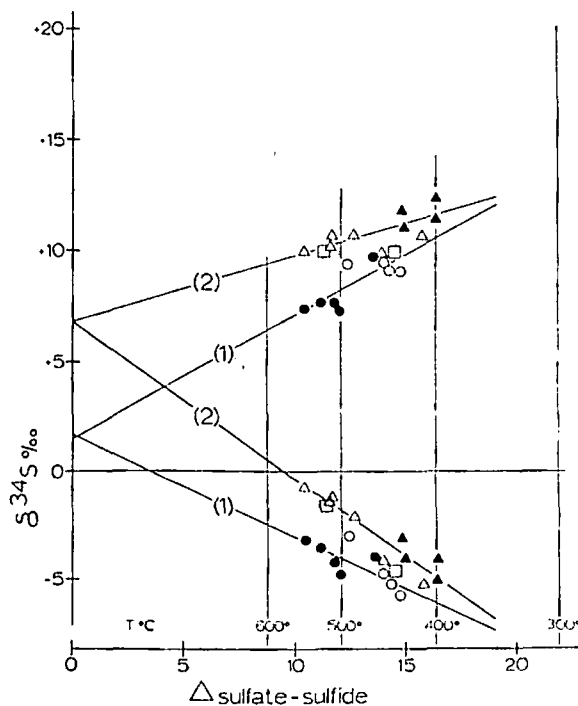


FIG. 4. Estimates of $\delta^{34}\text{S}_{\Sigma\text{S}}$ for the El Salvador hydrothermal system as determined from convergent lines of regression for plots of sulfate and sulfide $\delta^{34}\text{S}$ per mil values versus delta (Δ) values of coexisting sulfate-sulfide mineral pairs for paragenetic sample populations of Early K-silicate background and "A" vein assemblages (1) and Late sericite-chlorite background and "D" vein assemblages (2).

- (1) ● Anhy—Cp or Bn; Early K-silicate background
- Anhy—Cp or Bn; Early "A" veins
- Anhy—Cp or Py; Transitional "B" veins
- (2) ▲ Anhy or Gyp—Py; Late "D" veins
- △ Anhy—Cp or Py; Late sericite-chlorite background

The lines of regression designated 2 in Figure 4 are for the per mil-delta value points of sulfate-sulfide pairs from pyrite-bearing assemblages of Late "D" vein and "background" sericite-chlorite mineralization. Both lines intersect the vertical isotopic axis (where $\Delta = 0$) at +6.8 per mil. It may be inferred from the intercept and slopes of these two lines that the $\delta^{34}\text{S}_{\text{S}_2}$ was +6.8 per mil and the mole ratio of aqueous SO_4^{2-} to H_2S was about 70:30 in the late-stage hydrothermal system at El Salvador. Correlation coefficients for the per mil sulfate-delta value ($r = 0.746$) and per mil sulfide-delta value ($r = -0.938$) lines of regression on the 10 mineral-pair populations are statistically significant at the 95 and 99 percent confidence levels, respectively. The excellent linearity and convergence expressed by these data are rather unexpected in view of the apparent lack of isotopic equilibrium previously described for the Late pyrite-bearing assemblages which mostly formed at temperatures below 350°C. The two points that deviate most from linearity are the anhydrite-chalcopyrite pairs from samples (ES: 8237 and 1116) of fringing sericite-chlorite mineralization. Is it possible that there is a closer approach to isotopic equilibrium, or post-depositional preservation of that equilibrium, in the anhydrite-pyrite pairs than in the anhydrite-chalcopyrite (or bornite) pairs? The extent to which kinetic factors may have contributed to this linearity is unknown, but they are probably minimal as the assemblages were formed over a wide range of temperature, time, and space.

Data points for anhydrite-chalcopyrite and anhydrite-bornite pairs from Early disseminated K-silicate background and "A" vein assemblages shown in Figure 4 do not form tight linear groupings. Lines of regression (designated 1 in Fig. 4) for the per mil sulfate-delta value and per mil sulfide-delta value data converge on the vertical isotopic axis at +1.5 and +1.7 per mil, respectively. Nonetheless, correlation coefficients (r) for these lines based on nine mineral-pair populations are 0.808 and -0.763, respectively, and the linearity is statistically significant at confidence levels of 95 percent or higher. However, other groupings or line "fits" may be postulated for these scattered data. The slopes of the two regression lines suggest that the ratio of aqueous SO_4^{2-} to H_2S was slightly more than 40:60. Accordingly, the isotopic data indicate changes in $\delta^{34}\text{S}_{\text{S}_2}$ (from +1.6 to +6.8‰) and $x\text{SO}_4^{2-}:x\text{H}_2\text{S}$ (40:60 to 70:30) during the evolution from Early copper-bearing to Late pyrite-bearing assemblages at El Salvador.

It is tempting to interpret the two points of convergence in Figure 4 as representing a real difference in $\delta^{34}\text{S}_{\text{S}_2}$ of the reservoir between Early and Late

stages of mineralization. Gustafson and Hunt (1975) have portrayed Early mineralization as having been closely related to the emplacement of porphyry magmas, with the hydrothermal fluids and contained sulfur derived from these and the underlying magma chambers. In support of their interpretation, the indicated bulk composition of sulfur (+1.6‰) in the Early fluids is close to the 0 per mil value that is commonly accepted for "magmatic" hydrothermal sulfur (see Rye and Ohmoto, 1974). This similarity also argues against speculation that the abundance of sulfate at El Salvador might be attributable to remobilization of evaporites that conceivably may be part of the Jurassic or Lower Cretaceous marine section underlying the Indio Muerto district. Gustafson and Hunt (1975) have interpreted the Late fluids as having consisted largely of meteoric water, but the source of the abundant and isotopically heavy (+6.8‰) sulfur that was fixed during Late mineralization is not as clearly indicated by the geologic evidence. Possible sources might include (1) the underlying magma chambers that continued to provide sulfur and aqueous fluids, (2) additional sulfur derived from surrounding wall rock by the Late convecting meteoric-hydrothermal system, and (3) Early sulfur that subsequently was remobilized and emplaced at higher elevations during the Late hydrothermal activity. The isotopic evidence may indicate a choice among these alternatives.

Isotopic evidence for the apparent change in $\delta^{34}\text{S}_{\text{S}_2}$ between Early and Late stages of mineralization suggests that the Late sulfur was not simply derived from fluids continuing to emanate from the underlying magma chambers and that (2) or (3) are more probable interpretations. Although we have no isotopic data for traces of sulfur contained in the volcanic wall rocks that surround the El Salvador orebodies, the +6.8 per mil value indicated for Late sulfur is within the range measured for igneous rocks (Ault, 1959; Thode et al., 1962; Smitberingale and Jensen, 1963; and Sasaki, 1969), and such a source cannot be excluded by the present data.

A mass balance calculation for sulfur now preserved within the sulfate zone indicates that the bulk isotopic composition is approximately +6 per mil because there is roughly 5 to 6 times more sulfur contained in ^{34}S -enriched anhydrite than in the ^{34}S -depleted sulfides. It is therefore tempting to interpret the relatively heavy sulfur of Late mineralization (+6.8‰) as having been largely derived by remobilization of sulfur fixed during the period of Early mineralization. Gustafson and Hunt (1975) have noted the removal of Early copper from the halos of Late "D" veins deep in the deposit, and the enrichment of chalcopyrite, bornite, and enargite in these veins at higher elevations is presumably the

re-deposition of this copper. However, additional sulfur was fixed as both anhydrite and pyrite in these veins and halos at even the deepest levels of exposure. If there was leaching of anhydrite by the Late mineralization fluids, presumably it was confined to the deeper parts of the deposit.

Other difficulties are inherent to this interpretation. The apparent agreement between estimates of $\delta^{34}\text{S}_{\text{S}_2}$ derived from mass balance calculations for Early sulfur (+6‰) of the sulfate zone and that from regression line convergence for Late sulfur (+6.8‰) of the "D" vein and sericite-chlorite assemblages is probably coincidental. This is because the relative abundance of anhydrite versus sulfides was largely controlled by the relative activities of calcium ions versus those of iron and copper during mineralization and had little to do with the isotopic composition of the sulfur. Although it is difficult to estimate closely the total mass and proportions of sulfur-bearing minerals deposited in the El Salvador hydrothermal system, now that much of it has been removed by erosion and supergene activity and much lies hidden at depth, Gustafson and Hunt (1975) have indicated that up to 10^9 tons of sulfur may have been originally deposited. Probably about one-half of this amount was emplaced during Late stage alteration-mineralization. Unless this estimate for the quantity of Late sulfur is far too large, or the amount of Early sulfur is far more than is projected below the deepest level of exposure, there was not enough Early sulfur to account for all that was deposited in the Late event. It is also difficult to envisage a mineralization process, which derived its sulfur by the leaching of mixed sulfate and sulfide assemblages having different solubilities and isotopic compositions, that would maintain a constant $\delta^{34}\text{S}_{\text{S}_2}$ and a constant ratio of oxidized to reduced sulfur species over the paragenetic interval represented by the Late samples. Perhaps the most serious problem is the reduction potential required for converting large amounts of sulfate sulfur, derived from anhydrite, to sulfide sulfur forming Late pyrite, and especially at temperatures extending well below 300°C. Although the indicated mole ratio of oxidized to reduced sulfur increased paragenetically from Early to Late assemblages, the isotopic shift of $\delta^{34}\text{S}_{\text{S}_2}$ and mass balance constraints previously noted require that sulfur derived from Early anhydrite be the dominant source in this model. Approximately 10^8 tons of sulfate sulfur would have to have been reduced within a relatively small volume of rock that was probably less than 20 km³. The apparently dominant chemical trend to oxidation of sulfur during both Early and Late periods of mineralization (Gustafson and Hunt, 1975) would have to have been reversed. Estimating 10^8 tons of ferrous iron

in 1 km³ of rock, a volume of 20 km³ would provide enough potential reducing capacity to form the required amount of sulfide sulfur. However, simple reactions such as the direct sulfidation of magnetite or biotite are not adequate to provide the necessary reducing potential, and thus roughly one-half of the ferrous iron in 20 km³ of rock would have to have been oxidized. Although we do not have definitive data for the ferrous:ferric ratios of mafic silicates, the lack of visual evidence in these rocks for the pervasive oxidation of any element, other than sulfur, argues against this model.

If the Late sulfur had been derived from country rocks beyond the limits of obvious sulfur addition, most of the previously mentioned problems might be avoided. The sulfur from a source in the country rocks presumably would have been reduced and possibly isotopically homogeneous. However, there is no direct evidence that sulfur has been removed from these rocks, or that it had the appropriate isotopic composition.

Other groupings and associated line "fits" may be postulated from the data plotted in Figure 4 and these lead to markedly different interpretations. For example, three partly overlapping "isotopic" populations are suggested by the distributions of these data. They consist predominantly, but not exclusively, of assemblages representing Early disseminated, Early "A" vein and Transitional "B" vein, and Late sericite-chlorite and "D" vein mineralization. Regression lines for all three populations converge at about +6 per mil. They suggest an isotopically heavy and constant value for $\delta^{34}\text{S}_{\text{S}_2}$ throughout the mineralization sequence and isotopic variations resulting largely from changing mole ratios of aqueous SO_4^{2-} to H_2S (90:10 to 65:35) with paragenesis. This interpretation, however, is entirely speculative because of the small number of samples in the earlier populations and because of isotopic and paragenetic overlap among the data and samples comprising these populations.

On the basis of recent unpublished experimental studies by Ohmoto and Rye that indicate isotopic similarity between chalcopyrite and coexisting H_2S , and of the inordinately large fractionations we have measured between pyrite-chalcopyrite pairs, Ohmoto (1975, writ. and oral commun) has suggested that corrections of our pyrite data may be warranted. The correction involves subtracting -3 per mil (Table 3, average $\Delta_{\text{py-cp}}$ value) from each of the $\delta^{34}\text{S}$ per mil values for pyrite (Table 1). Hence, this correction transforms the per mil values for pyrite to those of "chalcopyrite" equivalents. Although the validity of these transformations are uncertain at best, the corrected data when plotted on a diagram similar to Figure 4 permit a very different geologic interpreta-

tion. Positions of the corrected anhydrite (gypsum)-pyrite data, which originally formed the majority of the data points for the regression lines designated 2 in Figure 4, are shifted to the right or downward and to the right by three units. As a consequence, the corrected data plot more closely as single linear trends that are aligned with the anhydrite-copper sulfide data points (regression lines designated 1, Fig. 4), and the entire set of isotopic data points more nearly approximates a single population. Convergence and slopes for the lines of regression suggest a value of about +2 per mil for $\delta^{34}\text{S}_{\Sigma_s}$ and a mole ratio of about 50:50 for aqueous SO_4^{2-} to H_2S in the hydrothermal system. This model implies a single source of sulfur, rather than two sources, for Early through Late stages of mineralization-alteration. The implication is that sulfur continued to emanate from the underlying magma chamber as meteoric waters invaded the cupola region of the mineralized intrusive complex. To what extent there may have been remobilization of heavy sulfur originally deposited as Early anhydrite, and later contributed to the apparent +2 permil composition of $\delta^{34}\text{S}_{\Sigma_s}$ for the total hydrothermal reservoir, is indeterminate from our data and the present state of the "art." A further implication of the single linear trends, if real, is that the ratio of oxidized to reduced sulfur in solution remained nearly constant over the time and temperature range of mineralization. Such a condition might have prevailed if f_{O_2} was externally controlled by conditions in the underlying fractionating magma chamber, but it conflicts with the previous argument that f_{O_2} was probably an internally controlled variable.

The available data do not warrant further speculation. Doubts remain concerning both the extent of isotopic equilibration among the pyrite-bearing assemblages and the true meaning of the linear configurations show in Figure 4. The scatter of data points for the anhydrite-copper sulfide assemblages allows other groupings and interpretations. This scatter probably indicates that the $\delta^{34}\text{S}_{\Sigma_s}$ of the reservoir and the ratio of oxidized to reduced species of sulfur did not remain constant throughout the complex series of events that accompanied Early alteration-mineralization (Gustafson and Hunt, 1975). The change from Early to Late environments was probably evolutionary rather than abrupt between the two separate stages of mineralization, and some retrograde effects might be expected.

The assumption of an effectively infinite reservoir of sulfur, which is implicit in constructions by Sakai (1968), Ohmoto (1972), and our Figures 3 and 4, must be questioned. Although the sulfate zone as presently exposed contains substantially more sulfate than sulfide minerals, we have no measure of

their original proportions beyond the top of this zone or throughout the entire deposit. The sulfate:sulfide mineral ratios presumably were lower toward the outer limits of anhydrite deposition and in the fringing zone of abundant pyrite. Moreover, it is possible that there were large volumes of rock in the upper and outer zones in which only sulfides were deposited. The bulk isotopic composition of sulfides in these zones would presumably be lighter than 0 per mil, especially if there had been any effect of ^{34}S -depletion during formation of Early sulfate-rich assemblages of the deep central zone because of a finite sulfur reservoir.

Eleven samples were collected from the uppermost and outermost parts of the pyritic zone as presently preserved to determine the existence of any such isotopic trends. With one exception (ES-5470, -10.1‰), the $\delta^{34}\text{S}$ values range from -3.9 to -1.1 per mil (see Tables 1 and 2) and thus they are isotopically not as light as would be expected had these pyrites equilibrated with anhydrite at the low temperatures postulated for fringing mineralization. This isotopic uniformity and small ^{34}S depletion of the pyrite is puzzling in that the outer and upper parts of the deposit are where the effects of low temperature and changing Eh and pH should produce the largest isotopic variations in the sulfides. We cannot offer any plausible reason for this constancy of composition other than to suggest that it represents some kind of "frozen" equilibrium from a higher threshold temperature and failure to re-equilibrate at subsequently lower temperatures of deposition.

The exceptionally light pyrite of ES-5470 (-10.1‰) is from a nearly unaltered ignimbrite. Sample ES-5472 (-3.9‰) represents a similar volcanic lithology with more local sericitization only 40 meters from ES-5470, and this pyrite is also depleted in ^{34}S relative to other sulfides of the fringe zone. We interpret the ^{34}S -depletion of these disseminated pyrites to some local phenomenon, perhaps fractionation accompanying diffusion, rather than to a broader mass balance effect related to a limited reservoir of sulfur.

Conclusions

The speculative interpretations offered herein must be considered more as questions than as answers. Clearly we have a need for additional samples and analytical data. Nonetheless, our results illustrate the potential wealth of information that may be derived from sulfur isotope studies of coexisting sulfate-sulfide assemblages in deposits for which the spatial and temporal complexities of mineralization are known. In addition, there is a need for further experimental determination and corroboration of frac-

tionation effects between the common sulfate and sulfide minerals.

Acknowledgments

We have benefitted from discussions with many colleagues, particularly John P. Hunt of Scripps Institution of Oceanography, Harold C. Helgeson of the University of California (Berkeley), Hiroshi Ohmoto of the Pennsylvania State University, Hugh P. Taylor, Jr., of the California Institute of Technology, J. Julian Hemley and Robert O. Rye of the U. S. Geological Survey, and Nicholas F. Davis of the Anaconda Company. Preliminary reviews and valuable criticisms of this manuscript were kindly given by N. F. Davis, H. Ohmoto, and R. O. Rye. We are particularly grateful to H. Ohmoto and R. O. Rye for bringing their unpublished work to our attention. The senior author wishes to acknowledge both the National Science Foundation, under the auspices of its International Decade of Ocean Exploration Program (the Nazca Plate Project), for the opportunity of visiting Chile in 1974, and Dr. Alvaro Tobar B., Superintendent of Geology for Compania de Cobre Salvador, for an outstanding tour of the El Salvador property. Finally, we extend our thanks and appreciation to the Anaconda Company for the financial support of this study and for permission to publish these results.

C. W. F.

DEPARTMENT OF GEOLOGY
OREGON STATE UNIVERSITY
CORVALLIS, OREGON 97331

L. B. G.

RESEARCH SCHOOL OF EARTH SCIENCE
THE AUSTRALIAN NATIONAL UNIVERSITY
CANBERRA, A.C.T., AUSTRALIA 2600
July 17, 1975; July 29, 1976

REFERENCES

- Ault, W. U., 1959, Isotopic fractionation of sulfur in geochemical processes, in Abelson, P. H., ed., *Researches in geochemistry*: New York, John Wiley and Sons, Inc., p. 241-259.
- Bachinski, D. J., 1969, Bond strength and sulfur isotope fractionation in coexisting sulfides: *ECON. GEOL.*, v. 64, p. 56-65.
- Czamanske, G. K., and Rye, R. O., 1974, Experimentally determined sulfur isotope fractionations between sphalerite and galena in the temperature range 600° to 275°C: *ECON. GEOL.*, v. 69, p. 17-25.
- Field, C. W., 1966a, Sulfur isotope abundance data, Bingham district, Utah: *ECON. GEOL.*, v. 61, p. 850-871.
- 1966b, Sulfur isotopic method for discriminating between sulfates of hypogene and supergene origin: *ECON. GEOL.*, v. 61, p. 1428-1435.
- 1973, Sulfur isotope abundances in hydrothermal sulfate-sulfide assemblages of the American Cordillera (abs.): *Geol. Soc. America, Abs. with Programs, 1973 (Ann. Mtg.)*, v. 5, n. 7, p. 619.
- and Lombardi, G., 1972, Sulfur isotopic evidence for the supergene origin of alunite deposits, Tolfa district, Italy: *Mineralium Deposita*, v. 7, p. 113-125.
- Field, C. W., and Moore, W. J., 1971, Sulfur isotope study of the "B" limestone and Galena fissure ore deposits of the U. S. mine, Bingham mining district, Utah: *ECON. GEOL.*, v. 66, p. 48-62.
- Field, C. W., Jones, M. B., and Bruce, W. R., 1971, Sulfur isotopic composition of Cordilleran hydrothermal sulfides and the role of Eh-pH (abs.): *Geol. Soc. America, Abs. with Programs, 1971*, v. 3, n. 2, p. 118.
- 1974, Porphyry copper-molybdenum deposits of the Pacific Northwest: *Am. Inst. Mining Metall. Petroleum Engineers Trans.*, v. 255, p. 9-22.
- Granger, H. C., and Warren, C. G., 1969, Unstable sulfur compounds and the origin of roll-type uranium deposits: *ECON. GEOL.*, v. 64, p. 160-171.
- Gustafson, L. B., and Hunt, J. P., 1975, The porphyry copper deposit at El Salvador, Chile: *ECON. GEOL.*, v. 70, p. 857-912.
- Helgeson, H. C., 1970, A chemical and thermodynamic model of ore deposition in hydrothermal systems: *Mineralog. Soc. America Spec. Paper 3*, p. 155-186.
- Jensen, M. L., 1971, Provenance of Cordilleran intrusives and associated metals: *ECON. GEOL.*, v. 66, p. 34-42.
- Ashley, R. P., and Albers, J. P., 1971, Primary and secondary sulfates at Goldfield, Nevada: *ECON. GEOL.*, v. 66, p. 618-626.
- Kajiwarra, Y., and Krouse, H. R., 1971, Sulfur isotope partitioning in metallic sulfide systems: *Canadian Jour. Earth Sci.*, v. 8, p. 1397-1408.
- Lange, I. M., and Cheney, E. S., 1971, Sulfur isotopic reconnaissance of Butte, Montana: *ECON. GEOL.*, v. 66, p. 63-74.
- Laughlin, A. W., Rehrig, W. A., and Manger, R. L., 1969, K-Ar chronology and sulfur and strontium isotope ratios at the Questa mine, New Mexico: *ECON. GEOL.*, v. 64, p. 903-909.
- Ohmoto, Hiroshi, 1972, Systematics of sulfur and carbon isotopes in hydrothermal ore deposits: *ECON. GEOL.*, v. 67, p. 551-578.
- Petersen, Ulrich, 1972, Nuevas investigaciones de yacimientos Peruanos: *Soc. Geol. Peru Bol.*, v. 42, p. 37-52.
- Rye, R. O., and Ohmoto, Hiroshi, 1974, Sulfur and carbon isotopes and ore genesis—a review: *ECON. GEOL.*, v. 69, p. 826-842.
- Sakai, Hitoshi, 1968, Isotopic properties of sulfur compounds in hydrothermal processes: *Geochem. Jour. (Japan)*, v. 2, p. 29-49.
- and Yamamoto, Masahiro, 1966, Fractionation of sulfur isotopes in and preparation of sulfur dioxide—an improved technique for the precision analysis of stable sulfur isotopes: *Geochem. Jour. (Japan)*, v. 1, p. 35-42.
- Sasaki, Akira, 1969, Sulphur isotope study of the Muskox intrusion, district of MacKenzie: *Canada Geol. Survey Paper 68-46*, 68 p.
- Sheppard, S. M. F., and Gustafson, L. B., 1976, Oxygen and hydrogen isotopes in the porphyry copper deposit at El Salvador, Chile: *ECON. GEOL.*, v. 71, p. 1549-1559.
- Smitheringale, W. G., and Jensen, M. L., 1963, Sulfur isotopic compositions of the Triassic igneous rocks of eastern United States: *Geochem. et Cosmochim. Acta*, v. 27, p. 1183-1207.
- Thode, H. G., Mounster, J., and Dunford, H. B., 1961, Sulphur isotope geochemistry: *Geochem. et Cosmochim. Acta*, v. 25, p. 159-174.
- Thode, H. G., Dunford, H. B., and Shima, M., 1962, Sulfur isotope abundances in rocks of the Sudbury district and their geological significance: *ECON. GEOL.*, v. 57, p. 565-578.

APPENDIX

Description of the El Salvador samples listed in approximate order of orebody zonation (deep central to shallow peripheral zones) and or paragenesis (Early to Late mineral assemblages), including host rock, mine coordinates and elevation (meters), min-

eralogy of alteration and vein assemblages, paragenetic occurrence, and mole ratios of sulfate to sulfide sulfur (see text for detailed elaboration of sample groups).

- ES-1910: Andesite; 19,894 N-8,160 W, 2,400 m; central; Early disseminated anhydrite-bornite-chalcopryrite with strong biotitic K-silicate alteration; cut by "A" veins bearing quartz, K-feldspar, anhydrite, bornite, and chalcopryrite; mole ratio sulfate/sulfide sulfur approximately 7:1, somewhat lower in the veins.
- ES-8230: "K" porphyry; 19,706 N-7,829 W, 2,400 m; central; low intensity Early disseminated anhydrite-chalcopryrite-bornite with K-silicate alteration; cut by Early "A" veins bearing quartz, bornite, chalcopryrite, and anhydrite.
- ES-2699: "X" porphyry; 19,875 N-8,200 W, 2,400 m; central; Early disseminated anhydrite-bornite-chalcopryrite with moderate K-silicate alteration; cut by Transitional "B" vein bearing quartz, anhydrite, and chalcopryrite; mole ratio of sulfate/sulfide sulfur approximately 6:1 in the wall rock, somewhat lower in the vein.
- ES-7536: Andesite; 19,950 N-7,613 W, 2,400 m; central; biotitic K-silicate alteration of host with disseminated chalcopryrite-bornite cut by Transitional "B" vein bearing quartz, anhydrite, chalcopryrite, molybdenite, and pyrite.
- ES-8237: Andesite; 19,808 N-8,530 W, 2,400 m; intermediate; intense Late sericite-chlorite alteration, and residual sodic plagioclase, with pyrite-chalcopryrite-anhydrite-(magnetite) mineralization; mole ratio sulfate/sulfide sulfur approximately 1:1.
- ES-1116: "X" porphyry; 19,720 N-8,420 W, 2,400 m; intermediate; intense sericite-chlorite alteration, and residual alkali feldspar, with Late anhydrite-chalcopryrite-pyrite mineralization; mole ratio of sulfate/sulfide sulfur is approximately 2:1.
- ES-8238: Andesite; 19,500 N-8,750 W, 2,400 m; peripheral; intense Late sericite-chlorite alteration, and residual biotite and traces of sodic plagioclase, with weak anhydrite-pyrite veinlets; mole ratio of sulfate/sulfide sulfur is approximately 3:1.
- SE-1173: Andesite; 19,502 N-8,748 W, 2,400 m; peripheral; moderately biotized with Late sericite-chlorite alteration and numerous pyrite-anhydrite veinlets lacing host; mole ratio of sulfate/sulfide sulfur is approximately 0.5:1.
- ES-7525: "L" porphyry; 19,946 N-7,742 W, 2,400 m; central; weakly mineralized host cut by Late "D" vein of pyrite-anhydrite which has a sericite-pyrite halo.
- ES-7576: "L" porphyry; 19,950 N-7,920 W, 2,400 m; central; very weakly mineralized host cut by Late "D" vein of pyrite-anhydrite; sericite-pyrite halo of vein contains minor chalcopryrite and anhydrite; anhydrite largely hydrated to gypsum.
- ES-7486: Pyroclastic; 19,340 N-8,740 W, 2,875 m; peripheral; sericitic host in the pyritic fringe cut by Late "D" vein of quartz and pyrite; finely crystalline supergene alunite fills vugs.
- ES-1855: Andesite; 19,580 N-8,519 W, 2,710 m; peripheral; pyritic host with sericite-kaolinite alteration; supergene "chalcocite," with pyrite, replaces original hypogene pyrite-chalcopryrite assemblage.
- DDH 65-182m: Andesite; 20,400 N-8,610 W, 2,630 m; intermediate; strongly enriched "chalcocite"-pyrite ore in host altered to kaolinite-sericite assemblage.
- DDH 599-24m: Andesite; 20,385 N-8,630 W, 2,570 m; intermediate; host with biotite-chlorite-sericite alteration contains chalcopryrite-pyrite protore below DDH 65.
- ES-1809: Andesite; 19,752 N-7,597 W, 2,710 m; central; host with kaolinite-sericite alteration contains strong "chalcocite" enrichment of hypogene chalcopryrite-bornite assemblage.
- ES-5827: Rhyolite; 19,832 N-7,535 W, 3,250 m; peripheral; jarositic leached capping with quartz-alunite alteration; coarsely crystalline hypogene alunite.
- ES-6573: Pebble dike; 20,118 N-8,875 W, 2,990 m; intermediate; jarositic leached capping in which coarsely crystalline hypogene alunite associated with pyrophyllite-diaspore-quartz in sandy pebble dike cuts quartz porphyry host that has been subjected to advanced argillic alteration.
- ES-1450: Pebble dike; 19,707 N-7,849 W, 3,100 m; central; jarositic leached capping that contains vein of finely crystalline supergene alunite in dike cutting "K" porphyry host with sericite-andalusite-pyrophyllite alteration.
- ES-8233: "X" porphyry; 20,044 N-7,830 W, 2,710 m; central; enriched and kaolinized host cut by vein of finely crystalline supergene alunite.
- ES-7466: Rhyolite; 19,804 N-9,040 W, 2,875 m; intermediate; coarsely crystalline jarosite filling cracks in leached capping formed by sericitized host over pyritic fringe mineralization.
- Gyp-2: Gypsum vein; 19,814 N-8,390 W, 2,600 m; central; massive granular gypsum in vein within upper hydrated capping of the sulfate zone.
- Gyp-1: Gypsum vein; 20,640 N-9,560 W, 2,600 m; peripheral; selenite gypsum filling cracks in leached capping over outer pyritic fringe.
- DDH 570-84m: Andesite; 21,500 N-9,650 W, 2,550 m; peripheral; propylitic alteration in waste rock containing disseminated pyrite.
- ES-5470: Pyroclastic; 18,106 N-7,738 W, 2,660 m; peripheral; disseminated pyrite in nearly fresh ignimbrite that contains traces of sericite; outer-

- most pyritic fringe with nearby propylitic alteration.
- ES-5472: Pyroclastic; 18,145 N-7,744 W, 2,660 m; peripheral; disseminated pyritic in host near ES-5470 that locally contains zones of sericite alteration.
- ES-5709: Pyroclastic; 19,100 N-7,981 W, 2,930 m; peripheral; strong pyritic waste mineralization in sericitized host from the upper level of the pyritic fringe.
- ES-5715: Pyroclastic; 19,100 N-7,891 W, 2,930 m; peripheral; strong pyritic waste mineralization in sericitized host from the upper level of the pyritic fringe.
- ES-2541: Pyroclastic; 19,400 N-8,691 W, 2,875 m; peripheral; strong pyritic waste mineralization in sericitized host from the upper level of the pyritic fringe; collected above ES: 1173 and 8238.
- ES-3196: Rhyolite; 19,950 N-7,233 W, 2,930 m; peripheral; strong pyritic waste mineralization in sericitized host that contains traces of diaspore, alunite, enargite, and covellite.
- ES-2079: Pyroclastic; 19,580 N-8,076 W, 2,930 m; intermediate; strong pyritic waste mineralization in host altered to an advanced argillic sericite-andalusite-pyrophyllite assemblage; sample overlies chalcopyrite-pyrite protore and secondarily enriched pyrite-bornite mineralization.
- ES-2087: Quartz porphyry; 19,464 N-8,133 W, 2,930 m; intermediate; strong pyritic waste mineralization in host altered to an advanced argillic sericite-andalusite-pyrophyllite assemblage; residual sulfides in relict pyrite-bornite zone of leached capping (see ES-2079) probably represent late pyritic copper-flushing mineralization.
- ES-3977: Pyroclastic; 19,838 N-8,553 W, 2,875 m; intermediate; strong pyritic waste mineralization in host altered to an advanced argillic sericite-andalusite-pyrophyllite assemblage; overlies secondarily enriched ore and pyrite-chalcopyrite protore.
- DDH 129A-105m; Andesite; 19,950 N-7,610 W, 2,840 m; central; secondarily enriched pyrite-"chalcocite" ore with traces of enargite in host altered to an advanced argillic sericite-alunite-kaolinite assemblage; overlies chalcopyrite-bornite protore.

UNIVERSITY OF UTAH
RESEARCH INSTITUTE
EARTH SCIENCE LAB.

AREA
Chile
El Tatio

The isotopic composition of waters from the El Tatio geothermal field, Northern Chile

WERNER F. GIGGENBACH

Chemistry Division, Department of Scientific and Industrial Research, Petone, New Zealand.

(Received 6 September 1977; accepted in revised form 22 February 1978)

Abstract—On the basis of isotopic and chemical analyses of 45 spring, well and meteoric water samples from the El Tatio geothermal field in Northern Chile, four main processes giving rise to the formation of a wide range of thermal discharges can be distinguished. (1) Deep dilution of a predominant, primary high chloride (5500 mg/l, 260°) supply water derived from precipitation some 15 km east of El Tatio with local groundwater produces a secondary chloride water. (4750 mg/l, 190°) feeding springs over a limited area. (2) Single step steam separation from these two waters leads to isotopic shifts and increases in chloride contents to 8000 and 6000 mg/l respectively. (3) Absorption of this separated steam and carbon dioxide into local ground water and mixing with chloride waters at shallow levels produces a series of intermediate temperature (160°), low chloride, high bicarbonate waters. (4) Absorption of steam containing H₂S into surface waters leads to the formation of zero chloride, high sulfate waters; the isotopic enrichment observed is governed by a kinetic, steady state evaporation process.

INTRODUCTION

A DETAILED description of the El Tatio geothermal field in Northern Chile was given by CUSICANQUI *et al.* (1975). On the basis of geochemical results, these authors came to the conclusion that the thermal discharges of El Tatio were derived from precipitation to the east which had acquired heat and chemical constituents while passing underneath a chain of volcanoes during their migration to the west. The existence of such largely horizontal movements of thermal waters has been described by HEALY and HOCHSTEIN (1973) on the basis of geophysical evidence.

At El Tatio three main types of thermal springs can be distinguished (ELLIS, 1969): Springs discharging high chloride waters (~8000 mg/l) located along a SW-NE trending line in the northern part of the main thermal area (Fig. 1), more dilute, intermediate chloride pools (~5000 mg/l) in the south-western part, and low chloride, high sulfate pools along the eastern margins. Exploration wells drilled to about 30 m depth produced waters with chloride contents of around 6000 mg/l. During a downhole sampling program, however, a highly mineralised brine was encountered at the bottom of wells T2 and T9.

A short description of the isotopic composition of El Tatio thermal waters was given by CUSICANQUI *et al.* (1975). In this study an attempt is made to delineate processes influencing the isotopic and chemical composition of the thermal waters and their origins in more detail.

RESULTS

Experimental
Isotope samples were collected in air-tight plastic bottles; soon after cooling to ambient temperature the waters were sealed into 150 ml glass ampoules. Isotopic analyses were carried out by established techniques. Hydrogen for D/H-measurements was produced by reduc-

tion over uranium at 700°C or zinc at 450°; the oxygen-18 content of the samples was determined by use of the CO₂-equilibration method. The relative errors over the three year analysis period were found to be within ±2‰ for deuterium and ±0.2‰ for oxygen-18.

Isotopic results

The isotopic composition of thermal and meteoric waters together with water temperatures, flows, and a short description of the sampling points are given in Table 1. The isotopic composition of well samples represents the

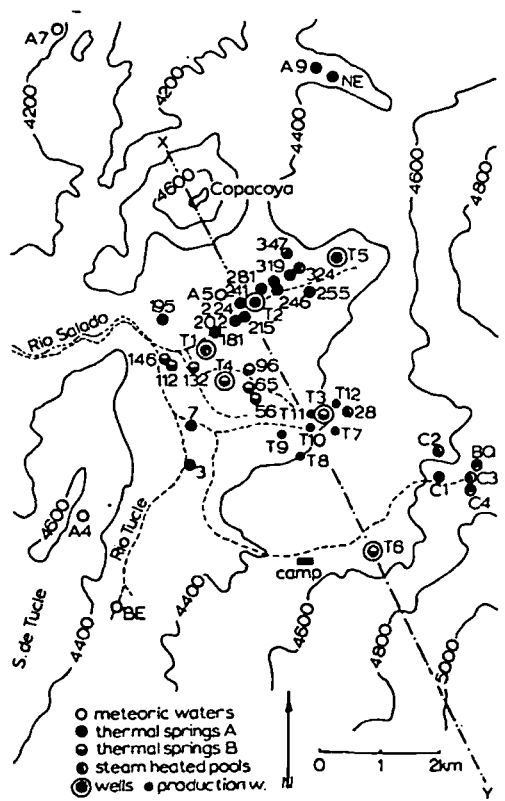


Fig. 1. Sketch map of El Tatio geothermal area.

Table 1. The isotopic composition of well, thermal spring and meteoric waters of the El Tatio geothermal field

No.	Date Coll.	T °C	Flow l/s	Short Description	δD ‰	δ ¹⁸ O ‰
<u>Wells</u>						
T1	12.69	211°	-	depth drilled 617m, solid casing 243m	-73	-6.0
T2	6.70	227°	-	" " 652m, " " 295m	-78	-6.3
T3	10.70	253°	-	" " 616m, " " 238m	-75	-6.8
T4	12.70	229°	-	" " 733m, " " 247m	-77	-6.6
T5	3.71	212°	-	" " 568m, " " 282m	-72	-5.6
<u>Chloride Springs</u>						
227	11.68	85°	0.5	vigorously spouting, clear pool, sinter	-69	-5.5
241	11.68	85°	0.5	spouting clear geyser, sinter	-68	-5.7
224	11.68	85°	0.1	variable discharge, clear pool	-68	-6.0
195	11.68	86°	0.2	spouting clear pool, sinter	-66	-6.0
146	11.68	86°	1.0	vigorous, periodic, clear geyser	-65	-6.0
96	11.68	86°	2.0	violently boiling, clear pool	-66	-6.2
202	11.68	86°	0.2	spouting, clear pool, sinter	-65	-6.2
112	11.68	86°	0.2	vigorously boiling clear pool	-68	-6.1
56	11.68	85°	0.1	small spouting clear pool, sinter	-64	-6.1
319	11.68	83°	-	boiling clear pool on sinter	-67	-6.0
65	11.68	86°	0.3	spouting, clear pool on sinter	-67	-6.5
132	11.68	79°	2.0	clear stream, sinter flat	-67	-6.9
246	10.69	64°	<0.1	clear pool on sinter flat	-63	-7.1
7	11.68	84°	0.1	jet of clear water, sinter	-66	-7.2
181	11.68	85°	0.3	clear pool on sinter	-64	-7.0
215	10.69	73°	2.0	clear stream from sinter	-61	-7.5
281	10.69	37°	0.1	gaseous opalescent pool	-61	-7.5
3	11.68	80°	-	clear spring from sinter flat	-61	-7.8
255	11.68	40°	0.1	clear pool on algae mound	-61	-8.3
NE	11.68	58°	2.0	clear stream, salt edges	-62	-8.4
A9	8.70	55°	-	quiet, clear pool	-57	-8.4
<u>Meteoric waters</u>						
A7	8.70	12°	-	cold spring	-48	-7.7
A4	8.70	14°	-	cold spring	-58	-8.2
A5	8.70	25°	-	cold spring	-53	-8.8
SN	11.68	0°	-	snow sample	-55	-9.5
BE	11.68	15°	-	drainage from SW	-50	-7.3
<u>Sulfate springs</u>						
C2	11.68	33°	0.5	clear flow, no sinter	-55	-8.7
C1	11.68	20°	0.1	clear flow, no sinter	-55	-8.6
BQ	11.68	18°	-	drainage from E, no sinter	-52	-7.3
C4	11.68	85°	-	violently boiling, milky pool	-44	-3.3
28	11.68	78°	0	boiling opalescent pool	-44	-0.9
C3	11.68	86°	<0.1	vigorously boiling, milky pool	-49	-3.7
347	10.69	56°	<0.1	gaseous, opalescent pool	-31	+6.3
324	10.69	78°	<0.1	gaseous, milky pool, no sinter	-26	+7.5
<u>Eastern samples</u>						
B1	8.70	60°	-	large pool	-66	-7.5
B2	8.70	6°	-	cold spring	-69	-9.5
B3	8.70	18°	-	warm stream	-67	-8.7
L1	8.70	-	-	cold spring N Laguna Colorada	-94	-12.4
L2	8.70	-	-	cold inflow into Laguna Colorada	-85	-11.3
LC	8.70	-	-	Laguna Colorada	-56	-4.3
<u>Postulated supply waters</u>						
A	-	260°	-	primary supply water	-78	-6.9
B	-	190°	-	diluted, supplying group B springs	-73	-7.2
C	-	160°	-	bicarbonate water	-58	-8.8
D	-	10°	-	local precipitation	-52	-8.5

weighted mean of analyses of steam and water samples obtained under controlled conditions by use of a sampling separator.

Chemical results

Chemical analyses of thermal and meteoric waters are given in Table 2. Again the composition for wells has been calculated on a total discharge basis, the values given are considered to represent the compositions of the waters under downhole conditions.

DISCUSSION OF RESULTS

Processes controlling the isotopic and chemical composition of El Tatio thermal waters

The pattern displayed by the isotopic data points in Figs. 2 and 3 suggests that several processes are active in producing thermal discharges with a wide range of isotopic compositions. In conjunction with

Table 2. T1

No.	T1	T2	T3	T4	T5
227	227	241	224	195	146
96	202	112	56	319	65
132	246	7	181	215	281
3	255	NE	A9	TB	19
A7	1	A4	1	A5	2
SN	2	BE	1	C2	3
C1	21	BQ	11	C4	81
28	71	C3	81	347	56
324	78	B1	52	B2	6
B3	18	L1	-	L2	-
LC	-	a this work		b ELLIS (15)	
		c CUSICANQ		chemical data	
		can be disti		centred aroun	
		-6‰ respect		long lines co	
		meteoric water		ing with a I	
		ascending awa		High chloria	
		thermal spring			

Table 2. The chemical composition of well and spring discharges and meteoric waters from the El Tatio geothermal field

No.	T °C	pH	Cl	SO ₄	HCO ₃	B	SiO ₂	Li	Na	K	Rb	Cs	Ca	T _{SiO₂}	T _{NKC}	ref.
<u>Wells</u>																
T1	211°	6.8	5820	47	21	127	293	23	3340	310	3.5	11.3	196	191°	212°	a
T2	227°	6.8	6020	33	35	127	298	28	3430	431	4.8	12.3	197	192°	232°	a
T3	253°	6.6	4490	44	9	107	173	21	2570	127	1.7	9.5	198	161°	171°	a
T4	220°	6.7	5650	45	59	129	246	20	3430	148	1.9	12.7	167	181°	170°	a
T5	212°	6.7	6690	34	48	150	343	32	3760	519	5.6	13.1	219	201°	239°	a
<u>Chloride springs</u>																
227	85°	7.4	8220	38	45	187	256	47	4600	520	6.7	15.8	280	183°	227°	b
241	85°	7.4	7870	26	44	170	280	45	4320	525	6.4	14.9	278	189°	231°	b
224	85°	7.2	6890	35	54	156	207	40	3860	445	-	12.0	244	171°	226°	b
195	86°	7.7	6280	29	68	141	125	34	3440	360	-	10.2	239	145°	218°	b
146	86°	7.7	6190	35	74	142	126	35	3500	306	-	-	249	145°	206°	b
96	86°	7.3	5840	46	46	137	180	32	3460	170	-	9.9	248	163°	174°	b
202	86°	7.3	5630	37	71	127	137	33	3140	336	-	10.2	218	149°	218°	b
112	86°	7.6	5560	35	69	127	130	30	3200	235	-	10.4	236	147°	195°	b
56	85°	7.6	5380	46	87	127	207	27	3060	150	2.1	9.9	232	171°	172°	b
319	83°	6.3	5370	22	65	123	149	27	3000	367	4.2	10.3	171	153°	229°	b
65	86°	6.7	5240	42	96	123	177	28	2880	145	2.1	10.0	225	163°	173°	b
132	79°	6.5	4970	45	92	136	181	27	2820	175	-	9.6	208	164°	184°	b
246	64°	6.2	4310	46	168	90	161	21	2360	235	-	-	160	157°	211°	b
7	84°	7.3	4210	62	288	101	258	24	2560	230	-	7.4	147	184°	207°	b
181	85°	6.9	4010	36	118	91	122	-	2250	230	2.5	8.0	170	143°	211°	b
215	73°	6.6	3120	44	138	70	150	-	1810	195	-	6.8	129	154°	213°	b
281	37°	3.2	2790	171	0	60	176	16	1570	200	-	6.4	90	162°	224°	b
3	80°	6.7	1830	78	242	45	218	11	1080	103	-	3.4	113	174°	196°	b
255	40°	7.2	1190	58	239	28	150	8	760	82	-	2.0	48	154°	205°	b
NE	58°	6.9	950	30	360	21	149	6	604	68	-	-	59	153°	201°	b
A9	55°	8.2	760	5	872	17	188	4	540	64	0.3	0.7	28	166°	209°	a
<u>El Tatio brine</u>																
TB	190°	2.0	185000	-	0	302	200	5	107000	4710	33	6.1	6270	169°	201°	c
<u>Meteoric waters</u>																
A7	12°	8.4	90	6	38	4	33	0.2	52	4	.01	<.01	8	-	-	a
A4	14°	7.5	53	<5	32	2	64	<0.1	35	4	.01	<.01	4	-	-	a
A5	25°	6.7	<5	5	5	<2	38	<0.1	6	1	<.01	<.01	4	-	-	a
SN	0°	-	<5	<5	5	<2	8	<0.1	4	1	<.01	<.01	1	-	-	a
BE	15°	8.3	<5	15	135	<2	69	<0.1	12	3	.01	<.01	22	-	-	a
<u>Sulfate waters</u>																
C2	33°	6.8	<5	98	135	<2	80	<0.1	12	10	-	-	67	-	-	b
C1	20°	7.1	<5	144	165	<2	60	<0.1	16	8	-	-	99	-	-	b
B0	18°	7.9	14	160	-	<2	66	<0.1	13	6	-	-	21	-	-	b
C4	85°	6.4	<5	180	4	<2	-	<0.1	15	10	-	-	27	-	-	b
28	78°	6.7	<5	180	91	<2	88	<0.1	53	18	-	-	37	-	-	b
C3	86°	6.9	<5	228	15	<2	127	<0.1	44	15	-	-	45	-	-	b
347	56°	4.9	<5	245	1	<2	87	<0.1	28	5	-	-	26	-	-	b
324	78°	3.6	<5	345	0	<2	112	<0.1	32	9	-	-	37	-	-	b
<u>Eastern springs</u>																
B1	52	7.4	35	320	62	<2	124	<0.1	52	23	0.1	<.01	71	-	-	a
B2	6	7.4	<5	54	16	<2	58	<0.1	5	4	<.01	<.01	13	-	-	a
B3	18	8.1	<5	450	232	<2	99	<0.1	10	13	0.1	0.03	165	-	-	a
L1	-	7.6	124	48	72	<2	74	0.3	83	12	<.01	<.01	8	-	-	a
L2	-	7.6	10	5	58	<2	41	0.1	9	5	<.01	<.01	8	-	-	a
LC	-	8.2	41660	4200	1120	350	79	80.0	27980	2700	7.0	2.00	1820	-	-	a

a this work. — not determined.
 b ELLIS (1969). T_{SiO₂} Silica temperature (adiabatic).
 c CUSICANQUI *et al.* (1975). T_{NKC} Na-K-Ca-temperature ($\beta = 1/3$).

chemical data, three main groups of thermal waters can be distinguished. The high chloride waters occurred around δD and $\delta^{18}O$ -values of -70‰ and -6‰ respectively, the chloride-bicarbonate waters along lines connecting the high chloride waters to meteoric waters, and the sulfate waters following a line with a positive slope of around 1.6 (Fig. 2) extending away from meteoric water positions. High chloride waters. The chloride contents of the thermal spring waters range up to about 8000 mg/l

with the highest chloride springs restricted to the northern part of the main thermal area (ELLIS, 1969). These waters are least diluted and can be considered to be most closely related to the deeper supply waters. The chemical and isotopic compositions of such deep waters as represented by well samples T1-5, however, are quite different with chloride contents of around 5500 mg/l and deuterium contents well below those of the spring waters. As proposed by MAHON (1974), the increased solute contents of the spring waters as

thermal
 $\delta^{18}O$
 -6.0
 -6.3
 -6.8
 -6.6
 -5.6

-5.5
 -5.7
 -6.0
 -6.0
 -6.0
 -6.2
 -6.2
 -6.1
 -6.1
 -6.0
 -6.5
 -6.9
 -7.1
 -7.2
 -7.0
 -7.5
 -7.5
 -7.8
 -8.3
 -8.4
 -8.4

-7.7
 -8.2
 -8.8
 -9.5
 -7.3

-8.7
 -8.6
 -7.3
 -3.3
 -0.9
 -3.7
 +6.3
 +7.5

-7.5
 -9.5
 -8.7
 -12.4
 -11.3
 -4.3

-6.9
 -7.2
 -8.8
 -8.5

ical comp
 data points
 processes are
 with a wide
 action with

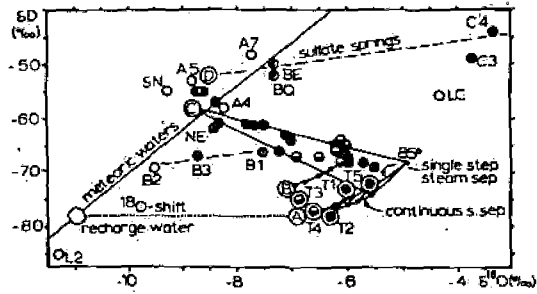


Fig. 2. Plot of δD vs $\delta^{18}O$ for thermal and meteoric waters of the El Tatio geothermal area (symbols see Fig. 1).

compared to the waters tapped by the wells is likely to be caused by steam separation due to adiabatic expansion of the deep fluids during their rise to the surface.

In Figs. 2 and 3 lines are drawn representing the shifts in isotopic composition and chloride content (TRUEDELL *et al.*, 1978) expected for steam separation from a water with an initial temperature of 260°, a chloride content of 5500 mg/l and an isotopic composition of -78‰ for deuterium and -6.9‰ for oxygen-18. The temperature chosen for the primary supply water is close to the maximum downhole temperature measured (CUSICANQUI *et al.*, 1975), its chloride and isotope contents were evaluated by initially assuming the well and high chloride spring discharges to be related by straightforward single step steam separation processes. Single step steam separation corresponds to the case where steam and water travel together and remain in contact and isotopic equilibrium until steam separates at a given depth and temperature. Continuous steam separation describes the other extreme situation where steam is removed continuously as soon as it is formed.

On the basis of isotopic data alone the formation of the chloride-spring waters could be explained in terms of steam separation and dilution of a single supply water. Preliminary evaluation of the chemistry

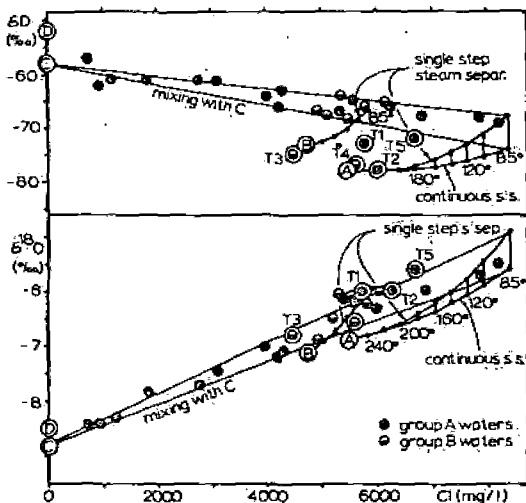


Fig. 3. Plot of δD and $\delta^{18}O$ vs chloride content for waters of the El Tatio geothermal area.

of these waters, however, indicates the existence of a group of springs characterised by low K/Cl weight ratios of around 0.025 as compared to those of around 0.060 for the rest of the springs. These springs, designated group B, occur within a limited area extending from the south-western end of the main thermal area to the south-east (Fig. 1). The similarity in the relative proportions of elements least likely to be affected by secondary processes (Cl, B, Cs) of El Tatio thermal waters (Fig. 4b) suggests common origins and formation conditions. The observed reduction in relative potassium contents for group B waters may then be explained in terms of some readjustment of the Na/K ratio to lower temperature conditions. Lower underground temperatures for the group B waters are also indicated by lower SiO₂ contents. This reduction in temperature is most likely due to dilution by the infiltration of surface waters possibly in combination with conductive heat loss through prolonged residence at shallow levels.

In order to explain the chemical and isotopic composition of the group B spring waters, a feed water with a reduced chloride content of 4750 mg/l at a temperature of 190° is postulated. The isotopic composition of this water B indicates a 1:6 mixture of local meteoric water with supply water A. As shown in Figs. 2 and 3, the position of data points observed for group B springs closely corresponds to that expected for waters produced through single step steam separation from such a pre-diluted, cooler water B.

Bicarbonate-chloride waters. The wide range in isotopic compositions observed for chloride springs can

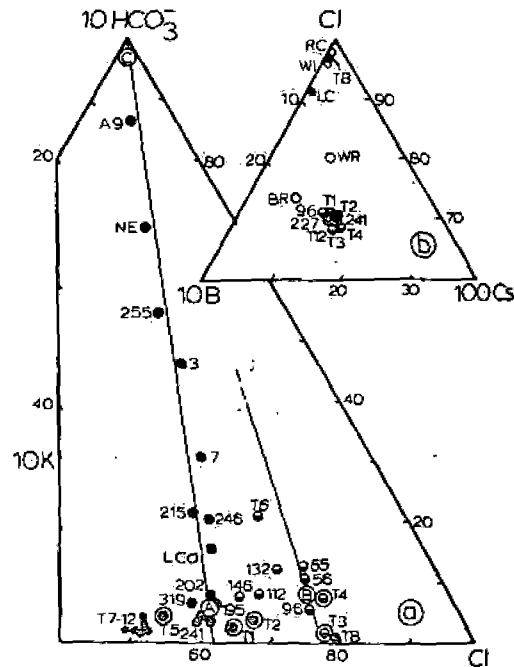


Fig. 4. (a) Relative HCO₃⁻, K and Cl contents of spring and well discharges at El Tatio; (b) relative Cl, B and Cs contents of thermal and volcanic waters at El Tatio and in New Zealand.

only partly be explained by secondary processes alone. The relative proportions of waters have to be considered. Data for all chloride waters indicate the existence of a group of waters with a deuterium and oxygen-18 composition of -8.8‰ respectively. This composition is inferred water I. The way by extrapolation of elements measured, the isotopic compositions remain close to those of the meteoric water. In a triangle of proportions of Cl, B and Cs group A are situated from the HCO₃⁻ constant ratio K/B however, occupying a position close to low HCO₃⁻ 0.025. The resulting mixture of the waters are an admixture of the water C.

The main constituent of the thermal water C is bicarbonate (170 mg/l), and its relative proportions indicate a tenfold dominance of bicarbonate over chloride. This represents a condensate of steam and CO₂ and TRUEDELL, 1978, is assumed to be assumed to be steam and condensed steam water, its isotopic composition is related to the weighted mean of the contributing phases and proportions of steam de-



Fig. 5. Plot of δD vs $\delta^{18}O$ for equilibrium steam and meteoric water.

existence of K/Cl weights to those of these springs. limited area of the main east likely to B, Cs) of El ommon or- rved reduc- up B waters eadjustment: conditions. he group B contents. This due to dilu- possibly in hrough pro-

otopic com- feed water g/l at a tem- ic composi- ure of local s shown in its observed ds. to that single step ited, cooler ange in iso- springs can

only partly be explained in terms of steam separation processes alone and other processes, such as admixture of waters with differing isotopic compositions, have to be considered. Extrapolation of the isotopic data for all chloride springs to zero chloride suggests the existence of a diluting water phase with deuterium and oxygen-18 contents of around -58‰ and -8.8‰ , respectively. The chemical composition of this inferred water phase may be obtained in a similar way by extrapolation to zero chloride. Of all constituents measured, only HCO_3^- , SO_4^{2-} and SiO_2 show appreciable intercepts. Whereas SO_4^{2-} and SiO_2 remain close to constant, a roughly inverse relationship exists between chloride and bicarbonate contents. In a triangular diagram showing the relative proportions of Cl, K and HCO_3^- , the data points for group A are stretched out along a line originating from the HCO_3^- corner and representing a close to constant ratio K/Cl of around 0.060, those for group B, however, occupy only a limited region corresponding to low HCO_3^- contents and K/Cl ratios of around 0.025. The resulting pattern suggests that only group A waters are affected by processes leading to the admixture of the low chloride, high bicarbonate water C.

The main constituents of this possibly only hypothetical water C are bicarbonate (~ 300 mg/l), silica (~ 170 mg/l), and sulfate (30–80 mg/l). The silica contents indicate a temperature of around 160° . The predominance of bicarbonate suggests water C to represent a condensate phase formed through absorption of steam and CO_2 in local groundwater (FOURNIER and TRUESDELL, 1970). The water phase C then has to be assumed to represent a mixture of groundwater and condensed steam derived from some deeper hot water, its isotopic composition is likely to correspond to the weighted mean of the isotopic composition of the contributing phases. In Fig. 5 the isotopic compositions of steam derived from supply water A after

either single step or continuous steam separation are shown. By considering the amounts of steam separated from A required to heat water from ambient temperatures (10°) to close to 160° , the isotopic composition of the local groundwater is found to be around -52‰ for deuterium and -8.5‰ for oxygen-18. These values fall within the range outlined by meteoric water samples collected in the El Tatio area.

The relatively high silica contents even for the lowest chloride springs would support the assumption of the existence of a definite, intermediate temperature underground water phase C. The alternative explanation for the high bicarbonate contents of low chloride springs, absorption of steam containing CO_2 and H_2S at shallow levels, after dilution by groundwater, should be reflected in silica contents decreasing with chloride contents and bicarbonate contents varying independently of chloride. The amounts of sulfate required to maintain close to constant sulfate contents could in either case be produced through oxidation of H_2S by the oxygen in air saturated groundwater. The low pH, low bicarbonate, high sulfate water of spring 281 (Table 2) is likely to have formed through absorption of steam and H_2S in dilute Cl-water under surface conditions.

The low meteoric precipitation rate at El Tatio may in some areas prevent the accumulation of sufficient amounts of groundwater for complete condensation and steam may escape to the surface leading to the formation of acid-sulfate type steam heated pools or, especially in elevated areas, fumaroles.

Sulfate waters. In Fig. 2, a series of isotopic data points fall along a line with a slope of around 1.6 extending away from the meteoric water line. The corresponding waters are characterised by very low chloride contents and sulfate contents increasing with increasing enrichment in the heavier isotopes. Such behaviour is explained in terms of extensive evapora-

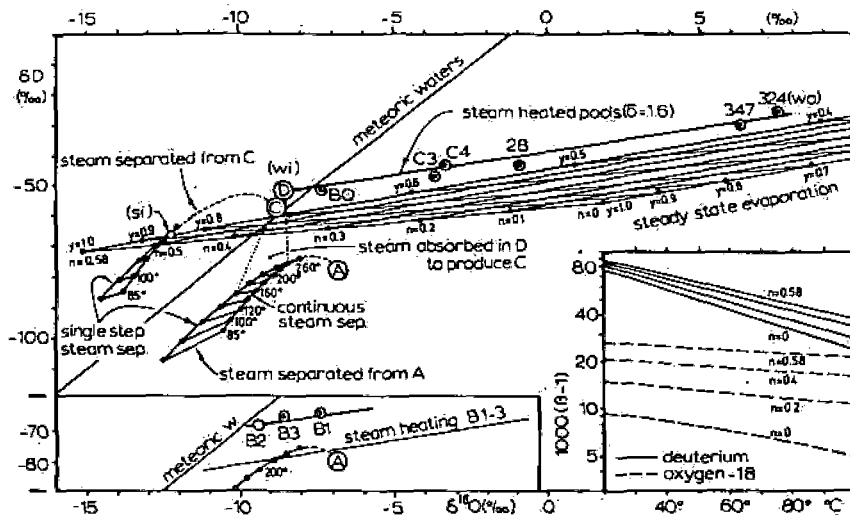


Fig. 5. Plot of δD vs $\delta^{18}\text{O}$ for El Tatio steam heated pools illustrating the effects of kinetic and equilibrium steady state evaporation. Inserts: variations in $1000(\beta - 1)$ with temperature and n for deuterium and oxygen-18 and steam heating relationships for pools B1-3.

70
100Cs
Cl
is of spring Cl, B and at El Tatio

ation from pools heated by the injection of geothermal steam (CRAIG, 1963). The $\delta D/\delta^{18}O$ slopes observed for such pools are usually in the range 2-3, considerably below those expected from the equilibrium fractionation ratio $\epsilon_D/\epsilon_{18O}$ of around 5 at boiling temperature. These deviations are considered to be due to kinetic fractionation effects to some degree influencing evaporation processes from hot pools (CRAIG, 1963).

In recent studies on the evaporation of falling water drops, isotopic fractionation was found to take place in two steps (STEWART, 1975). Removal of water vapor from the drop surface to a vapor boundary layer was found to correspond to an equilibrium fractionation process governed by the vapor pressure ratios α_D and α_{18O} of H_2O to HDO and $H_2^{18}O$ respectively. Exchange between the boundary layer and the atmosphere, however, is strongly influenced by a kinetic fractionation process controlled by the ratio of diffusion coefficients (D/D') for H_2O to HDO or $H_2^{18}O$ in air. The isotopic shifts actually observed also depend on evaporation temperature, relative humidity of the atmosphere and the difference in isotopic composition of the evaporating water and that of atmospheric water vapor. Because of the very low relative atmospheric humidity generally observed at El Tatio, especially if referred to the elevated temperature at which evaporation from hot pools takes place, the effects of atmospheric humidity and those of the isotopic composition of atmospheric water vapor can be assumed to be negligible. Under these circumstances, the overall fractionation factor for water evaporating from the surface of a hot pool is taken to be given by

$$\beta = \alpha_D D/D'^n.$$

The exponent n is derived empirically and decreases with increasing size of the evaporating water body (STEWART, 1975). For falling water drops it was found to be 0.58. In the absence of further information on the influence of kinetic effects on the evaporation from steam heated pools, initially two extreme situations are considered, pure equilibrium evaporation ($n = 0$) and behaviour found for the evaporation of water drops ($n = 0.58$).

Accepting very low values for the effective relative atmospheric humidity at El Tatio, evaporation from steam heated pools can be expected to be described by relationships valid for evaporation in dry atmospheres (STEWART, 1975). Two limiting evaporation processes for hot pools are considered: a steady-state process describing evaporation from continuously replenished, well mixed pools, with relatively high steam injection rates, and batch (Rayleigh) evaporation assumed to represent evaporation from flow channels. The effects of conductive or radiative heat losses or gains are considered to be negligible.

In the case of steady state evaporation, the amount of steam required to heat cold surface waters to evaporation temperatures is taken to be insignificant com-

pared with the total amounts of steam involved in the evaporation processes, the quantities of steam and hot water leaving, therefore, can be set equal to the quantities of steam and surface water entering the pool, the isotopic balance then is given by

$$\delta_{wi} - y(\delta_{wi} - \delta_{si}) = \delta_{wo} - y(\delta_{wo} - \delta_{so})$$

where δ_w and δ_s refer to the deuterium or oxygen-18 content of the water or steam phase respectively, i and o to fluids entering or leaving the pool; y represents the fraction of total fluid entering and leaving the pool as steam. By use of the respective values for β , the difference in isotopic composition of water and steam leaving the pool is given by

$$(\delta_{wo} - \delta_{so}) = 1000(\beta - 1)$$

The above relationships then allow the isotopic composition of the steam heating the pool to be calculated from the known composition of local meteoric waters, δ_{wi} , and that of the pool water sampled, δ_{wo} as a function of y according to

$$\delta_{si} = \delta_{wi} + ((\delta_{wo} - \delta_{wi})/y) - 1000(\beta - 1).$$

The values for β were obtained by use of data reported for the water vapor pressure ratios α_D at 85° of 1.034 and α_{18O} of 1.0057 by MAJOUBE (1971), and values for the ratio of diffusion coefficients (D/D') taken to be those of 1.024 for HDO and 1.0289 for $H_2^{18}O$ reported by MERLIVAT (1970) for room temperature. (D/D') depends largely on the mass ratios of the diffusing molecules and can therefore be assumed to be only little affected by variations in temperature. Variations in $1000(\beta - 1)$, the fractionation factors in the delta notation, with temperature and n are given in Fig. 5 (insert).

The other evaporation process considered is described by the Rayleigh batch-distillation equation

$$R/R_0 = (1 - y)^{(1/\beta) - 1}$$

where R_0 represents the initial isotopic ratios of HDO or $H_2^{18}O$ to H_2O , R the ratios after evaporation of the fraction y of steam. Again by taking R_0 to correspond to the weighted mean of steam and surface water entering the system and R to the composition of the water after removal of the fraction y of steam, the isotopic composition of the steam entering is given by

$$\delta_{si} = \delta_{wi} + [(\delta_{wo} + 1000)(1 - y)^{(1/\beta) - 1} - (\delta_{wi} + 1000)]/y.$$

The batch distillation process closely approximates steam loss accompanying adiabatic cooling of the thermal discharges in flow channels or fast flowing pools with low steam injection rates. In the absence of further heat gains the amount of steam produced depends on the temperature difference of the discharges before and after steam loss. At an initial temperature of 85°, adiabatic cooling to 10° can produce a maximum amount of steam corresponding to $y = 0.12$. Insertion of this value into the above equa-

area for both kinetic and equilibrium evaporation, shows that in order to achieve the isotopic enrichment observed for springs 324 and 347, the steam injected would have to be enriched in deuterium and oxygen-18 corresponding to δ -values between +100 to +150‰, a range far beyond that ever encountered in natural systems. Pure batch evaporation can, therefore, be discounted to represent an effective process in bringing about the observed isotopic enrichments in steam heated pools.

Restricting further considerations to the effects of steady state evaporation an area outlining the ranges of composition expected for the steam entering pool 324 can be calculated as shown in Fig. 5. The range of steam compositions obtained for pure equilibrium fractionation ($n = 0$) is outside that of steam likely to have separated from either waters A, B or C, according to single step or continuous steam separation, the calculated fractionation are much too small, even for high degrees of evaporation corresponding to values of y approaching unity.

By assuming evaporation from pools to be governed by kinetic processes similar to those observed for falling water drops, the range of isotopic compositions for the steam injected into pool 324 is found to intersect the compositional range of steam separated from water C at temperatures between 140–160°. These findings would point to some re-evaporation of the high-bicarbonate water phase C at around 150° which in turn is formed by absorption of steam separated from the deep, original supply water A. The overall process then corresponds to double stage steam separation modified by the interaction with local ground water during the second stage.

In the case of evaporation from hot pools, the value of $n = 0.58$, derived for the evaporation of falling water drops, is likely to be somewhat too high. By assuming the isotopic composition of pools 324 and 347 to represent the maximum obtainable enrichment ($y = 1.0$), n is found to be in the order of 0.50. In the absence of further evidence this value is taken to be characteristic for the evaporation from steam heated pools.

Accepting the isotopic composition of steam heated pools to be governed by an overall kinetic steady state evaporation process the slope σ of the line connecting the isotopic data points for such pools is given by

$$\frac{\delta D_{wi} - \delta D_{wo}}{\delta^{18}O_{wi} - \delta^{18}O_{wo}} = \sigma$$

$$= \frac{\delta D_{wi} - \delta D_{si} - 1000(\beta_D - 1)}{\delta^{18}O_{wi} - \delta^{18}O_{wo} - 1000(\beta_{18O} - 1)}$$

Inserting the found values for δ_{si} , δ_{wi} and β ($n = 0.50$), a slope of +1.62 is obtained, almost identical to that of the least squares line of 1.58 for all steam-heated pools of the El Tatio area. The relationships derived above, therefore, can be assumed to describe the isotopic behaviour of steam heated pools satisfactorily.

Because of the predominant effect of the temperature insensitive kinetic factor $(D/D)^*$, β and correspondingly σ are close to independent of the actual evaporation temperature (Fig. 5). The higher slopes in the order of 2–3 usually observed for other geothermal areas can largely be explained by variations in the differences in isotopic composition between local meteoric water and heating steam. In addition, the assumption of the effects of atmospheric humidity to be negligible may not be valid for lower lying thermal areas.

Applying the above procedures to a set of three samples collected from obviously steam heated pools 7 km to the east of El Tatio (B1–B3), the range of possible compositions of the steam injected can then be calculated. This range intersects the curves representing steam separated from water A for temperatures above 200°, those for steam from water B for temperatures below 120° (Fig. 5, insert). Since water B is assumed to be restricted to the main thermal area, the steam heating pools B1 and B3 is possibly derived from an underground body of water A extending beneath the eastern ranges (Fig. 5, insert).

The main chemical constituent of steam heated pools is sulfate derived from oxidation of H_2S by atmospheric oxygen. Sulfate contents increase with increasing enrichment in the heavier isotopes. Assuming complete absorption and oxidation of H_2S in the pool and isotopic enrichment to be governed by kinetic, steady-state evaporation processes, an attempt can be made to calculate the concentration of H_2S in the steam injected. By use of the known values of δ_{si} , δ_{wo} and δ_{wi} for oxygen-18 and the observed sulfate contents (in mg/l), the concentration of H_2S (in mol%) is given by

$$(H_2S)_s = 1.88 \times 10^{-3} (SO_4^{2-}) [\delta_{si} - \delta_{wo} + 1000(\beta - 1)] / (\delta_{wo} - \delta_{wi})$$

The values obtained for pools 324 and 347 are 1.3×10^{-3} mol% as compared to 0.6×10^{-3} mol% found for fumaroles of the northern part of the thermal areas (CUSICANQUI *et al.*, 1975), for pools 28, C3 and C4 in the southern part, the values are with 7×10^{-3} mol% considerably higher, possibly reflecting the higher H_2S contents of around 2×10^{-3} mol% determined in fumarolic steam there.

Origin of thermal waters

In the preceding sections the isotopic composition of the three main underground water phases and that of the local meteoric water was defined. The data points for waters C and D lie close to the meteoric water line, waters A and B occupy positions off this line towards higher oxygen-18 values. This oxygen shift is explained in terms of ^{18}O -exchange between rock and water at elevated temperatures. While affecting the oxygen isotopic composition of thermal waters, the deuterium content of the waters, thought to be largely of meteoric origin, remains preserved. In the case of the main supply water A, the deuterium

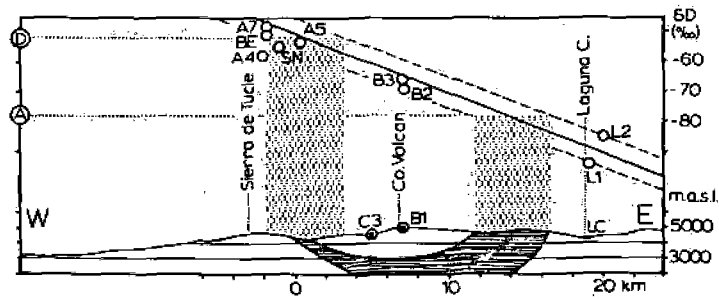


Fig. 6. Variation in deuterium content of precipitation with distance from El Tatio to the east.

content is well below that of El Tatio meteoric waters thus indicating a different origin.

Geographical conditions influencing the deuterium content of precipitation are the altitude of the catchment area, and its latitude and distance from the sea (FRIEDMAN *et al.*, 1964). Since El Tatio lies on the western flanks of the Andes, the deuterium content of precipitation can be expected to decrease both with increasing altitude and distance inland to the east. In order to evaluate the influence of these geographical parameters, samples from cold springs to the east of El Tatio were analysed. Their deuterium contents with respect to geographical position is shown in Fig. 6. The combined effects of increases in altitude and distance from the sea lead to a roughly linear decrease in deuterium content by about 2‰ per km. Local and annual variations in the isotopic compositions are assumed to correspond to deviations from this line by about $\pm 5\%$. With a deuterium content of the main supply water of -78% , the catchment area for water A then is found to lie some 12–16 km to the east of El Tatio. Geophysical and geochemical considerations suggest the thermal waters enter the El Tatio area from the southeast, in this case the overall picture is still valid, the actual distance travelled by the waters would be larger.

GENERAL DISCUSSION

Application of mixing models

Recently TRUESDELL and FOURNIER (1975) proposed a mixing model allowing deep supply water temperatures to be evaluated from the chloride and silica contents of boiling springs. The model assumes temperatures as indicated by the quartz geothermometer to be controlled by two main processes: adiabatic steam loss and dilution by low chloride, low silica and low temperature surface waters. In an enthalpy-chloride diagram (Fig. 7), deep water enthalpies derived from silica temperatures are marked on steam separation lines radiating from a point corresponding to steam at elevated temperatures (zero chloride, enthalpy 2775 J/g) to points representing sampling temperatures and chloride contents. Dilution is represented by lines radiating from the low chloride, low temperature surface water position through the silica-enthalpy points on the steam separation lines. The intersection of the dilution lines with the highest chloride steam separ-

ation line is taken to represent the enthalpy and chloride content of the primary supply water. In this evaluation, two sets of samples assume exceptional importance: the highest chloride springs, presumed to be unaffected by dilution and to represent pure steam loss, and the lowest chloride springs, with silica contents below that of amorphous silica solubility at sampling temperatures, taken to reflect the effects of both surface water dilution and steam separation.

In Fig. 7, data points derived by use of the analytical results given in Table 2 together with those of wells T7, 10, 11, and 12, as reported by CUSIGNOLI *et al.* (1975), are shown. As outlined above, the composition of the low chloride springs has to be explained in terms of mixing with the 160° high silica bicarbonate water C and not dilution by cold surface waters as required by the mixing model. Straightforward application of this method to an unselected group of samples would lead to unreasonably high estimates of the deep temperatures. Restricting mixing model considerations to springs and wells with bicarbonate contents below 100 mg/l, maximum supply water temperatures and corresponding chloride contents identical to those of the deep production well T7, 10, 11 and 12 are obtained.

The data points for the shallow wells T1–5 lie close to a line indicating gradual dilution with cool, low chloride waters from north to south. The undiluted end member of this series, as represented by T5, is derived from water A by steam loss; this process apparently also affected the deeper production wells

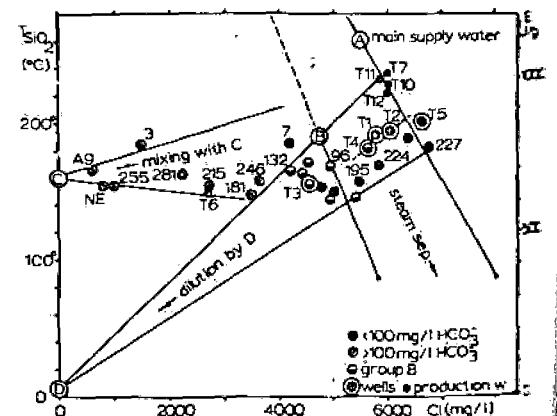


Fig. 7. Application of boiling springs mixing model to El Tatio thermal discharges.

Fig. 10, 11 and 12, though to a lesser degree. The low-temperature supply water for group B springs is likely to have formed by dilution of waters represented by the production well discharges. Steam separation and some dilution with water D is likely to be responsible for the small but noticeable variations in composition observed for group B waters.

The large area of data points occupied by the high bicarbonate (<100 mg/l) waters suggests that in addition to mixing with water C and steam separation, the waters may have also been subject to minor degrees of dilution by water D.

In order to avoid interference from admixture of low chloride, high silica secondary underground waters, in the application of the boiling spring mixing model, conclusions based on data points from waters with high bicarbonate or sulfate contents should be treated with caution.

General hydrology

According to the above findings, the El Tatio thermal discharges are likely to be derived from precipitation some 15 km to the east. During their passage to the west, contact with rock at elevated temperatures leads to an increase in temperature and to an exchange of oxygen-18. In the absence of further evidence, the increase in solute content of the thermal waters may also be explained in terms of rock-water interaction (ELLIS and MAHON, 1964). During a down-hole sampling program, however, highly concentrated waters with chloride contents up to 190 g/l were encountered in wells 2 and 9. According to MAHON (1974), these brines may have formed through leaching of buried evaporite deposits by the thermal waters. The low room-temperature pH of around 2 of the brines, however, is far below that expected for such a simple leaching process, but is very similar to that of fluids formed through contact with acid magmatic emanations. Again, considering the relative proportions of the three constituents of thermal waters, Cl, B and Cs, likely to be least affected by secondary reactions at temperatures below 300°, the data point in Fig. 4b for the El Tatio brine (TB) occupies a position far removed from those of the thermal waters, however, close to points obtained for highly mineralised waters resulting from the interaction of acid volcanic fluids with andesitic rock. WI represents an acid brine from White Island, New Zealand (GIGGENBACH, 1977), RC the more dilute waters of Ruanuku Crater Lake (GIGGENBACH, 1974), BR and WR represent typical waters from the Broadlands and Wairakei geothermal areas. The distribution of data points shows that the relative positions of the acid brines to the neutral waters in New Zealand is similar to that observed for the El Tatio samples.

The New Zealand volcanic samples, WI and RC, are typical for waters formed through interaction of acid waters with andesitic rock at comparatively low temperatures (<200°). Interaction of waters derived by absorption of magmatic steam with rock at higher

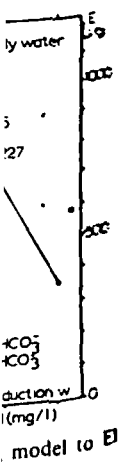
temperatures (300–500°) and greater depth is assumed to finally lead to the production of near neutral waters as represented by BR and WR (GIGGENBACH, 1977). This rough classification might suggest that the El Tatio brine represents a water phase produced through absorption of magmatic steam at relatively low temperatures (~200°). The thermal waters discharged then are likely to be derived in a similar way, their neutral pH and lower solute content have to be explained in terms of more intense rock-water interaction of the initial brines at higher temperatures followed by dilution with the east-west moving tongue of meteoric water.

The data point in Fig. 4b for the highly mineralised waters of Laguna Colorada (LC), some 20 km to the east of El Tatio, occupies a position close to that for volcanic brines; differences in the relative proportions of chemical constituents and the higher pH, however, suggest that the LC-waters and the El Tatio brine are not directly related. The possibility of both brines to be of related origins, however, cannot be discounted, the differences observed then being due to secondary reactions of the original waters with rock contacted under different temperature and pH conditions. The position of the isotopic data points for Laguna Colorada, far from the meteoric water line, suggests some considerable rock-water oxygen-shift or evaporation at above ambient temperatures caused by steam heating. In discussions on a possible connection between the two brines and their relationship to the thermal waters, information on the isotopic composition of the El Tatio brine would be required, which is unfortunately not available.

The two main processes affecting the thermal waters during their migration westward are steam separation and dilution. In contrast to most other geothermal areas around the globe where dilution by local meteoric waters represents one of the most important processes influencing the chemical and isotopic composition of the discharges, the very low annual precipitation rate at El Tatio (<10 cm) limits such direct dilution to the waters of group B discharged in the southern part of the main thermal area. This dilution takes place under circumstances allowing the equilibria controlling both SiO₂ and relative Na-K-Ca contents to readjust to the lower temperatures of around 160° as compared to that of the primary supply water of 240–260°. Readjustment of the silica contents is likely to be comparatively fast, reequilibration of the feldspar equilibria controlling relative Na-K-Ca contents at temperatures below 250°, however, are considered to be much slower (FOURNIER and TRUESDELL, 1973) suggesting long residence times for the dilute waters underground. In Fig. 8 an attempt is made to illustrate the possible paths of the thermal waters. The diagram closely resembles that given by HEALY and HOCHSTEIN (1973) derived by use of geological and geophysical evidence. According to these authors two main water conducting strata can be distinguished, a hot water carrying

thaly and
ater. In the
exceptional
presumed
resent part
with silica
solubility
re effects of
paration.
the analyt
th those of
CUSICAN
e, the con
has to be
high silica
cold surface
Straightfor
unselected
onably high
ting mixing
with bicar
um supply
chloride co
uction well

1-5 lie close
h cool low
e undiluted
d by T5. a
this process
uction well



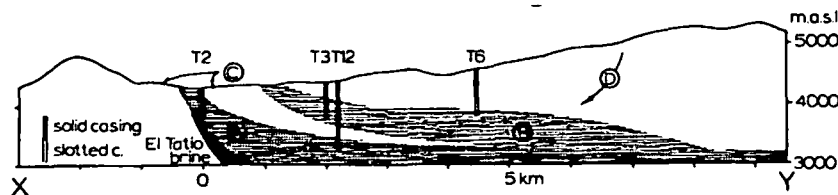


Fig. 8. Hydrological profile of the El Tatio thermal area.

ignimbrite formation and a more shallow dacite formation containing the cooler diluted waters.

The chemistry of the group B springs can largely be explained in terms of steam loss and straightforward dilution of the original supply water with local meteoric water. The chemistry of group A springs, however, points to admixture of a secondary water phase possibly resulting from the absorption of steam separated from the deep water in local meteoric water. The overall effect of these processes could still be considered dilution by local meteoric waters, the creation of a different chemical environment for rock-water interaction and the resulting formation of the low chloride, high silica, bicarbonate water phase C, however, leads to marked differences in the chemical nature of the waters produced.

In order to explain these differences, the existence of definite underground steam zones associated predominantly with the high temperature water phase A and separating the deep thermal waters from the shallow ground water was invoked. The formation of these 'vapor dominated' zones or pockets (WHITE *et al.* 1971) is likely to be favoured by the lack of a significant recharge of cooler surface waters to counteract steam separation from the rising thermal waters. At present it is not possible to evaluate the geometry of these steam zones and that of the associated condensate layer. The finding that widely scattered springs to the north (A9, NE) and south (3, 7) of the main area are obviously affected by similar processes, the likelihood that the steam heating pools to the east (28, C3, C4) is derived from the proposed intermediate bicarbonate water, its uniformity in temperature indicated by the SiO_2 -contents, and the close to linear, inverse relationship between bicarbonate and chloride contents would favour the possibility of the existence of extensive vapor or, in cooler regions, gas dominated zones capped by a close to uniform layer of bicarbonate water. Of the wells drilled only T4 showed evidence for the inflow of a gas-rich steam phase at shallow levels, (MAHON, 1974), the fact that wells at El Tatio are solidly cased down to about 250 m may prevent the detection of these steam or gas zones in the vicinity of other wells.

Acknowledgements—The author wishes to thank A. J. ELLIS and H. CUSICANQUI for the collection of most of the water samples, M. K. STEWART and R. L. GOGUEL for assistance with the isotopic and chemical analyses respectively, and A. J. ELLIS, W. A. J. MAHON and M. K. STEWART who reviewed the manuscript for helpful comments.

REFERENCES

- CRAIG H. (1963) The isotopic geochemistry of water and carbon in geothermal areas. In *Nuclear Geology of Geothermal Areas* (editor E. Tongiorgi), pp. 53–92.
- CUSICANQUI H., MAHON W. A. J. and ELLIS A. J. (1975) The geochemistry of the El Tatio Geothermal Field, Northern Chile. In *Second United Nations Symposium on the Development and Utilisation of Geothermal Resources*, San Francisco, pp. 703–711.
- ELLIS A. J. (1969) Survey for Geothermal Development in Northern Chile. Preliminary geochemistry report, El Tatio geothermal field. UNDP-Report.
- ELLIS A. J. and MAHON W. A. J. (1964) Natural hydrothermal systems and experimental hot-water/rock interactions. *Geochim. Cosmochim. Acta* 28, 1323–1357.
- FRIEDMAN I., REDFIELD A. C., SCHOEN B. and HARRIS J. (1964) The variations of the deuterium content of natural waters in the hydrological cycle. *Rev. Geophys.* 2, 177–223.
- FOURNIER R. O. and TRUESDELL A. H. (1970) Chemical indicators of subsurface temperature applied to hot spring waters of Yellowstone National Park, Wyoming, USA. *Geothermics, Special Issue 2*, Vol. 2, Part 1, pp. 529–536.
- FOURNIER R. O. and TRUESDELL A. H. (1973) An empirical Na–K–Ca geothermometer for natural waters. *Geochim. Cosmochim. Acta* 37, 1255–1275.
- GIGGENBACH W. F. (1974) The chemistry of the Crater Lake on Mt Ruapehu (New Zealand) during and after the 1971 active period. *N.Z. J. Sci.* 17, 33–45.
- GIGGENBACH W. F. (1977) The isotopic composition of sulphur in sedimentary rocks bordering the Taupo Volcanic Zone. In *Geochemistry 1977*. N.Z. DSIR Bull. 218, 57–64.
- GIGGENBACH W. F. and GLASBY G. P. (1977) The influence of thermal activity on the trace metal distribution in marine sediments around White Island, New Zealand. In *Geochemistry 1977*. N.Z. DSIR Bull. 218, 121–126.
- HEALY J. and HOCHSTEIN M. P. (1973) Horizontal flow in hydrothermal systems. *N.Z. J. Hydrology* 12, 71–82.
- MAHON W. A. J. (1974) The Geochemistry of the El Tatio geothermal system. Unpublished Report-UNDP, New York.
- MAJOUBE M. (1971) Fractionnement en oxygene-18 et en deuterium entre l'eau et sa vapeur. *J. Chim. Phys.* 68, 1423–1436.
- MERLIVAT L. (1970) L'étude quantitative de bilans de lac à l'aide des concentrations en deuterium et oxygene-18 dans l'eau. In *Isotope Hydrology*, pp. 89–107. IAEA, Vienna.
- STEWART M. K. (1975) Stable isotope fractionation due to evaporation and isotopic exchange of falling water-drops: application to atmospheric processes and evaporation of lakes. *J. Geophys. Res.* 80, 1133–1146.
- TRUESDELL A. H. and FOURNIER (1975) Calculation of deep temperatures in geothermal systems from the chemistry of boiling spring waters of mixed origin. In *Second United Nations Symposium on the Development and Utilisation of Geothermal Resources*, San Francisco, pp. 837–844.
- TRUESDELL A. H., NATHENSON M. and RYE R. O. (1978) The effects of subsurface boiling and dilution on the isotopic composition of Yellowstone thermal waters. To be published.
- WHITE D. E., MUFFLER L. J. P. and TRUESDELL A. H. (1971) Vapor dominated hydrothermal systems compared with hot-water systems. *Econ. Geol.* 66, 75–97.